HETEROCYCLES, Vol. 100, No. 10, 2020, pp. 1513 - 1578. © 2020 The Japan Institute of Heterocyclic Chemistry
Received, 18th December, 2019, Accepted, 24th April, 2020, Published online, 8th May, 2020
DOI: 10.3987/REV-19-924

NEW AND PRACTICAL APPLICATIONS OF FUNCTIONALIZED CYCLOTRIPHOSPHAZENE CORE-BASED MATERIALS

Manabu Kuroboshi* and Hideo Tanaka

Graduate School of Natural Science and Technology, Okayama University, Tsushima-naka 3-1-1, Kita-ku, Okayama, Japan, 700-7530. mkurohos@cc.okayama-u.ac.jp

Abstract – Hexachlorocyclotriphosphazene (HCCP) is a very old compound, and used as a starring material of a variety of cyclotriphosphazene derivatives. Some of them have unique properties, and have been used in not only frame retardants but also functional materials and biomaterials. To develop cyclotriphosphazene derivatives having a desired function, numbers of substituents, regio-, and stereochemistry should be controlled in the reaction between HCCP and nucleophiles. In this review, selectivity in the reaction between HCCP and nucleophiles as well as application of the cyclotriphosphazene derivatives are summarized.

1. INTRODUCTION

Cyclotriphoaphazenes have formula $(NPR_2)_3$, in which three nitrogen atoms and three phosphorus atoms are connected alternately to form planer six-membered ring structure. Each phosphorus atom has two substituents directed toward upper and lower sides of the ring. Simplest and most basic cyclotriphosphazene is hexachlorocyclotriphosphazene (HCCP, Figure 1-1). HCCP was firstly synthesized in 1834 by Liebig from reaction between PCl_5 and ammonia.[1] Its cyclic structure was suggested in 1895,[2] and confirmed by electron diffraction[3] and X-ray diffraction.[4] All P-N bonds in HCCP have a same length (158 pm, about 10% larger than benzene (139 pm)), and angles of N-P-N and P-N-P are about 120º (Figure 1-1).

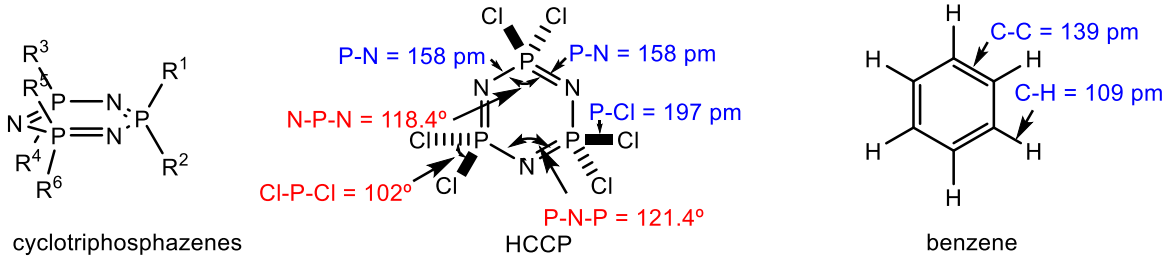

Figure 1-1. Bond length and bond angle of HCCP and benzene

HCCP itself is stable solids under air, but has relatively reactive six P-Cl bonds, which can easily react with several types of nucleophiles such as amines (ammonia, primary/secondary aliphatic/aromatic amines), alcohols and phenols, thiols and thiophenols, and so on. Number of substituents and regio/stereo-chemistry of the products depend on the introduced nucleophiles and the reaction conditions. For example, ammonia and thiophenols tend to be introduced two by two in *gem*-position to make 2,2-disubstituted, 2,2,4,4-tetrasubstituted, and 2,2,4,4,6,6-hexasubstituted cyclotriphosphazenes,[5,6] whereas phenols are introduced randomly.[7] Since all P-Cl bonds are equivalent, control of the selectivity is difficult. It makes the situation more complicated that, in some cases, intramolecular and intermolecular recombination (rearrangement) of the substituents can occur frequently. However, HCCP is small, compact, and rigid compounds and can be equipped with six units having different functionality. Moreover, since the substituents are closely located, interactions between the substituents can be expected. If we can control the selectivity, HCCP can be a core of the multifunctional compounds, molecular factories.

HCCP has a flat $(-N=P-)_3$ ring, and most of cyclotriphosphazene derivatives have a flat $(-N=P-)_3$ ring. In some cases, the cyclophosphazene ring is a little twisted and the maximum deviation from the mean plane of the cyclophosphazene ring being 1.115(9) pm (on P2 atom) (Figure 1-2).[8]

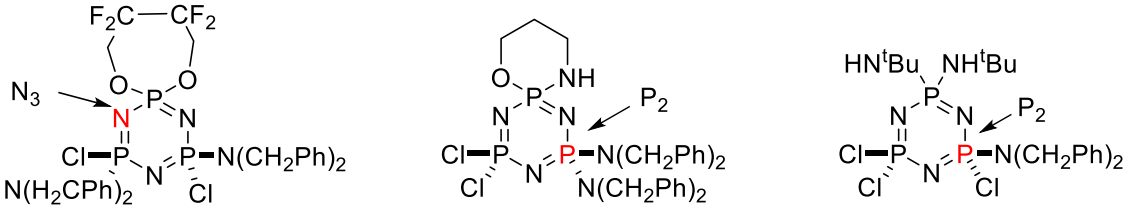

5-1	**5-2**	**5-3**
Max. Deviation for P_3N_3 ring		
0.0695 (16) (N3)	0.0791 (15) (P2)	0.1115 (9) (P2)

Figure 1-2. The cyclotriphosphazenes **5-1**, **5-2,** and **5-3**, and max deviation for P_3N_3 ring

HCCP is a versatile starting material for syntheses of cyclotriphosphazene derivatives. A wide range of cyclotriphosphazene derivatives have been synthesized by nucleophilic substitution of reactive P-Cl bonds in HCCP with a variety of functionalized nucleophilic reagents having -NH or –OH reaction points, such as primary and secondary amines, polyamines, and phenols. Six Cl atoms of HCCP may be replaced sequentially by the same/different organic/inorganic nucleophiles. Therefore, a variety of geometrical (regio/stereo) and optical isomers can be generated. When two Cl atoms in HCCP are substituted by the monodentate nucleophiles, *gem*, non-*gem*/*cis*, and non-*gem*/*trans* geometrical isomers are obtained. When the nucleophile is bidentate, there are *spiro*- and *ansa*-type isomers (Figure 1-3).

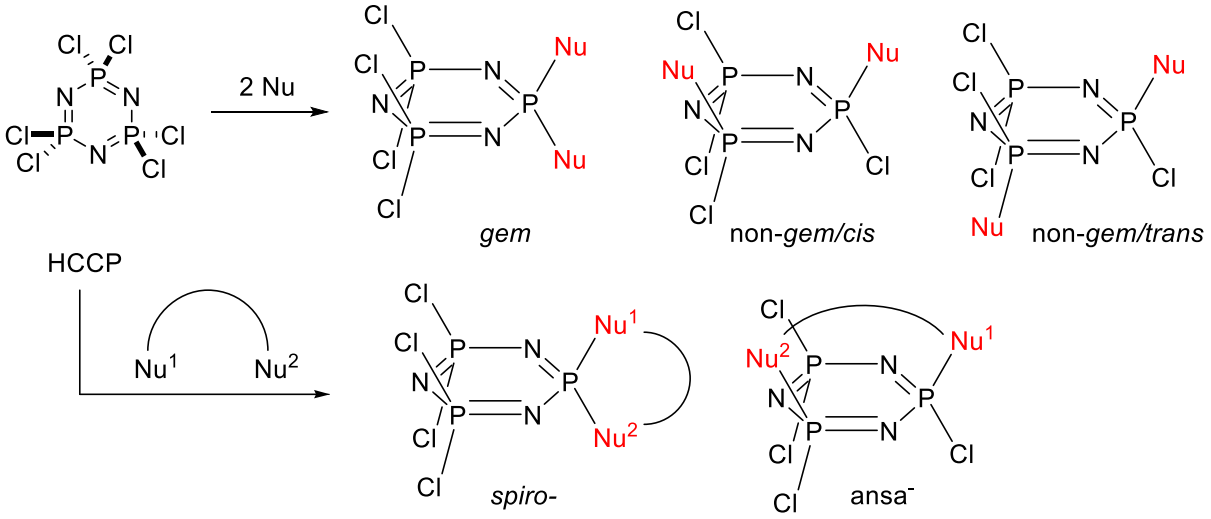

Figure 1-3. Di-substituted derivatives of HCCP

Tri-substituted, $N_3P_3Cl_3R_3$, and tetra-substituted, $N_3P_3Cl_2R_4$, phosphazenes also have the *gem*, non-*gem*/*cis*, and non-*gem*/*trans* isomers. The di-substituted $N_3P_3Cl_4R_2$, tri-substituted $N_3P_3Cl_3R_3$, and tetra-substituted $N_3P_3Cl_2R_4$ structures can have optical isomers.

^{31}P NMR can be used to determine the structure of the cyclotriphosphazene derivatives. The representative data are shown in Figures 1-4,[5] 1-5,[6] and 1-6.[7] The reactions of HCCP with nucleophiles can also be easily monitored by ^{31}P NMR.

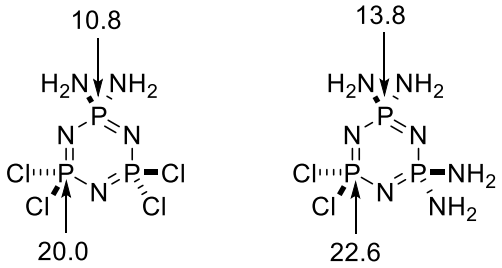

Figure 1-4. ^{31}P NMR of *gem*-$N_3P_3Cl_4(NH_2)_2$ and *gem*-$N_3P_3Cl_2(NH_2)_4$

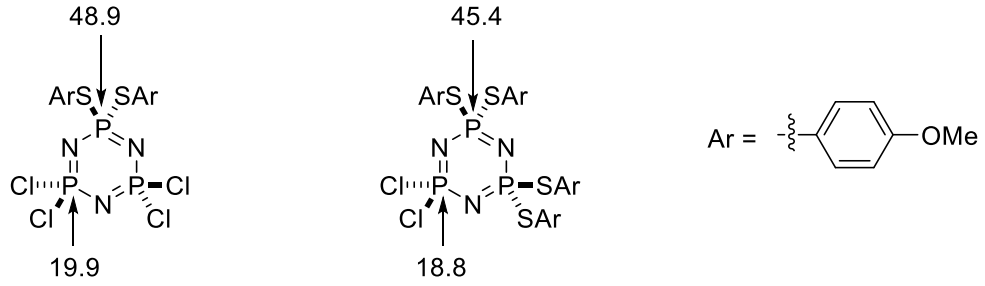

Figure 1-5. ^{31}P NMR of *gem*-$N_3P_3Cl_4(SAr)_2$ and *gem*-$N_3P_3Cl_2(SAr)_4$ (Ar = 4-$MeOC_6H_4$)

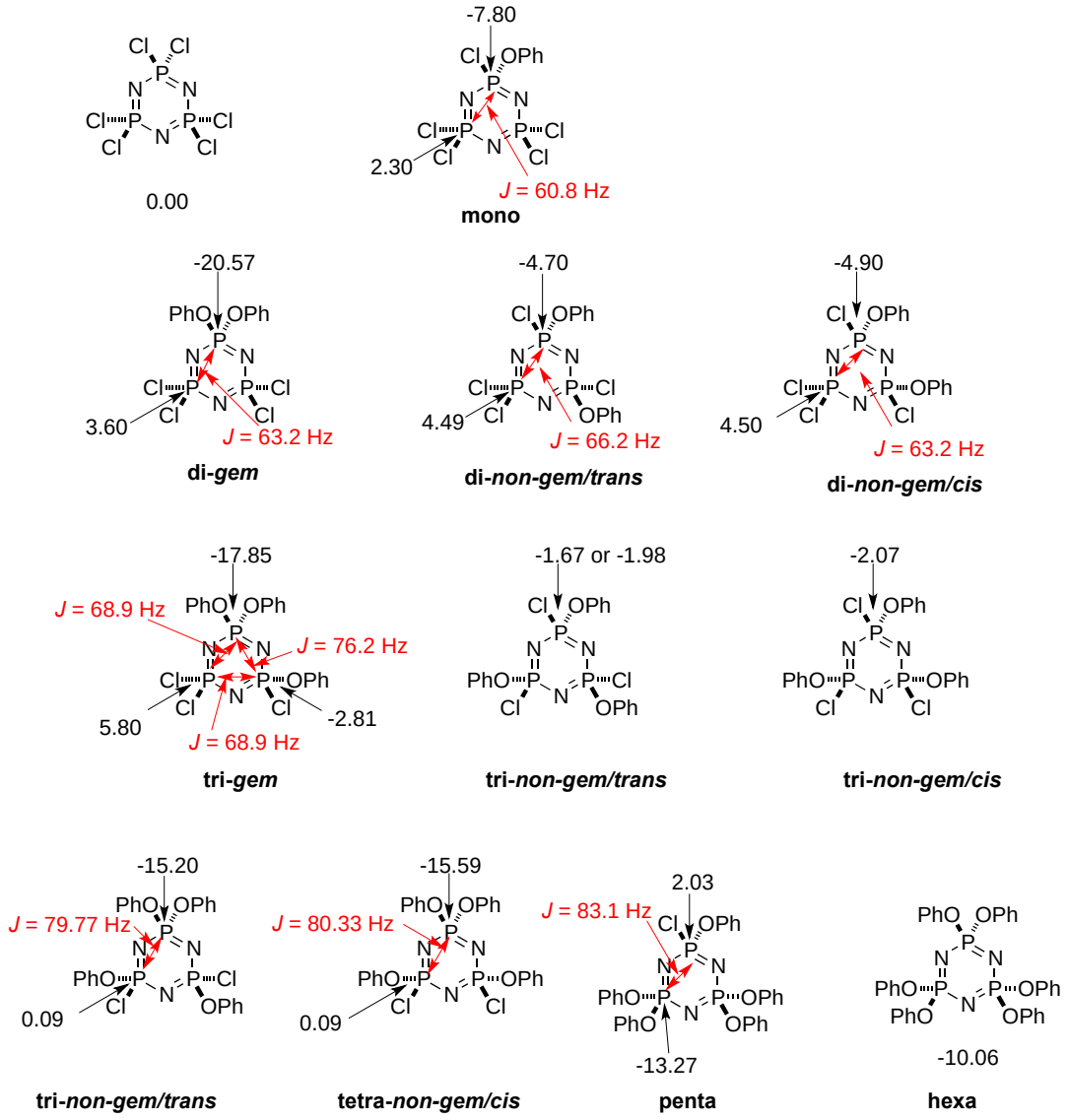

Figure 1-6. ^{31}P NMR of $N_3P_3Cl_x(OPh)_{6-x}$. Relative to HCCP (20.0 ppm from 85% H_3PO_4 external standard).

Historically, HCCP was treated with large excess of nucleophiles to make six-same-substituted derivatives (R^1-R^6 = same), which were used as a frame retardant.[9] On the other hand, in recent years, synthesis of partial substituted cyclotriphosphazenes and the geometrical selectivity were reported, and

especially about after 2010, reports about multi-functionalized interesting cyclotriphosphazenes increased (Figure 1-7). Search by SciFinder using Keyword "cyclotriphosphazene" (Nov. 29, 2019) hits over 2500 literatures. In this manuscript, such compounds used as functional materials and biomaterials are introduced.

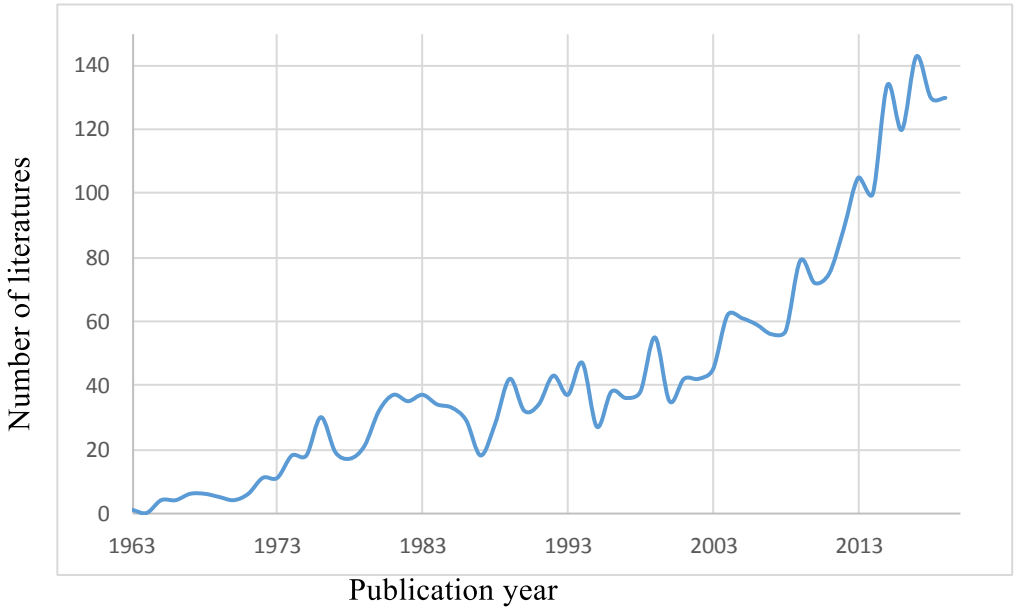

Figure 1-7. Number of literatures by years (searched by SciFinder, Keyword is "cyclotriphosphazene", Nov. 29, 2019)

2. SELECTIVITY FOR NUMBER, REGIO- AND STEREOSELECTIVITY FOR INTRODUCING NUCLEOPHILES INTO CYCLOTRIPHOSPHAZENES

2-1. Single nucleophile

Chen-Yang reported phase-transfer catalyst-promoted reaction of HCCP with phenol in organic solvent/water two-phase system to synthesize the partially substituted (phenoxy)chlorocyclotriphosphazenes, $N_3P_3Cl_{6-x}(OPh)_x$ (x = 0 - 6).[7b] In this reaction, mono-, di- (*gem*, non-*gem*/*cis*, non-*gem*/*trans*), tri- (*gem*, non-*gem*/*cis*, non-*gem*/*trans*), tetra- (*gem*, non-*gem*/*cis*, non-*gem*/*trans*), penta-, and hexaphenoxy products were obtained. Table 2-1 summarizes the distribution of the products varying ratio of phenol : HCCP. It indicates that, under the condition used, the first to fifth phenols were introduced smoothly according to the equivalent of the phenols, but introduction of the sixth phenol required increasing reaction temperature and longer reaction time.

On the other hand, when HCCP was treated with gaseous NH_3, diamino-product *gem*-$N_3P_3Cl_4(NH_2)_2$ and tetraamino-product *gem*-$N_3P_3Cl_2(NH_2)_4$ were obtained in Et_2O and MeCN solvent, respectively (Scheme 2-1).[6] Amino (-NH_2) groups were introduced only in *gem*-position, and no mono-, tri-, and

penta-aminocyclotriphosphazenes were detected. 2,2,4,4,6,6-Hexaaminocyclotriphodphazene was also obtained when HCCP was treated with liquid NH_3.

Table 2-1. Phenoxylation of HCCP in aqueous/organic solvent two-phase system in the presence of phase transfer catalyst, $Me(Oct)_3NCl$

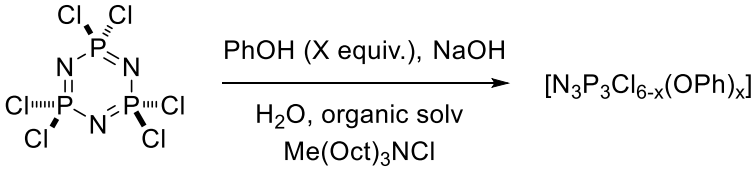

ratio	temp.	time	organic solv	x						
				0	1	2	3	4	5	6
1.0	rt	20 min	CH_2Cl_2	6.7	76.5	10.0				
2.0	rt	20 min	CH_2Cl_2		5.3	77.2	7.0			
3.0	rt	20 min	CH_2Cl_2			4.3	81.8	7.7		
4.0	rt	40 min	CH_2Cl_2				13.5	77.8	1.7	
5.5	reflux	1 h	$(CH_2Cl)_2$					7.2	82	5.7
7.0	reflux	8 h	$(CH_2Cl)_2/CH_2Cl_2$						39.6	50.4

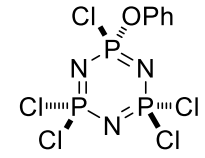
x = 1: mono-

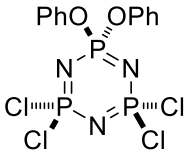
x = 2: di-*gem*

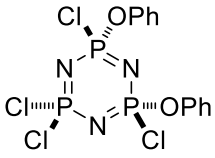
di-non-*gem/cis*

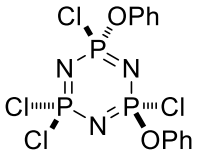
di-non-*gem/trans*

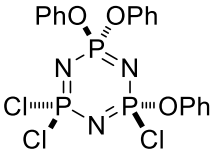
x = 3: tri-*gem*

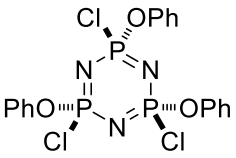
tri-non-*gem/cis*

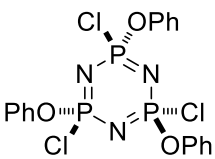
tri-non-*gem/trans*

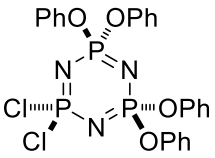
x = 4: tetra-*gem*

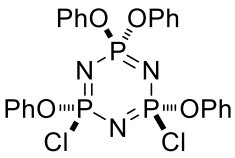
tetra-non-*gem/cis*

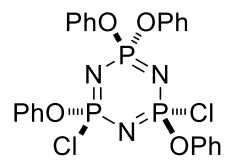
tetra-non-*gem/trans*

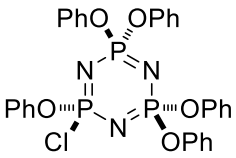
x = 5: penta

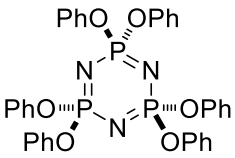
x = 6: hexa

Also, reaction of HCCP with two and four equivalents of thiophenols/Et_3N in MeCN gave 2,2-bis(arylthio)-4,4,6,6-tetrachlorocyclotriphosphazene and 2,2,4,4-tetrakis(arylthio)-6,6-dichlorocyclo-

triphosphazene, respectively (Scheme 2-2).[7] In this case, *gem*-arylthio-substituted products were produced, and mono-, tris-, and pentakis-(arylthio)-substituted cyclotriphosphazenes were not obtained.

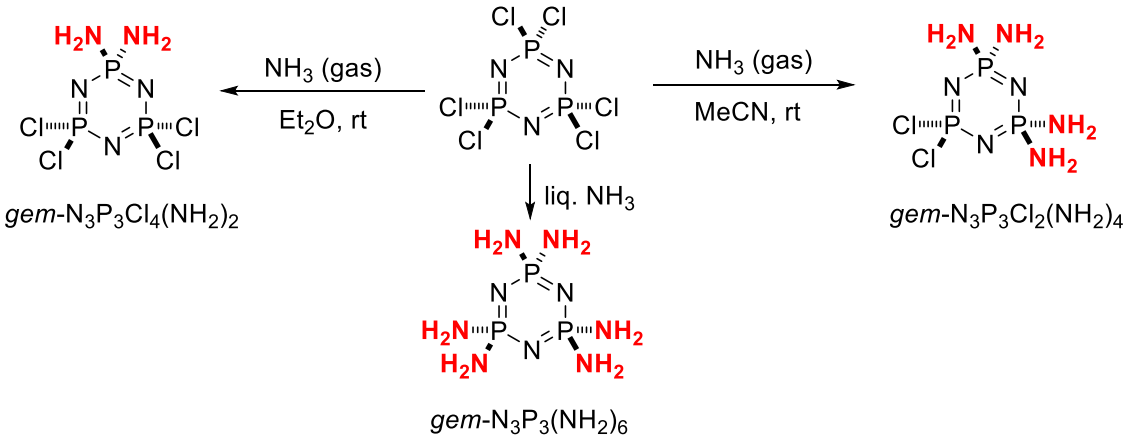

Scheme 2-1. Aminolysis of HCCP

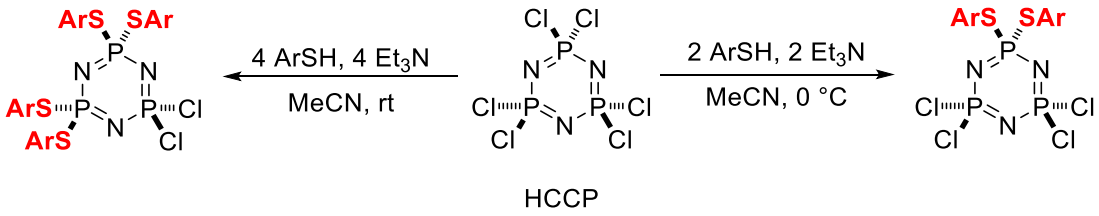

Scheme 2-2. Reaction of HCCP with ArSH

2-2. Introducing the second kind of nucleophiles into substituted cyclotriphosphazenes

Beşli reported reactions of mono *ansa* fluorodioxycyclotriphosphazenes $[N_3P_3Cl_4[OCH_2(CF_2)_2CH_2O]$ (**10-1**) with sodium phenoxide in THF at different molar ratios (Scheme 2-3).[10] This work aimed to determine the reaction pathways and the mechanism of the nucleophilic substitution at PCl_2 and PCl(OR) phosphorus atoms by phenol.

Ten new products were formed, namely mono-phenoxy derivatives (**10-2a** – **4a**), di-phenoxy derivatives (**10-5a** – **7a**), tri-phenoxy derivatives (**10-8a** – **10a**), and tetra-phenoxy derivatives (**10-11a**). When 1 equiv. of PhOH was used, mono-phenoxy derivatives **10-2a** (non-*gem/cis*), **10-3a** (non-*gem/trans*), and **10-4a** (*gem*) were obtained in 25, 45, and 8% yield, respectively. In the second stage of the reaction of **10-1**, the bis non-*gem*/*cis* compound (**10-7a**) formed as the major product (40% yield), which may be derived from **10-3a.** Together with them, tri-phenoxy compounds **10-8a** – **10a** were also obtained. Consequently, 3 equiv. of phenol gave the tris non-*gem*/*cis* compound (**10-9a**) (23% yield) and the tris *gem* compound (**10-8a**) (55%) as major products.

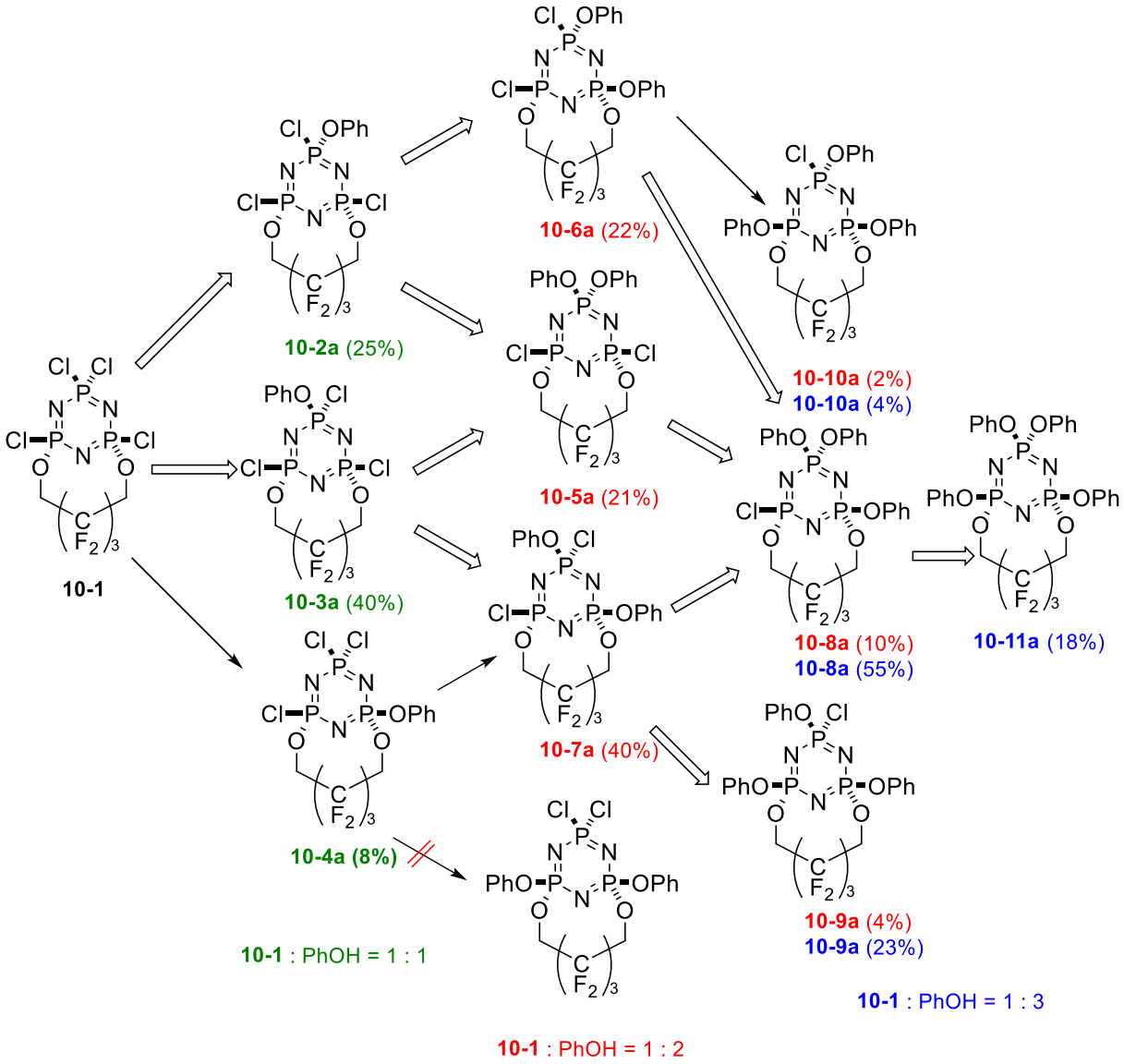

Scheme 2-3. Reaction of $[N_3P_3Cl_4(OCH_2(CF_2)_2CH_2O)]$ (**10-1**) with sodium phenoxide at different molar ratios

The authors also reported reactions of cyclotriphosphazenes with 10-membered *ansa*-$N_3P_3Cl_4[OCH_2(CF_2)_3CH_2O]$ (**11-1a**) ring with sodium methoxide in a THF solution at different molar ratios (Scheme 2-4).[11] The reactions afforded eight products, mono-methoxy derivatives (**11-2a** – **4a**), di-methoxy derivatives (**11-5a** – **7a**), tri-methoxy derivatives (**11-8a**), and the tetra-methoxy derivatives (**11-9a**).

Nucleophilic substitution reactions at the *ansa*-ring PCl(OR) phosphorus atoms of the cyclotriphosphazene compounds **11-1** occurred with a retention of configuration for the 10-membered fluorodioxy *ansa*-rings to give **11-4a**. When 1 equiv. of MeOH was used, mono-methoxylated products **11-2a**, **11-3a** (reacted at PCl_2 phosphorus atom), and **11-4a** (reacted at P(OR)Cl phosphorus atom) were obtained in 32, 27, and 7% yield, respectively. The result confirmed that the reactions with **11-1**

containing the 10-membered *ansa*-ring occurred competitively at both the PCl_2 and P(OR)Cl moieties with an approximate 8 : 1 preference at the PCl_2 group. The results were mainly rationalized in terms of the P–Cl bond lengths of the reactants and the cation-assisted mechanism of reaction.

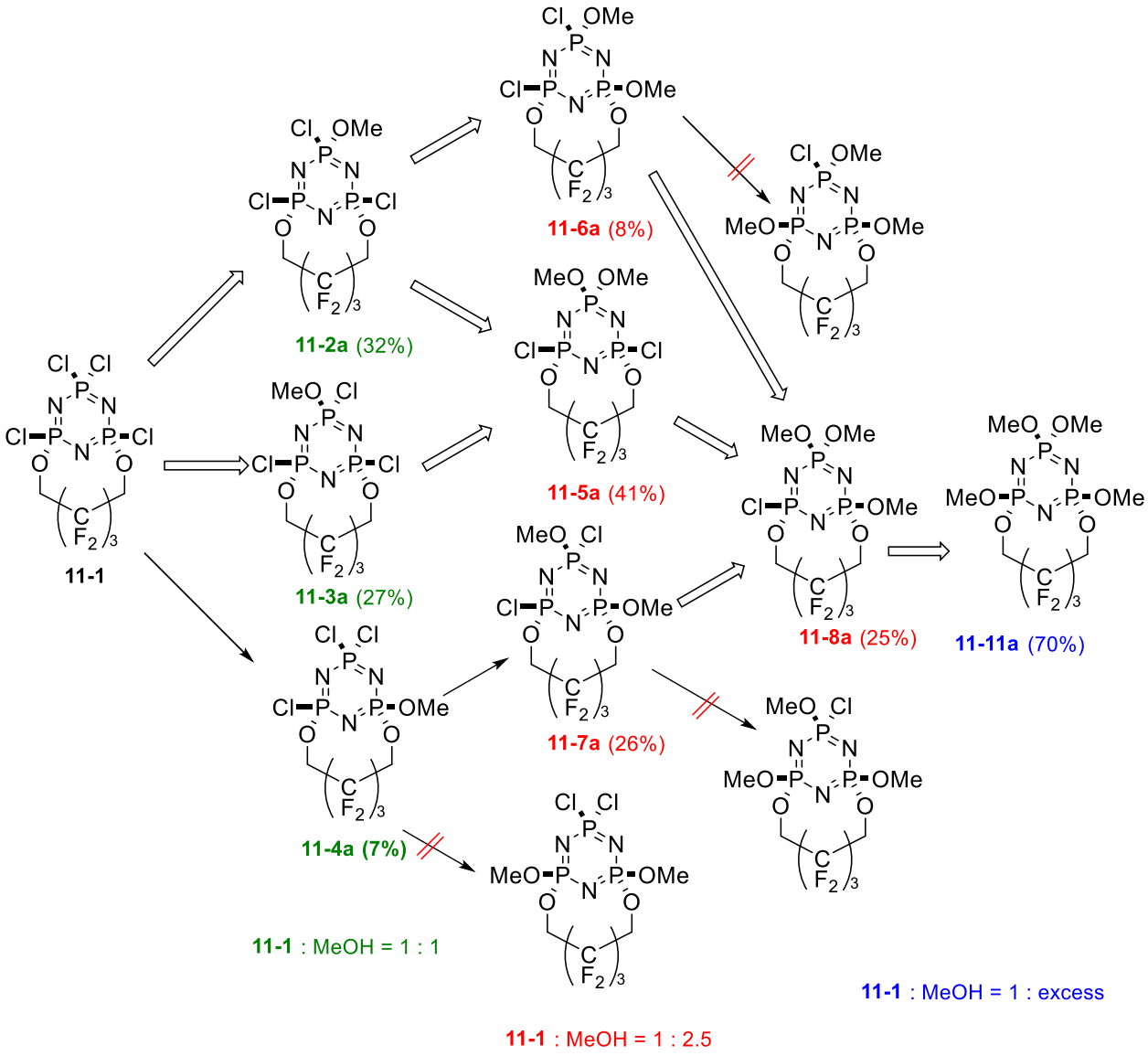

Scheme 2-4. Reaction of $[N_3P_3Cl_4[OCH_2(CF_2)_2CH_2O]$ (**11-1**) with sodium methoxide in different ratios

Reactions of dibenzylamine with selected mono-*spiro* and *gem* di-substituted cyclotriphosphazene derivatives, $N_3P_3Cl_4R_2$ [R = $(OCH_2(CF_2)_2CH_2O)$ (**12-1a**), SPh (**12-1b**), NHPh (**12-1c**), $(OCH_2CH_2CH_2NH)$ (**12-1d**), and $NHBu^t$ (**12-1e**)] were systematically studied (Table 2-2).[12] The influence of the electron-supplying properties of the R groups on the reaction pathway and degree of substitution of the product was investigated. The aminolysis reactions of *spiro*-$N_3P_3Cl_4[NH(CH_2)_3O]$ (**12-1d**) and *gem*-$N_3P_3Cl_4[NHBu^t]_2$ (**12-1e**) with dibenzylamine formed *bis gem*-dibenzylamino

derivatives (**12-4d** and **12-4e**), respectively, whereas **12-1a – c** did not give **12-4a – c**. The reaction of *gem*-$N_3P_3Cl_4[NHPh]_2$ (**12-1c**) was carried out with dibenzylamine at the same mole ratio to give the fully substituted product (*gem*-$N_3P_3[(PhCH_2)_2N]_4[NHPh]_2$, **12-5c**).

The R groups were selected in the order of the electron-supplying capacity as measured by their reported basicity: The basicity of the R_2 groups was calculated about 3.9 for *spiro*-($OCH_2CF_2CF_2CH_2O$) (**12-1a**), 6.0 for $(SPh)_2$ (**12-1b**), 8.8 for $(NHPh)_2$ (**12-1c**), 9.7 for *spiro*-($OCH_2CH_2CH_2NH$) (**12-1d**), and 11.8 for $(NHBu^t)_2$ (**12-1e**). Although it has known that the reaction of cyclotriphosphazene with secondary amines gives non-*gem* products,[9a] the authors showed that the yield of *gem* product increased proportionally with the increase of electron releasing capacity of the R groups on the cyclophosphazene ring.

The regio- and stereoselectivity depends on the balance of steric effects *vs* substituent electron releasing capability. Compound **12-1a** with dibenzylamine gave only bis non-*gem/trans* products (**12-3a**, ca. 63%). However, a small amount of the bis *gem* isomer (**12-4e** ca. 5%) in addition to the bis non-*gem/trans* isomer (**12-3e**, ca. 38%) was obtained in the reaction of **12-1e**. The bis *gem* product (**12-4d**, ca. 29%) formed in almost equal amounts of bis non-*gem* product (**12-3d** ca. 37%) from **12-1d**. Furthermore, a *gem* tetra-substituted product (**12-5c** ca. 11%) was obtained from **12-1c**.

Table 2-2. Aminolysis of $N_3P_3R_2Cl_4$ (**12-1**) with dibenzylamine

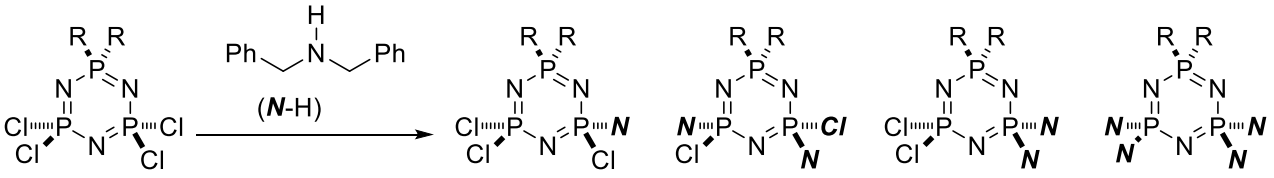

12-1 **12-2** **12-3** **12-4** **12-5**

R	mono	di-non-*gem*/*trans*	di-*gem*	tetra
a -$OCH_2CF_2CF_2CH_2O$-		**12-3a** (63%)		
b -SPh	**12-2b** (38%)	**12-3b** (62%)		
c -NHPh		**12-3c** (27%)		**12-5c** (11%)
d -$OCH_2CH_2CH_2NH$-		**12-3d** (37%)	**12-4d** (29%)	
e -NH^tBu	**12-2e** (44%)	**12-3e** (38%)	**12-4e** (5%)	

Possible reaction mechanisms are suggested in Scheme 2-5 for the non-*gem* and *gem* product formation. Once a secondary amine is substituted to $N_3P_3R_2Cl_4$ (**12-1a** – **e**), there are both the S_N1 (Route I) and the S_N2 (Route II) reaction mechanisms. Non-*gem* products are typically obtained *via* the Route I, while the *gem* products would arise from Route II. The stronger electron donor substituents decrease the formal positive charge on the ring phosphorus atoms thus favoring the initial dissociation of the phosphorus-chlorine bond. In the case of the mono-dibenzylamino derivatives, the electron donating

property of the amine causes a further decrease in the charge on the phosphorus center and consequently increases the tendency for the dissociative pathway and hence formation of the *gem* product as shown in Scheme 2-5 (Route II).

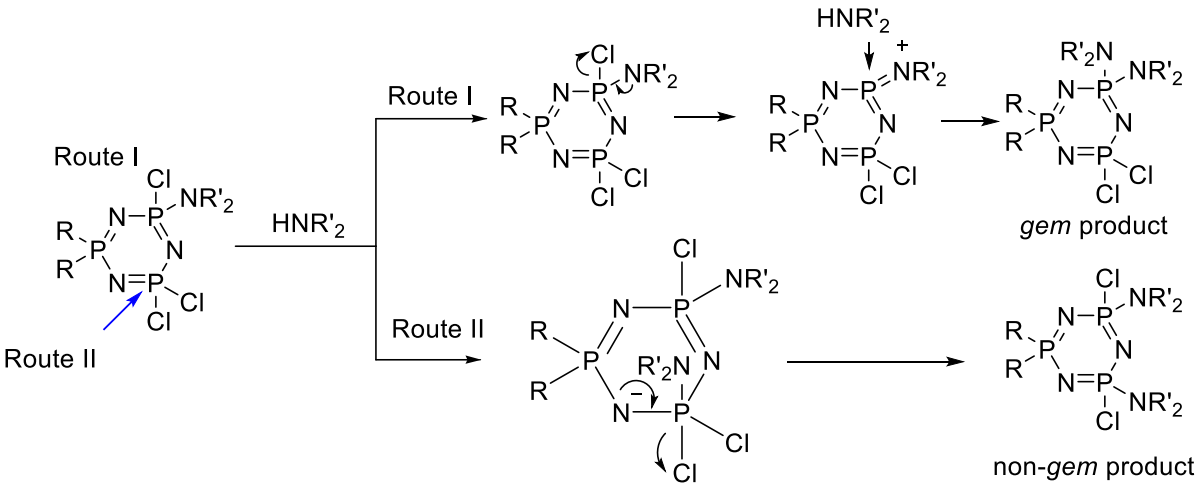

Scheme 2-5. Possible reaction mechanisms for Route I: *gem* product formation and Route II: non-*gem* product formation

The aminolysis of *gem*-$N_3P_3Cl_4R_2$ type cyclophosphazene derivatives with the highly sterically demanding dibenzylamine. Secondary amines are expected to follow a non-*gem* pathway in the reactions with HCCP. Although this rule is largely valid, it was confirmed that bulky dibenzylamine can give *gem* products depending on the basicity of the R group. The steric demands of certain of these derivatives can lead to a debenzylation reaction to relieve excess steric strain.

Substitution reaction of $N_3P_3Cl_4R_2$ (**13-1**) with other *sec*-amines, such as dimethylamine and pyrrolidine, were also investigated.[13] The relative amounts of isomeric products, *gem* and non-*gem*/*trans* or *cis*, was established quantitatively from the ^{31}P NMR spectra of the reaction mixtures. Although secondary amines generally follow a non-*gem* pathway in the reactions with HCCP, the reactions of two different secondary amines with *spiro*- and *gem*-$N_3P_3Cl_4R_2$ (R = $OCH_2CH_2CH_2NH$, NHPh, $NHBu^t$) derivatives lead to the formation of *gem* products.

In the current investigation, the aminolysis reactions of these two amines resulted in the formation of the *gem* and/or non-*gem* isomer in different ratios, depending on the basicity of the starting compound (Table 2-3). In the reactions of **13-1c** with the amines, pyrrolidine gave again only non-*gem*/*trans* (**13-4c**, 63%) and *cis* (**13-5c**, 37%) derivatives, whereas a small amount of *gem* isomer (**13-3c**, 12%) in addition to the non-*gem/trans* (**13-4c**, 47%) and *cis* (**13-5c**, 31%) isomers are formed in the reaction with $HNMe_2$. Compound **13-1e** gave the *gem* isomer (**13-3e**, 65%) with $HNMe_2$ in an approximately 22 : 1 ratio in comparison to the non-*gem* isomers (**13-4e** or **13-5e**, 3%), whereas with pyrrolidine both *gem* (**13-3e**,

57%) and non-*gem* (**13-4e** or **13-5e**, 14%) isomers were formed, albeit in a ratio of about 4 : 1. On the other hand, **13-1d** and **13-1f** with the corresponding amines gave the *gem* products (*gem*/non-*gem* ratios for dimethylamine 3 : 1 and 6 : 1, respectively, and *gem*/non-*gem* ratios for pyrrolidine 2.5 : 1 and 4 : 1, respectively).

Table 2-3. Aminolysis of $N_3P_3R_2Cl_4$ (**13-1**) with $HNMe_2$ and pyrrolidine

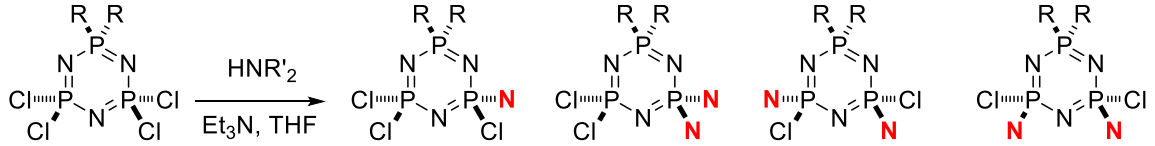

13-1 **13-2**, mono- **13-3**, *gem* **13-4**, non-*gem*/*trans* **13-5**, non-*gem*/*cis*

		$HNMe_2$ (4.5 eq.)			
	13-1 (R)				
a	$-OCH_2CF_2CF_2CH_2O-$	-	-	59	35
b	SPh)	10	-	56	34
c	$-OCH_2CH_2CH_2O-$	-	12	47	31
d	NHPh	47	38	7	6
e	$-OCH_2Ch_2CH_2NH-$	23	65	3 (**4** and **5**)	
f	NH^tBu	43	45	4	3

		$HN(CH_2)_4$ (4.5 eq.)			
	13-1 (R)				
a	$-OCH_2CF_2CF_2CH_2O-$	13	-	46	41
b	SPh)	21	-	48	30
c	$-OCH_2CH_2CH_2O-$	-	-	63	37
d	NHPh	36	35	9	6
e	$-OCH_2Ch_2CH_2NH-$	23	57	14 (**4** and **5**)	
f	NH^tBu	45	43	7	3

It is likely that a dissociative mechanism, S_N1, would be preferred to the bimolecular mechanism, whereas S_N2 yielding the *gem* product increases in the case of substituents such as anilino and *tert*-butylamino groups, which supply electrons to the cyclophosphazene ring. The decrease in formal positive charge on the cyclophosphazene starting material decreases its electrophilic character to render the bimolecular pathway less favorable energetically. Additionally, the increased negative charge will lower the activation energy of the dissociative process by stabilizing the positively charged phosphorus atom in the intermediate. The electron-supplying properties of the R groups (R = NHPh (**13-1d**), $OCH_2CH_2CH_2NH$ (**13-1e**), $NHBu^t$ (**13-1f**)) make the *gem*-disubstituted starting materials less reactive toward nucleophiles compared to the other R groups (R = $OCH_2(CF_2)_2CH_2O$ (**13-1a**), SPh (**13-1b**),

$OCH_2CH_2CH_2O$ (**13-1c**)). Hence, the yield of mono substitution products (**13-2d** (47%) and **13-2f** (43%) for dimethylamine; **13-2d** (36%) and **13-2f** (45%) for pyrrolidine) is quite high. In the non-*gem* pathways, stereoselectivity was also observed, and it is expected that steric requirements will favor a *trans* disposition of bulky groups.

Substitution reaction of $N_3P_3Cl_4R_2$ (**14-1**) [R = Cl (**14-1a**); ($OCH_2(CF_2)_2CH_2O$) (**14-1b**); ($OCH_2CH_2CH_2O$) (**14-1c**); NHPh (**14-1d**); ($OCH_2CH_2CH_2NH$) (**14-1e**) and $NHBu^t$ (**14-1f**)] with 1,3-propanediol in THF solution at 1 : 1 mole ratio in the presence of two different bases, NaH and Et_3N, was also investigated (Table 2-4).[14] The ratio of isomeric products, *spiro*- and *ansa*- were established quantitatively from the ^{31}P NMR spectra of the reaction mixtures. Although the ratio of the *ansa*-product decreased with the increase of the electron releasing capacity of R_2 group, it was formed in all the reactions in which the sodium salt of diol was used.

It was found that the ratio of *spiro*-product increased as the electron releasing capacity of R_2 groups substituted on cyclophosphazene ring increased. Furthermore, NaH/THF system was more preferable than Et_3N/THF system for the reactions of cyclophosphazene derivatives with diols in terms of reaction efficiency.

The reaction of HCCP with 1,3-propanediol predominantly gave *spiro*-derivatives in the presence of Et_3N. When disodium salts of 1,3-propanediol are used, ratio of *ansa*-derivatives significantly increases. The electronic and steric properties of the substituents on the cyclophosphazene ring also played an important role in the formation of *spiro*-isomers which is formed with *gem* pathway and *ansa*-isomers which is formed with non-*gem* pathway.

In the reaction of disodium salts of 1,3-propanediol (NaH was used) with the compounds **14-1d** – **f** [R = NHPh, $NH(CH_2)_3O$ and $NHBu^t$] the *spiro* compounds (**14-3d – f**) formed predominantly than the *ansa* compounds (**14-2d** – **f**). In contrast, the reaction with compounds **14-1b** and **14-1c** [R = $OCH_2CF_2CF_2CH_2O$ and $O(CH_2)_3O$] gave the *ansa* isomers (**14-2b** and **14-2c**) in significant quantity. Moreover, the reaction of compound **14-1a** with disodium salts of 1,3-propanediol gave *ansa* isomer (**14-2a**, ca. 46%) which about two times more likely than the *spiro* isomer (**14-3a**, ca. 26%). Comparing the results with the reaction of **14-1** with *sec*-amines, there are differences in the reactivity of the starting cyclophosphazene compounds **14-1a** – **f** because of electronic and steric effects of R_2 group on cyclophosphazene ring. The whole of the starting compounds **14-1a** – **c** reacted and their reactions led to formation of di*spiro*-1,3-propanedioxy products (**14-4a** – **c**). However, the ratio of **14-1d** – **f** (**14-1d**, 19%; **14-1e**, 23%; **14-1f**, 20%) remained unchanged in the reaction medium under the same reaction conditions. It is likely that increase the basicity of the R group [R = NHPh, $NH(CH_2)_3O$ and

Table 2-4. Reaction of $N_3P_3Cl_4R_2$ with 1,3-propanediol

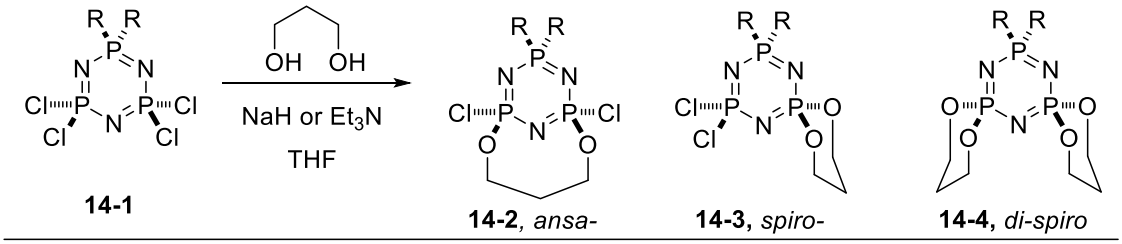

14-1 **14-2**, *ansa*- **14-3**, *spiro*- **14-4**, *di-spiro*

		Ratio/%					
		NaH			Et_3N		
	R	*ansa*-	*spiro*-	*di-spiro*	*ansa*-	*spiro*-	*di-spiro*
14-1a	Cl	46	26	24	-	64	-
14-1b	$-OCH_2CF_2CF_2CH_2O-$	25	68	7	-	8	-
14-1c	$-OCH_2CH_2CH_2O-$	16	81	3	-	7	-
14-1d	NHPh	5	76	-	-	13	-
14-1e	$-OCH_2CH_2CH_2NH-$	8	69	-	-	6	-
14-1f	NH^tBu	3	77	-	-	1	-

$NHBu^t$] causes the starting compound to be less reactive to nucleophiles. Hence, *ansa* isomer (**14-2d**, ca. 5%; **14-2e**, ca. 8%; **14-2f**, ca. 3%) formed as minor products compared to *spiro* isomer (**14-3d**, ca. 76%; **14-3e**, ca. 69%; **14-3f**, ca. 77%). Compound **14-1b** has a very low electron-supplying capacity because of low basicity of the *spiro*-[$OCH_2CF_2CF_2CH_2O$] moiety. Therefore, 1,3-propanediol/NaH in THF gave *ansa* isomer (**14-2b**, ca. 25%). Compound **14-1c** (R = *spiro*-[$O(CH_2)_3O$]) also formed *ansa* isomer (**14-2c**) in 16% yield.

On the other hand, when Et_3N was used as a base, most of the starting materials **14-1b** – **f** remained unchanged under reflux conditions for 24 h. In these reactions, *ansa* isomers were not detected and small amount of *spiro* isomers (**14-3b**, 8%; **14-3c**, 7%; **14-3d**, 13%; **14-3e**, 6%; **14-3f**, 1%) were obtained. The reaction of HCCP with 1,3-propanediol/Et_3N afforded *spiro* isomer **14-3a** in 64% yield.

The reaction of the *N,N-spiro* bridged octachlorobis(cyclotriphosphazene), {$N_3P_3Cl_4$[br-$N(CH_2)_5Me]_2N_3P_3Cl_4$} (**15-1**), in three stoichiometries (1 : 0.7, 1 : 2, and 1 : 4) with the disodium salt of 1,3-propanediol in THF at room temperature produced seven products, rearranged derivatives (**15-2**, **15-4** and **15-5**) in which the central four membered cyclotriphosphazene ring expanded into a six-membered ring, and the normal substituted derivatives (**15-3**, **15-6** – **8**) (Scheme 2-6).[15]

^{31}P NMR data for compounds **15-2**, **15-3**, **15-5** – **8** are shown in Table 2-5.

Table 2-5. ^{31}P NMR data for compounds **15-2**, **15-3**, **15-5** – **8**

		PCl_2	PCl(NR)	P(NR)(OR)	P(OO)*spiro*	P(NN)*spiro*
15-2	AMX, ABX	25.53 20.78, 20.11	28.28	15.14	-	8.77
15-3	AMX, A_2X	29.28 25.43	-	-	9.49	4.84, 0..65
15-5	AMX, ABX	25.20 23.86	28.34	15.38	6.61	13.04
15-6	AMX	29.13	-	-	9.55	4.85
15-7	AMX	28.85	-	-	9.82	5.10
15-8	A_2X	-	-	-	15.48	8.75

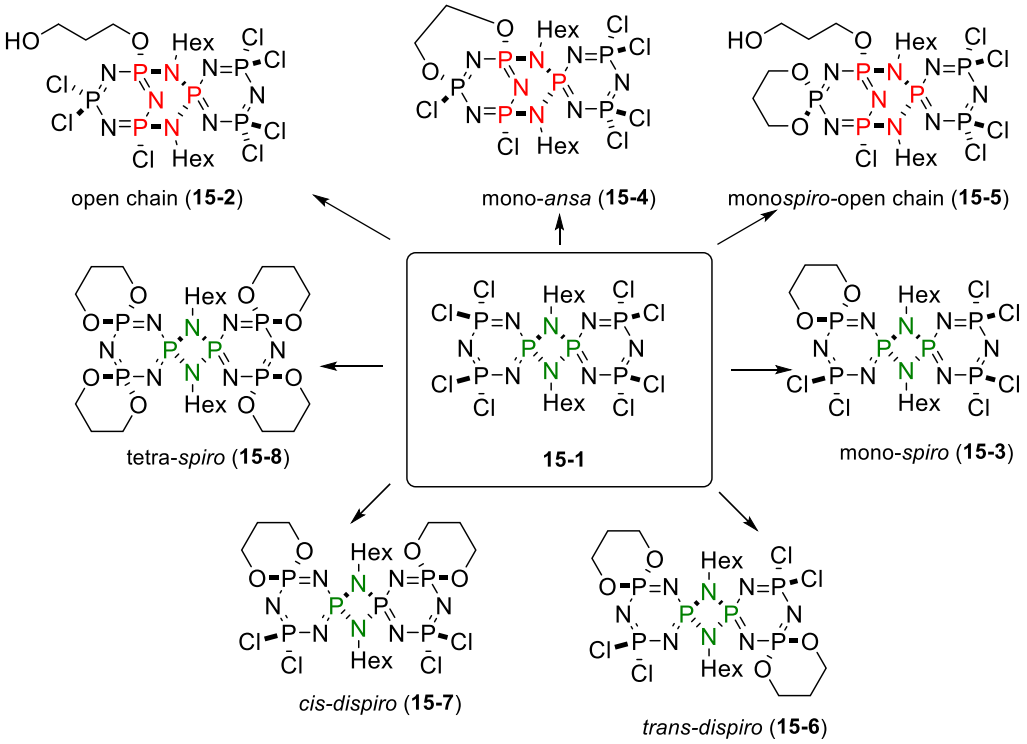

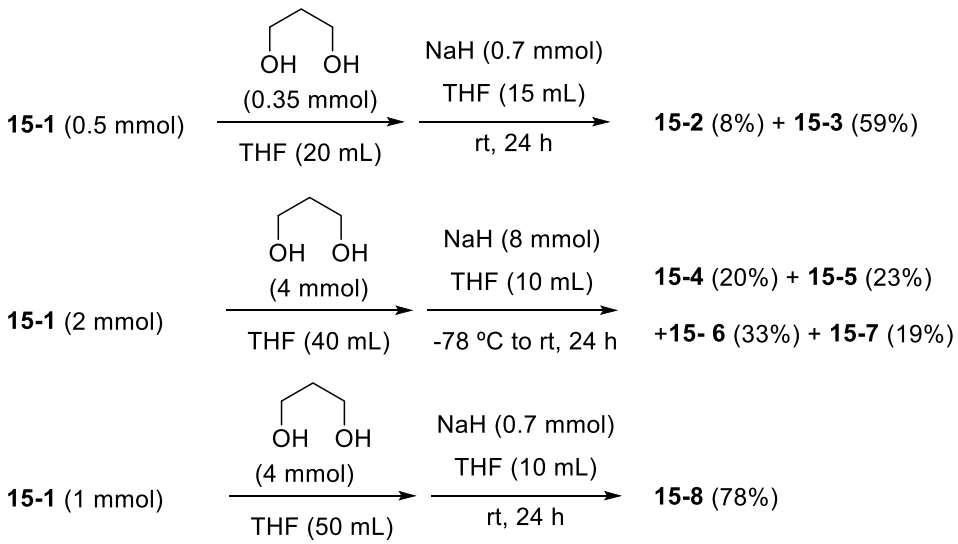

Scheme 2-6. Reaction of **15-1** with the disodium salt of 1,3-propanediol

A plausible mechanism for the formation of compounds **15-2** and **15-5** is described in Scheme 2-7.

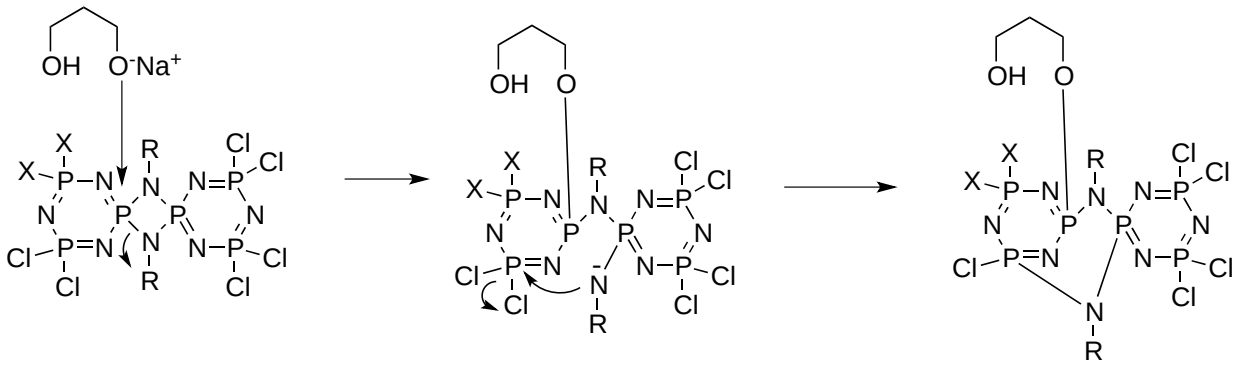

Scheme 2-7. A proposed mechanism for the formation of compounds **15-2** and **15-5**

3. NEW AND PRACTICAL APPLICATIONS OF FUNCTIONALIZED CYCLOTRIPHOSPHAZEN CORE-BASED MATERIALS

3-1. New Applications of Cyclotriphosphazene Materials

3-1-1. Hosts (channels) for molecular motors and other molecules

Tris(*o*-phenylene)cyclotriphosphazene (TPP) (Figure 3-1), which can easily prepared from HCCP and 3 equivalents of catechol in the presence of Na_2CO_3 in boiling THF, makes a crystal of ca. 50 pm-thick layers with the neighboring layers rotated by 60°. The layers have voids that are superimposed to form channels and located about 110 pm apart in a triangular arrangement. The staggered layers make hexagonal channels when viewed from upwards. The internal diameter is ca. 50 pm. The channel-to-channel spacing can be expanded by as much as 10% when the channels are filled with guest molecules (Figure 3-2).[16]

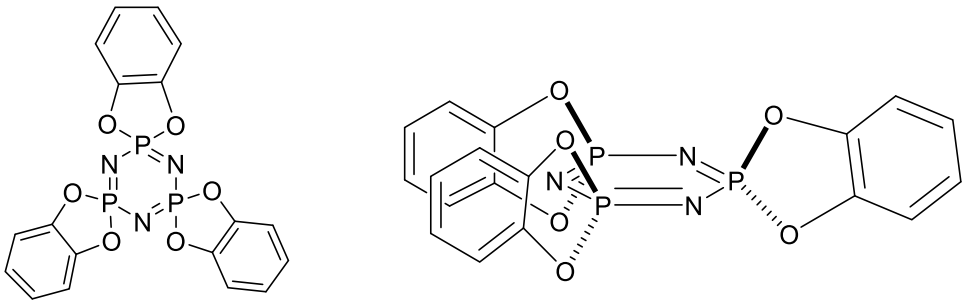

TPP

Figure 3-1. Tris(*o*-phenylene)cyclotriphosphazene (TPP)

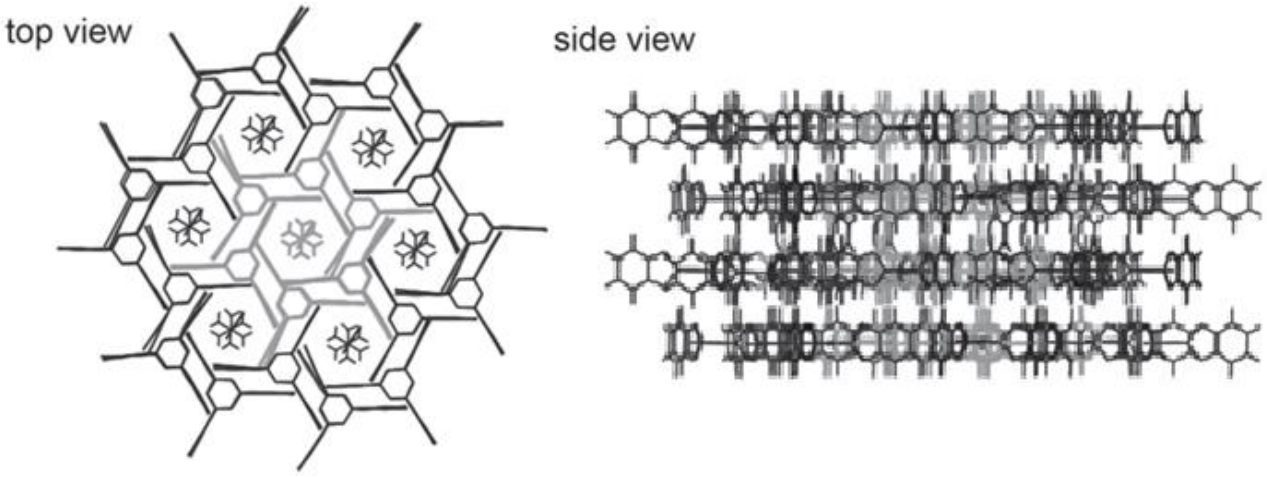

Figure 3-2. The seven-channel model of TPP lattice used in the calculations of rotational potential. These figure were originally printed in lit. 16.

Structure of the molecular rotors and method for the inclusion of the rotors in TPP-d_{12} are illustrated in Scheme 3-1.

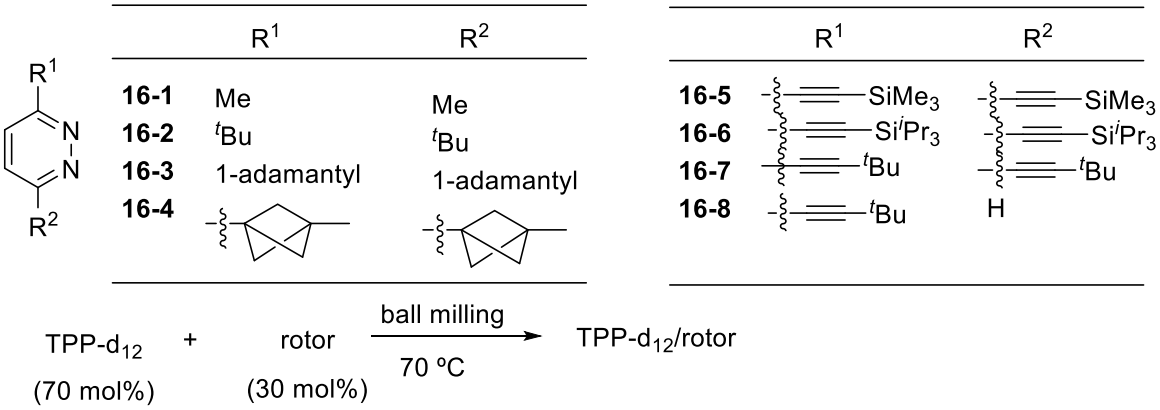

Scheme 3-1. Structure of molecular rotors and including complexes

Since size of the end group (Si^iPr_3) in **16-6** is so huge, **16-6** can not enter into TPP-d_{12} channels, which was confirmed that the ^{13}C CP MAS NMR spectrum of 30% **16-6**@TPP-d_{12} did not contain TPP peaks and was identical to that of **16-6**. The other seven dipolar rotor molecules (**16-1** – **5**, **16-7**, **16-8**) form hexagonal bulk inclusion compounds.

The authors found that (1) though the pyridazine is a small, it makes dipolar rotor suitable for use in TPP; (2) the pyridazine rotational barrier depends on the nature of R^1 and R^2; (3) competition between antiferroelectric intrachannel and ferroelectric interchannel rotor is exist.

The authors also synthesized five double pyridazine molecular rotors **17-1** – **5** having a different intra- and intermolecular dipole-dipole spacing (Figure 3-3).[17] All rotor molecules formed bulk inclusions with TPP host (Scheme 3-2).

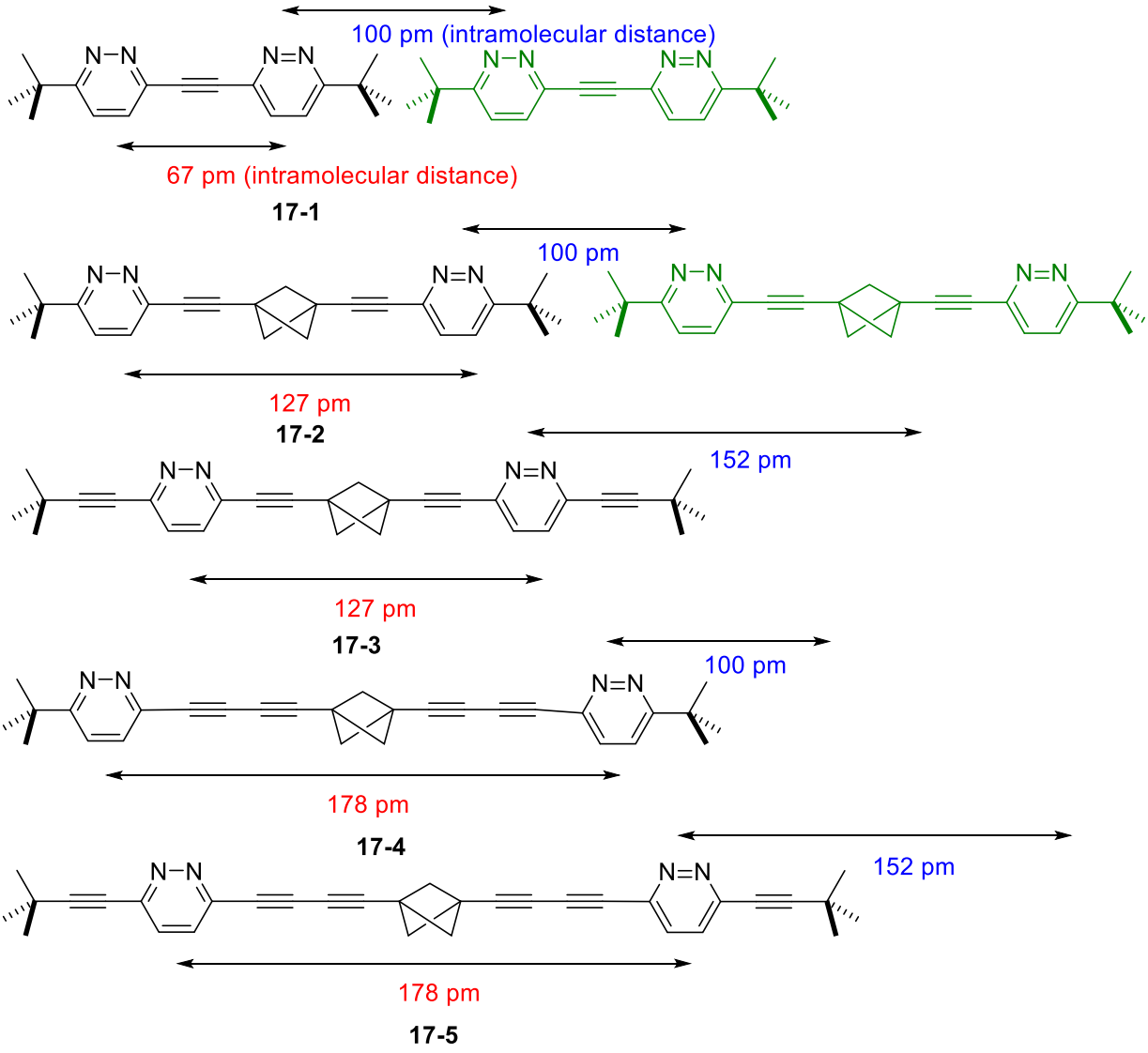

Figure 3-3. Structures of the guest molecules **17-1** – **5**. Intramolecular and intermolecular distances between the pyridazine rings are shown in red and blue letters.

Dielectric spectroscopy, fitted to a pair of nine-state models that accounted for interactions of neighboring dipoles at either an aligned or opposed possible orientation of the local threefold dipole rotation potentials within a channel of the TPP host, indicated that dipoles preferentially populates a subset of low-energy configurations, determined from strength of dipole-dipole interaction at the 100 to 200 K scale. They also revealed that pyridazine derivatives having two ethynyl substituents in both 3- and 6-positions have slightly higher rotational barriers (3.2 − 3.5 kcal/mol) than those carrying one ethynyl and one *tert*-butyl group (1.9 − 3.0 kcal/mol).

The authors examined the fluorescence anisotropy of rod-shaped guests **18-1** − **5** held inside the channels of TPP host (Figures 3-4, 3-5).[18]

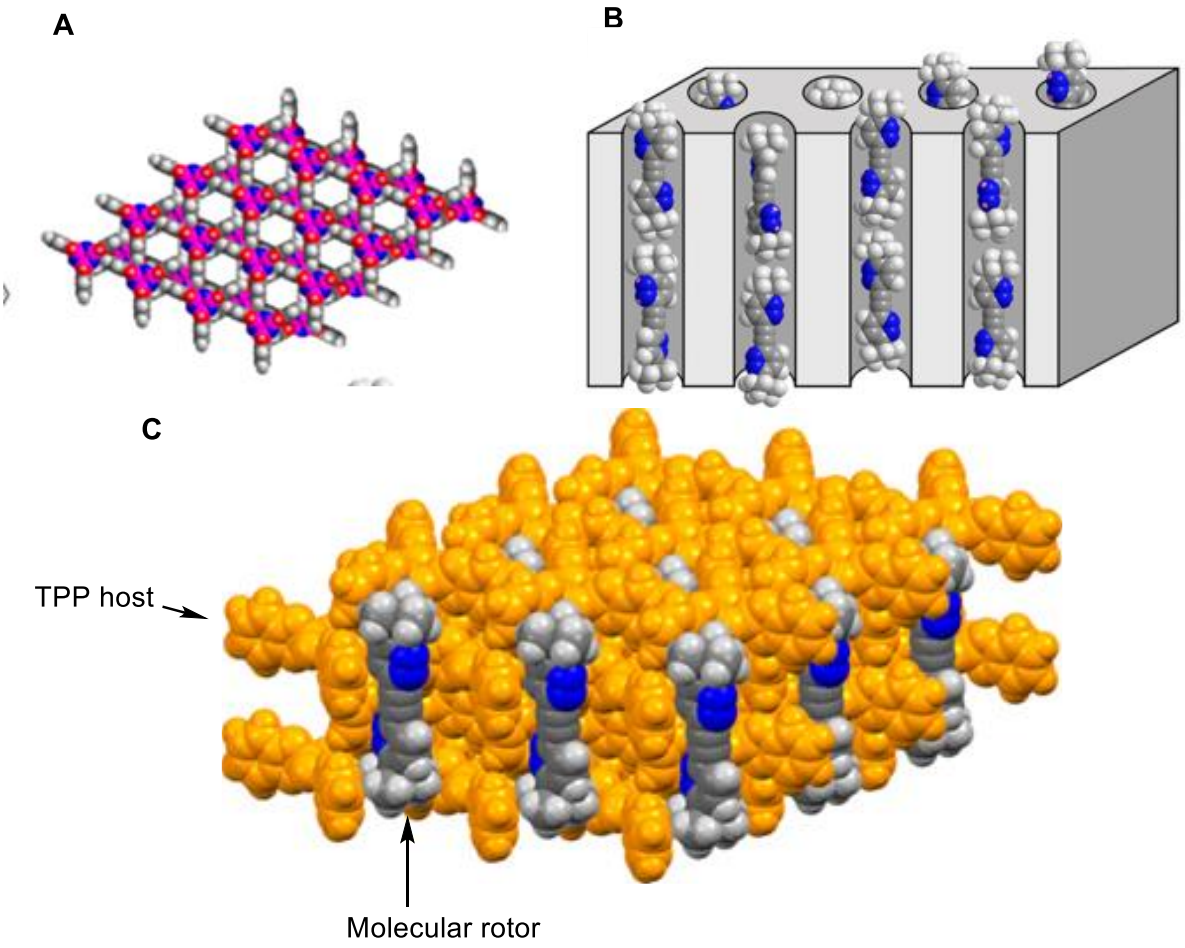

Scheme 3-2. (A) Top view of two successive layers of TPP. (B) Idealized model of molecular rotors anchored inside the TPP host. (C) Inclusion complex. These Figures were originally reported in lit. 17.

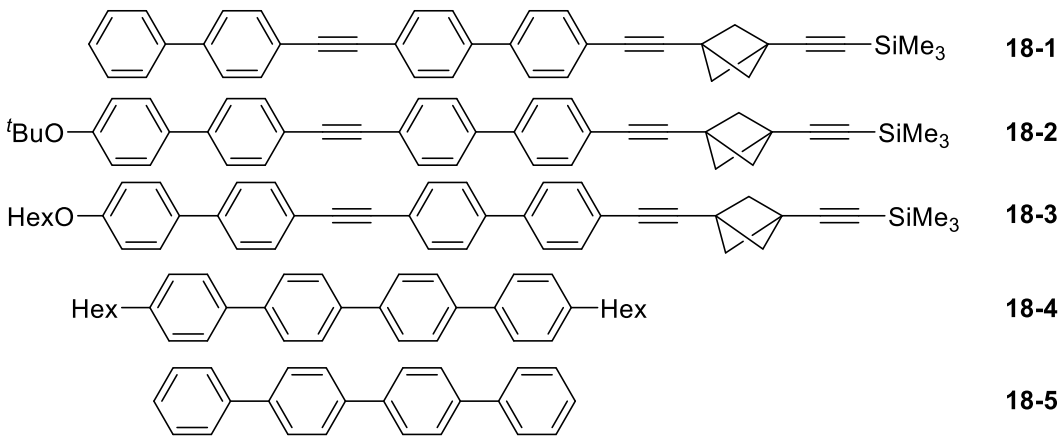

Figure 3-4. Structures of the guest molecules **18-1** – **5**

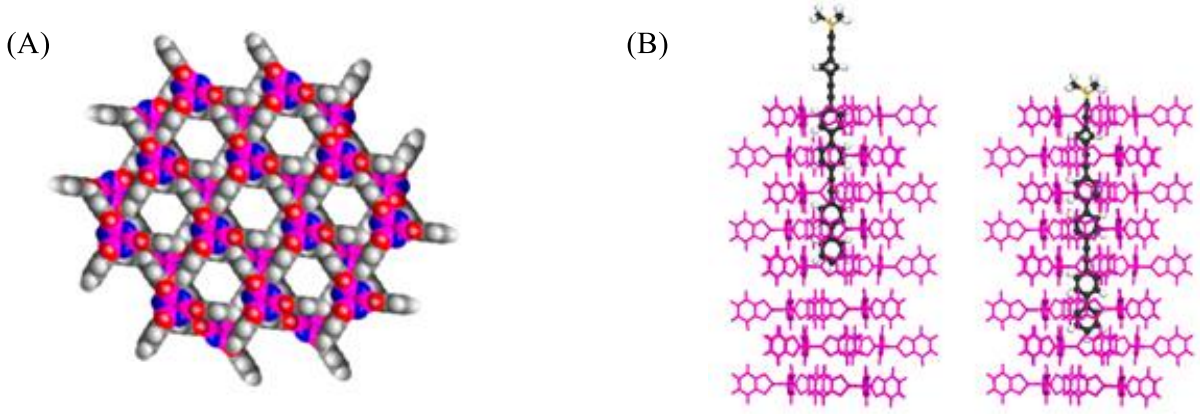

Figure 3-5. (A) Two layers of crystal viewed from above. (B) Proposed structure of **18-1**@TPP. The location of 4/5 of the guest molecules (left). The location of 1/5 of the guest molecules (right). These figures were originally drawn in lit. 18.

They reported colloidal solutions of TPP nanoparticles carrying the guest molecules as time-resolved fluorescence anisotropy studies. They pointed out that these solutions would be equally suitable for polarized transient absorption measurements. Rotation of dipolar rotators in real time and the time-resolved measurements indicated that the long axis of **18-1** − **4** is essential to immobilize them in the TPP channel (Figure 3-6).

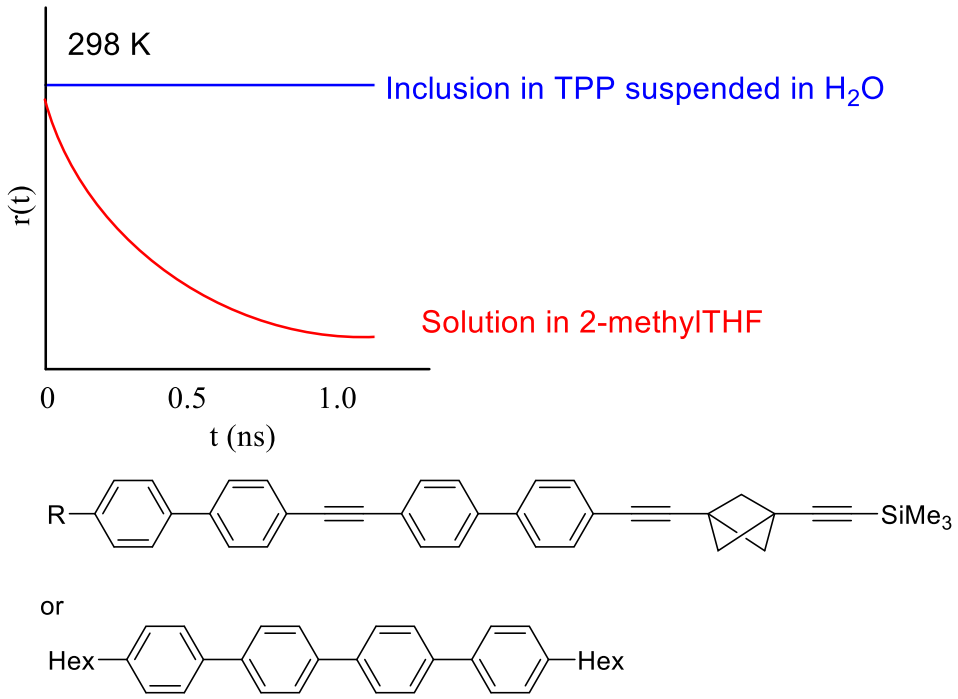

Figure 3-6. Rotation of dipolar rotators in real time and measurements of the time-resolved anisotropy decay

3-1-2. Gas storage

TPP has a honeycomb structure and can also include organic and inorganic small molecules, such as water, benzene, THF and I_2. TPP can storage gaseous compounds and intriguing electro-optical properties due to the extended π conjugated systems.[19,20] Thermodynamic (**19-1a**) and kinetic (**19-1b**) guest-free forms of TPP can be respectively obtained by sublimation under vacuum or by careful desolvation of TPP-benzene channel inclusion compound (**19-1b**·benzene). Crystals of guest-free TPP can be prepared by three-times sublimation at 175.1 ºC under vacuum (13 Pa, 0.1 mmHg).

TPP in **19-1a** resembles a three-bladed paddle wheel in which the *spiro*cyclic *o*-phenylenedioxy rings are perpendicular to the plane of the central phosphazene ring. However, the *o*-phenylenedioxy rings are bent at the bridging oxygen atoms to avoid the perpendicular symmetry plane positions of the central ring or steric hindrance. As a result, HCCP molecule is bent away from the trigonal symmetry and showed low Cs symmetry.

Crystals of guest-free **19-1b** were obtained by careful evacuation of benzene molecules in TPP·benzene complex, as reported by Sozzani.[21] TPP in **19-1b** form a hexagonal array of microporous channels about 5 Å in diameter. Each TPP occupies ca. 577 $Å^3$ of lattice volume, a 23% increase compared to the monoclinic system (468 $Å^3$) making a large empty pore. The packing efficiency of **19-1b** is 0.56 and the value is significantly lower than **19-1a** (0.69). As a result, density of **19-1b** is low (1.321 $g \cdot cm^{-3}$ vs. 1.628 $g \cdot cm^{-3}$, **19-1a**) and 25% of the volume is available to trap guest molecules (Figure 3-7).

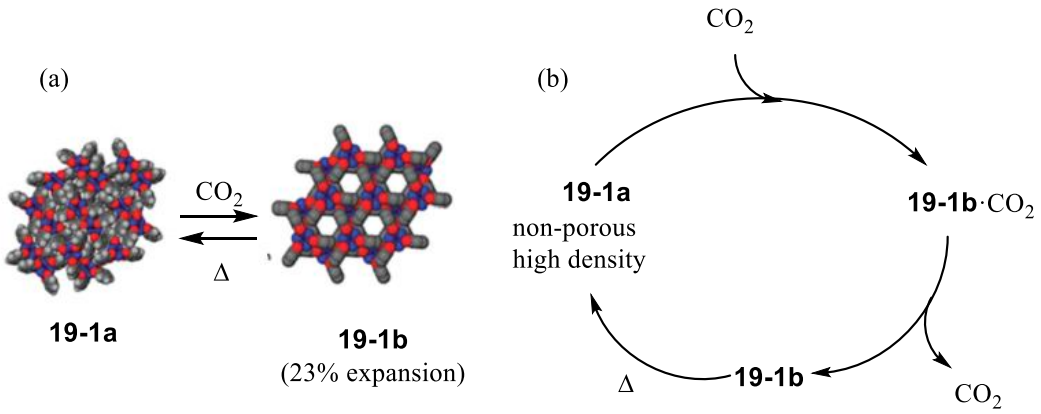

Figure 3-7. (a) Gas-induced conversion of a nonporous high density phase **19-1a** (left) to hexagonal porous phase **19-1b** (right) with moderate pressures of CO_2. (b) Schematic diagram of conversions from **19-1a** to **19-1b** by absorbing/desorbing of CO_2.

The authors demonstrated a gas-induced phase transformation of a well-known host TPP from a high density nonporous form to a low density porous form with changing from Cs to D_{3h} symmetry. Such an expedient approach may hold great implications for the polymorphic control of molecular materials and

pharmaceutical solids.

3-1-3. Gas-separation

Gas-storage by organic zeolite (OZ) is a forefront issue, and gas recognition, separation, and the absorption properties of gases by materials should be controlled. Since TPP makes a regulated large empty pore, TPP is a candidate for OZ and focused about potential applications.[22] The results show a tight dependence of the electron-donor capacity of the entire molecule on that of the free side group, resulting in some interesting implications for some aspects of OZ use: The electron-donor capacity of the side groups is tunable, allowing that the stability of the inclusion compounds of OZ and molecules is predictable (Figure 3-8). The optimized structures for the neutral and cationic species for **22-1a**, **22-3a**, and **22-4a** were almost unchanged (Figure 3-9). It was concluded that the total O/NH substitution may significantly enhance the electron-donor capacity without altering the tolerance of the host materials to the guest molecules.

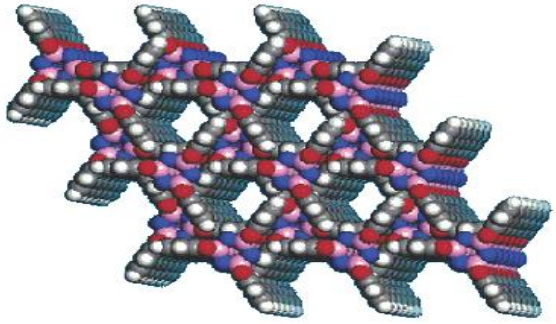

Figure 3-8. Crystal structure of TPP. This figure was originally shown in lit. 22.

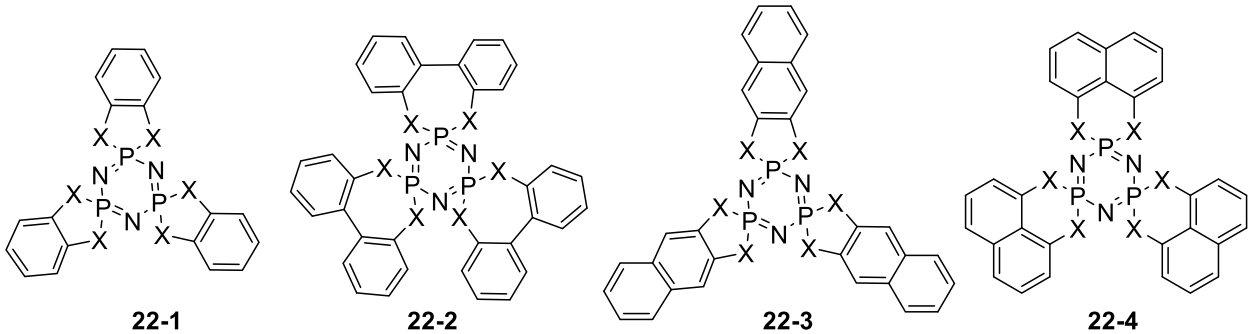

a: (X, Y) = (O, O), **b**: (X, Y) = (O, NH), **c** (X, Y) = (NH, NH)

Figure 3-9. Candidates of cyclotriphosphazenes for gas-storages

3-1-4. Nanotweezers

Architecturally designed cyclotriphosphazene derivatives constituted from perylene and glycol units were issued, and the non-covalent dispersion of cyclotriphosphazene derivatives with precise stereo isomer bearing perylene units for π-π interaction and glycol moieties for hydrophilicity was discussed. For this

purpose, a variety of perylene-cyclotriphosphazene hybrid compounds decorated with triethylene glycol monomethyl ether moieties were prepared to investigate spectroscopic, dispensability, and morphological properties study of the soluble perylene/cyclotriphosphazene/single-wall-carbon nanotubes (SWCNT) nanocomposites.[23,24]

HCCP was treated with triethylene glycol monomethyl ether (1 : 3 mole proportion)/NaH in THF at -60 °C. Isomers (non-*gem/cis*-2,4,6 (**24-1a**); non-*gem/trans*-2,4,6 (**24-1b**); *gem*-2,2,4 (**24-1c**)) were isolated (Scheme 3-3). Compound **24-1a** was allowed to react with pyrene-modified alcohol gave **23-5P** (Scheme 3-4). Similarly, di-pyrene-modified cyclotriphosphazene **23-6P** and mono-pyrene-modified cyclotriphosphazene **23-7P** were synthesized (Figure 3-10).

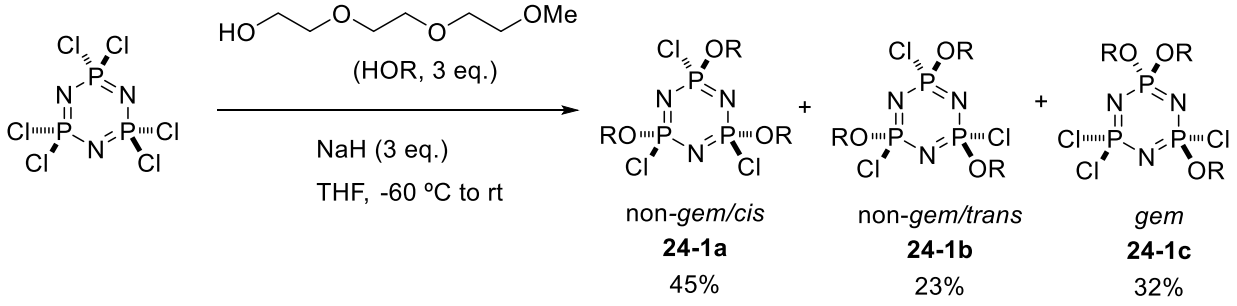

Scheme 3-3. Reaction of HCCP with triethylene glycol monomethyl ether

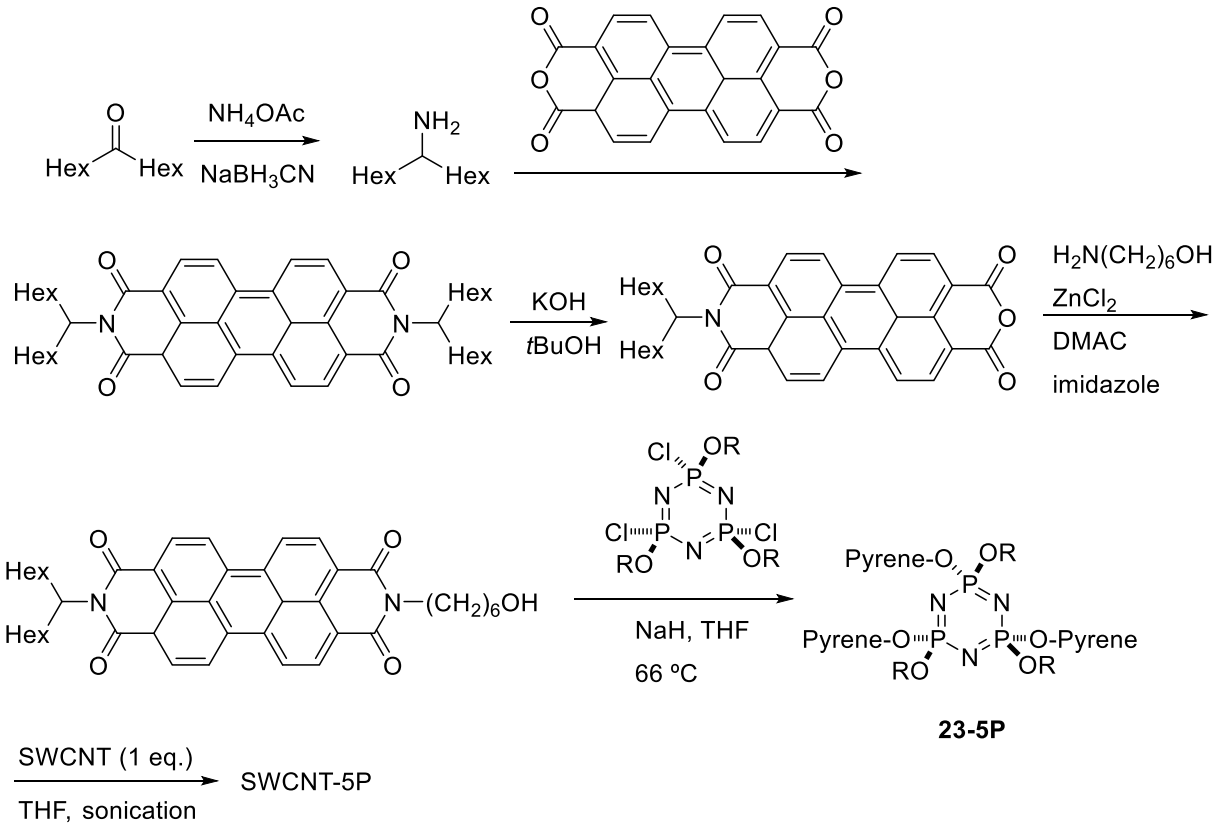

Scheme 3-4. Synthesis of pyrene-modified alcohol, cyclotriphosphazene, and its SWCNT complex

The authors established the perylene excimer on a dilute solution (5 mM) of molecule. Red-shifted emission of compound **23-5P** is observed owing to important intramolecular excimer emission among the substituted asymmetric peryleneoxy groups.

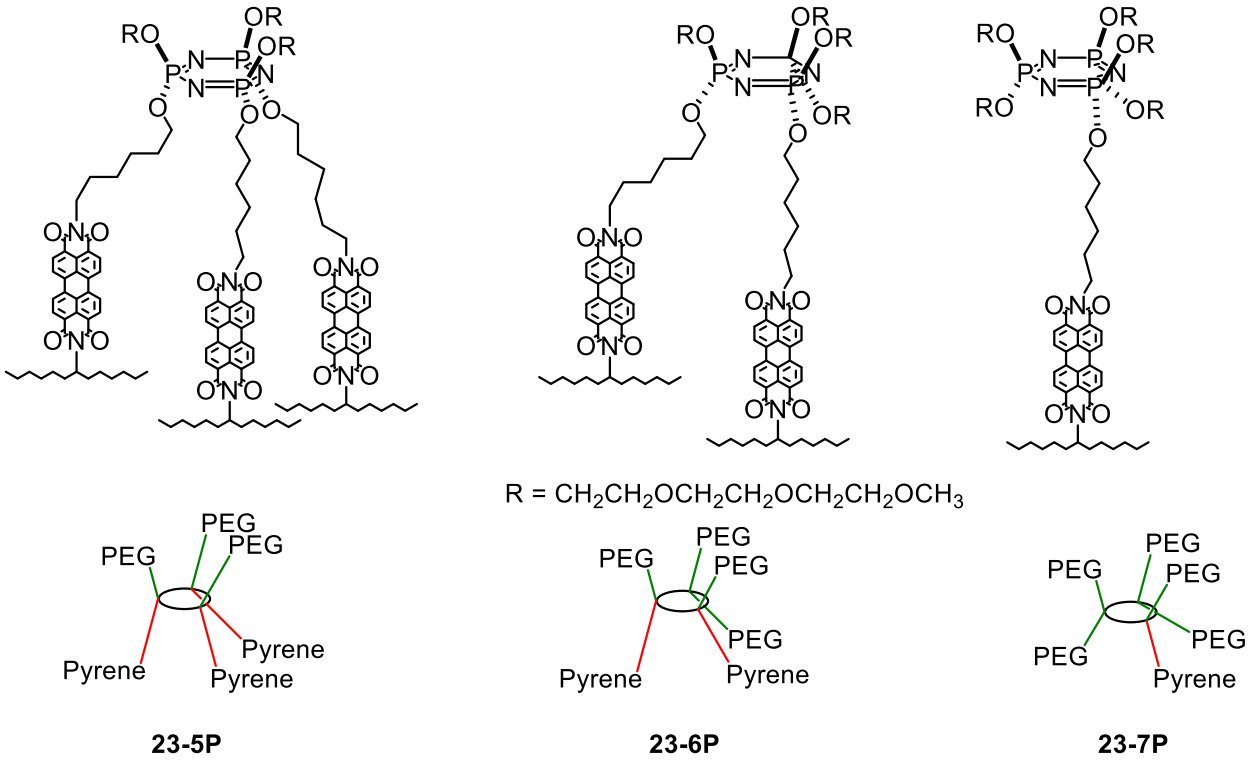

Figure 3-10. Molecular structures of glycol/perylene/ cyclotriphosphazene systems (**23-5P**, **6P**, **7P**)

Table 3-1. Photophysical features of compounds **23-5P** − **7P** and **SWCNT-23-5P** − **7P**

Compounds	Absorption wavelength (nm)	Emission wavelength (nm)
23-5P	456, 487, 521	530, 572, 623
23-6P	456, 487, 521	530, 572, 623
23-7P	456, 487, 521	530, 572, 623
SWCNT-23-5P	490, 528	535, 577, 629
SWCNT-23-6P	490, 528	535, 577
SWCNT-23-7P	490, 528	535, 577

3-1-5. Singlet Oxygen Generator

Okutan reported cyclotriphosphazene derivatives having perylenebisimide (PBI) as a singlet oxygen generator.[25] The substitution reaction of asymmetric PBI derivative with HCCP resulted in the formation of fully PBI decorated cyclotriphosphazene (**25-5**). The photophysical (UV-Vis absorption, fluorescence emission, fluorescence lifetime, and fluorescence quantum yield) and photochemical (singlet

oxygen generation and photostability) properties of this conjugate were investigated as heavy atom free triplet photosensitizers. The singlet oxygen quantum yield of **25-5** was 0.86, which is good for a triplet photosensitizer.

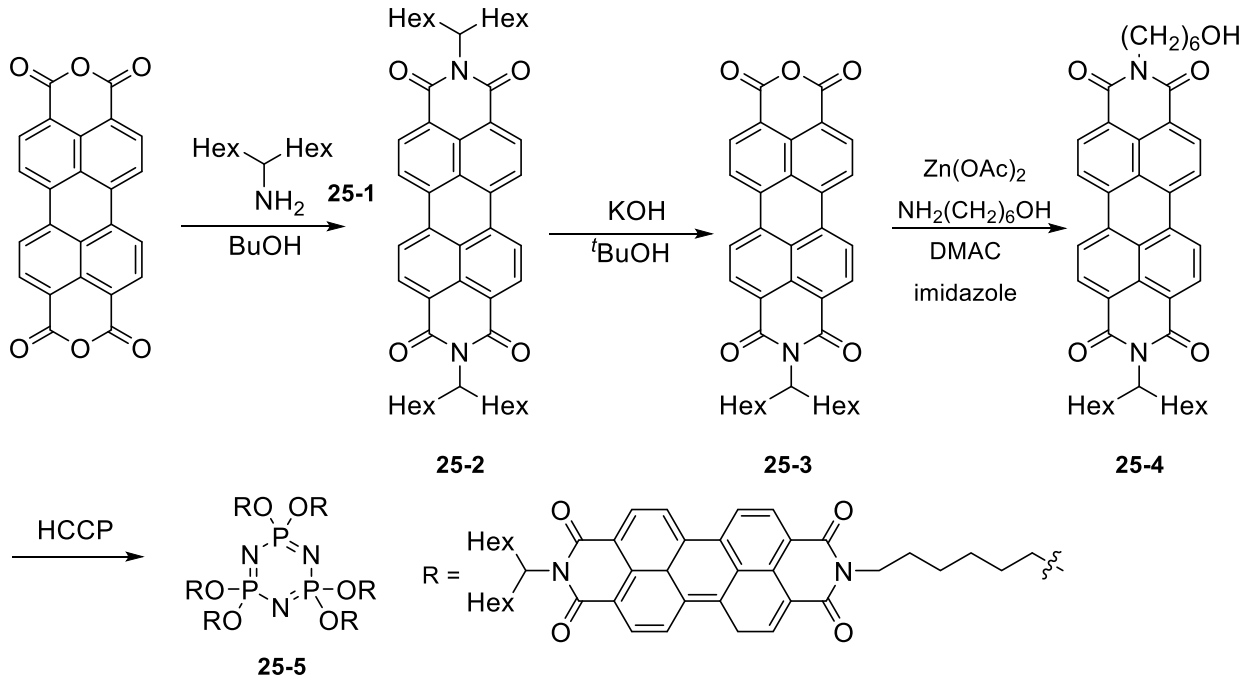

Scheme 3-5. Synthesis of perylenebisimide-cyclotriphosphazene

Two constitutionally isomers (**26-4** and **26-6**) and their cyclotriphosphazene derivatives (**26-5** and **26-7**) were designed and synthesized (Figure 3-11).[26] The thermal and photophysical properties of these compounds were examined. The geometric optimization of the constitutional isomers and their dendrimer-like derivatives, HOMO–LUMO energy levels, and molecular interactions were performed using DFT calculation at the wB97XD/6-31G(d) level (Figure 3-12). The fluorescence behaviors of **26-5** and **26-7** were evaluated for nitro-aromatic compounds. Results of measurements showed that explosive nitroaromatics efficiently quenched fluorescence emission, suggesting that these dendrimer-like cyclotriphosphazene derivatives (**26-5** and **26-7**) could be promising candidates as sensors.

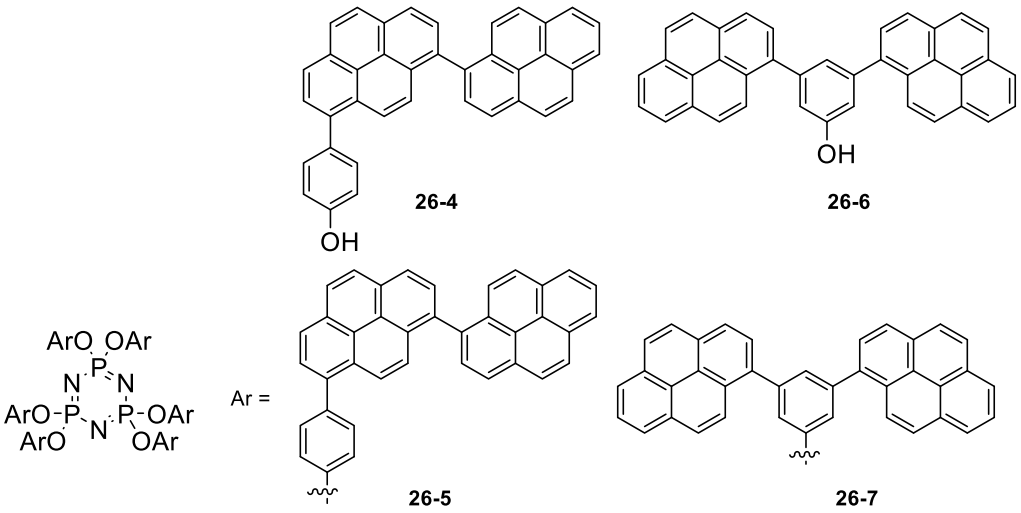

Figure 3-11. Synthesis of bis-pyrenyl-phenol dendrons

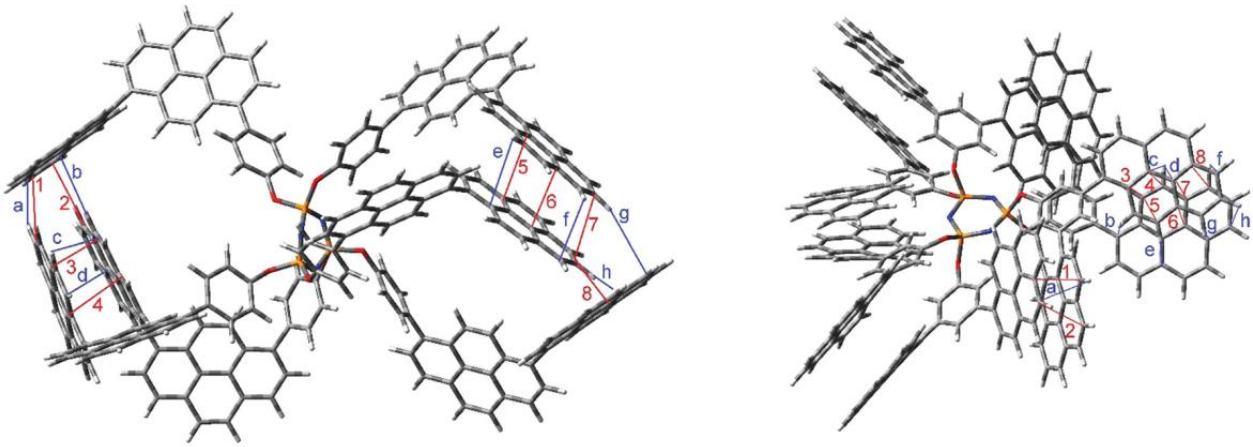

Figure 3-12. Intramolecular π–π and CH–π interactions in the structures of compounds **26-5** and **26-7**. These figures were originally drawn in lit. 26.

3-1-6. Liquid crystal

Hexakis[*p*-(dodecyloxy)phenoxy] derivative of cyclotriphosphazene **27-2** was synthesized to investigate its mesogenic properties as liquid crystals (Figure 3-13).[27] Hexakis(*p*-(Dodecyloxy)phenoxy)cyclotriphosphazene (**27-2**) was synthesized from reaction of HCCP (**27-1**) with *p*-dodecyloxyphenol. HCCP was treated with 8 equivalent of *p*-dodecyloxyphenol in THF in the presence of NaH as a base at room temperature for 24 h and then under the reflux for a day. Thermal and monomorphic behaviors of **27-2** were examined by differential scanning calorimetry, polarizing optical microscopy, and X-ray diffraction techniques to reveal that compound **27-2** has liquid crystal behavior (Figure 3-14). The three dodecyl chains on both upper and lower sides of the $-(N=P)_3-$ ring gave rise to smectic phase of calamitic mesomorphism. As a result, it can be concluded that compound **27-2** might be a suitable candidate for new liquid crystalline materials.

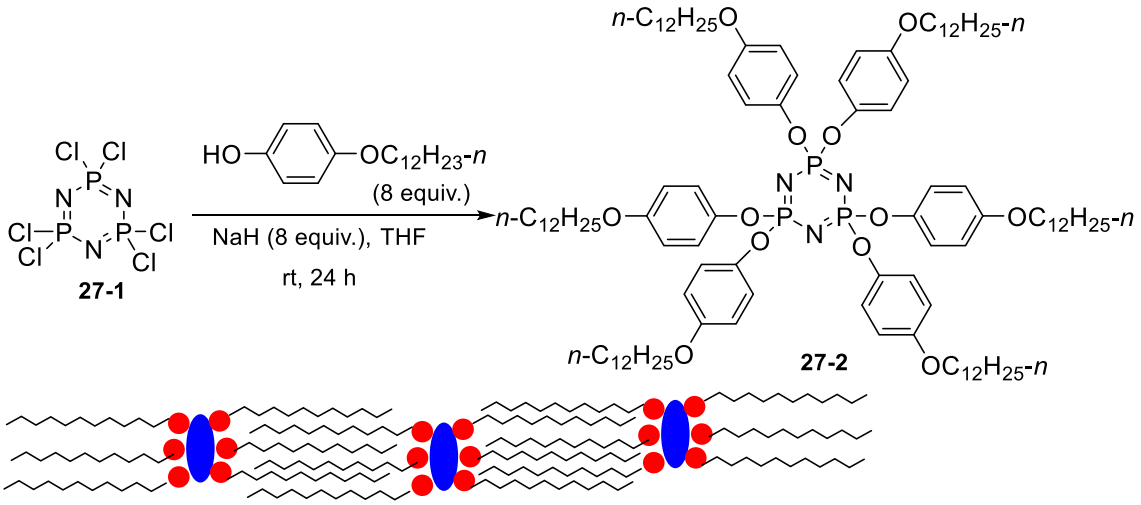

Figure 3-13. Synthesis and illustration of possible arrangement of **27-2**

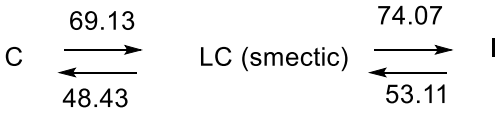

Figure 3-14. Liquid crystal phase transitions of **27-2**

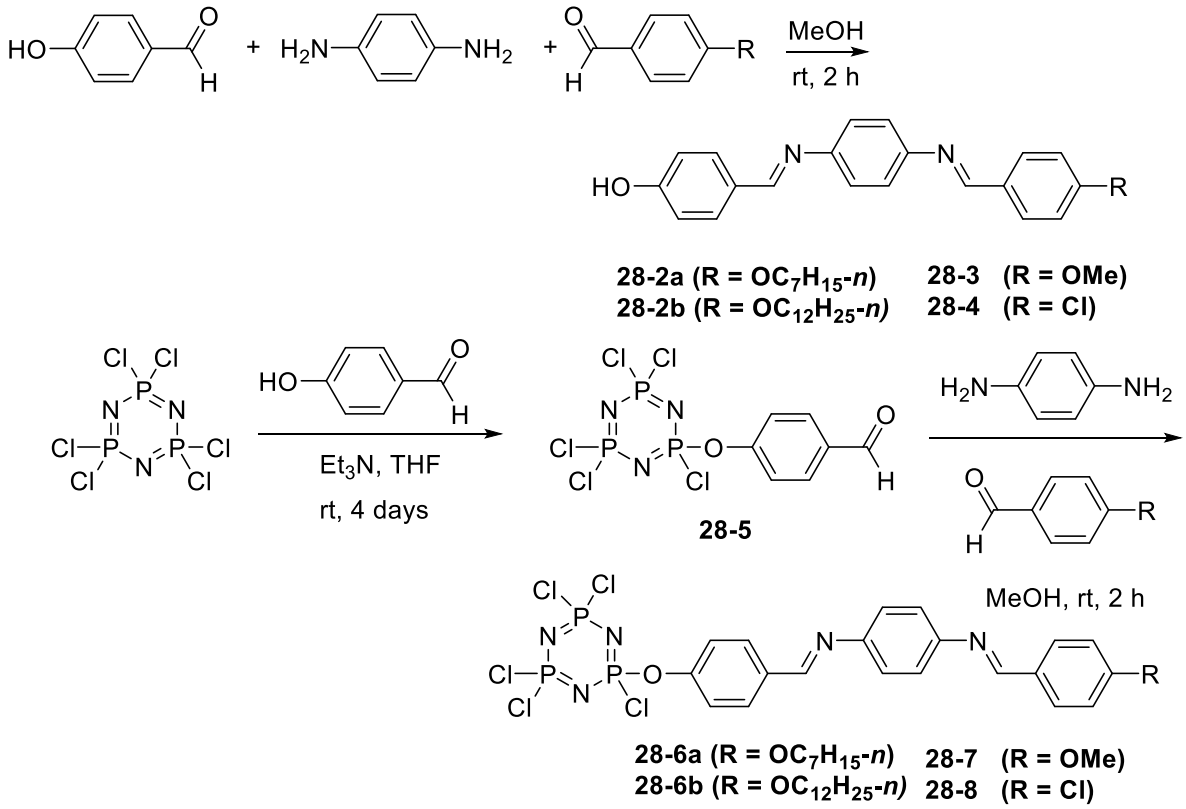

Scheme 3-6. Synthesis of Schiff bases **28-2a**, **28-2b**, **28-3**, and **28-4** and Schiff base-carrying cyclotriphosphazenes **28-6a**, **28-6b**, **28-7,** and **28-8** having four different substituents (R = heptyl, dodecyl, methoxy, and chloro)

A series of Schiff base compounds, **28-2a**, **28-2b**, **28-3**, and **28-4,** was synthesized from 4-hydroxybenzaldehyde, 1,4-phenylenediamine, and *p*-substituted benzaldehyde derivatives.[28] Similarly, reaction of 4-hydroxybenzaldehyde with HCCP gave **28-5**, which was further allowed to react with 1,4-phenylenediamine and *p*-substituted benzaldehyde derivatives to afford **28-6a**, **28-6b**, **28-7,** and **28-8** (Scheme 3-6). Their liquid crystal mesophase was observed by using polarized optical microscope to reveal that **28-2a** and **28-2b** with heptyl and dodecyl chains, respectively, exhibited smectic C phases, whereas **28-6a** showed a smectic C and nematic phases and **28-6b** showed only a nematic phase. However, compounds **28-3**, **28-4**, **28-7** and **28-8** did not show liquid crystal phases (Table 3-2).

Table 3-2. Thermal transitions of the synthesized compounds

	R	Cr ⟶	SmC ⟶	N ⟶	I ⟶	N ⟶	SmC ⟶	Cr
28-2a	OC_7H_{15}-*n*	116.05	145.25	-	-	140.95	100.27	
28-2b	$OC_{12}H_{25}$-*n*	121.16	127.51	-	-	123.07	109.68	
28-6a	OC_7H_{15}-*n*	119.04		161.39	174.81	156.90	141.96	
28-6b	$OC_{12}H_{25}$-*n*	122.30	146.58	201.73	194.70	-	111.53	

3-1-7. Ionic liquid

2,2-{1-(4-Fluorobenzyl)-2-alkyl-1,2-ethanediamino}cyclotriphosphazene derivatives with (trimethylammonium)ethoxy (**29-PzIL1a** − **2a**) and (trimethylammonium)propoxy (**29-PzIL1b** − **2b**) chains and $N(SO_2CF_3)_2^-$ counter anion were synthesized (Scheme 3-7).[29] Thermal properties of all compounds were observed by thermogravimetric analysis. These PzILs were liquid at room temperature, and used as the dielectric layer in organic field effect transistors (OFETs). The fabricated OFETs with PzILs operated in low voltage range. Though the iodide salts (**29-PzIL1** − **4**) showed excellent solubility in water, the NTf_2^- salts **29-PzIL1a** − **4a** did not soluble in water. In addition, **29-PzIL1a** − **4a** were thermally stable than **29-PzIL1** − **4.**

3-1-8. Ion receptor

Gutowska reported preparation of new single and double-lariat ether derivatives **L1** and **L2.** HCCP was treated with 3,6,9-trioxaundecane-1,11-diol to give single lariat ether MONO-ANSA and double lariat ether BIS-ANSA. **L1** and **L2** were synthesized from MONO-ANSA and BIS-ANSA precursors, respectively, by substitution of chlorine atoms with piperidine (Scheme 3-8).[30] **L1** and **L2** made complexes of different types with Ag^+ ion in MeOH and MeCN solutions. All of the stability constants were higher in the case of in MeOH than in MeCN, since MeCN is solvate Ag^+ more efficient than MeOH. **L1** made three types of complexes, *e.g.*, Ag**L1**$_2$, Ag**L1**, and Ag_2**L1**.

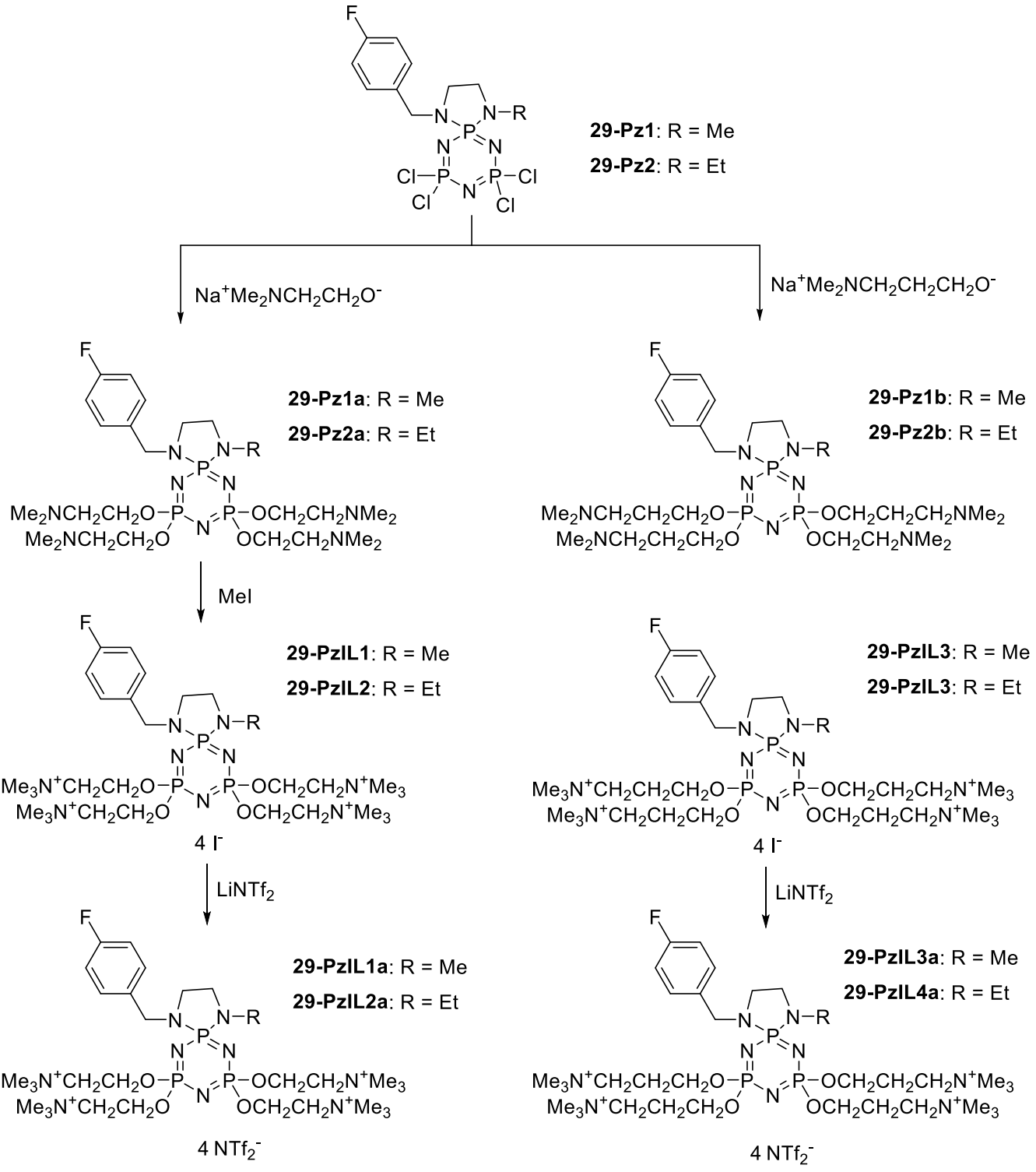

Scheme 3-7. Syntheses of the mono(4-fluorobenzyl)cyclotriphosphazene derivatives (**29-Pz1a** – **2a**, **29-Pz1b** – **2b**) and their ILs (**29-PzIL1a** – **4a**)

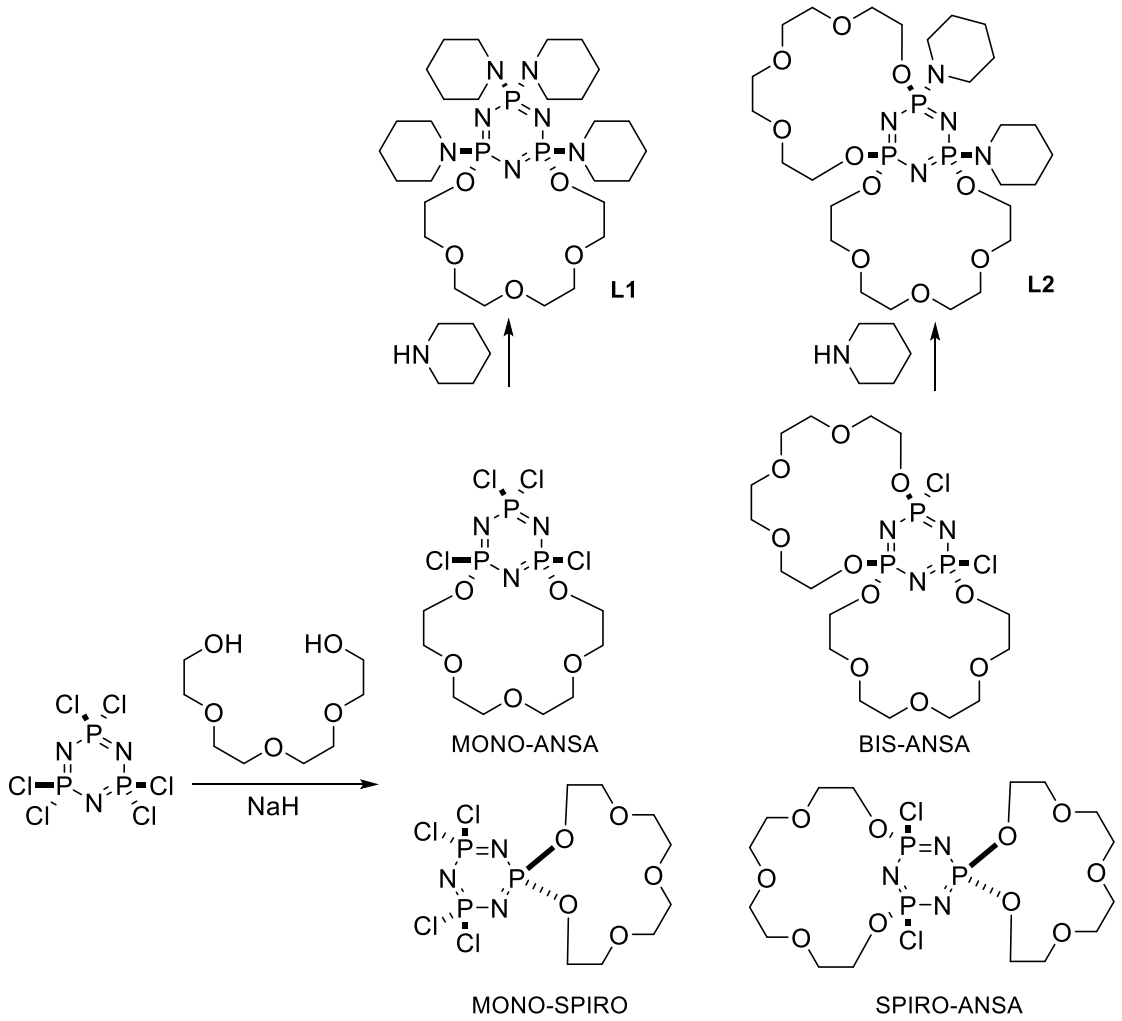

Scheme 3-8. Synthesis of ligands **L1** and **L2**

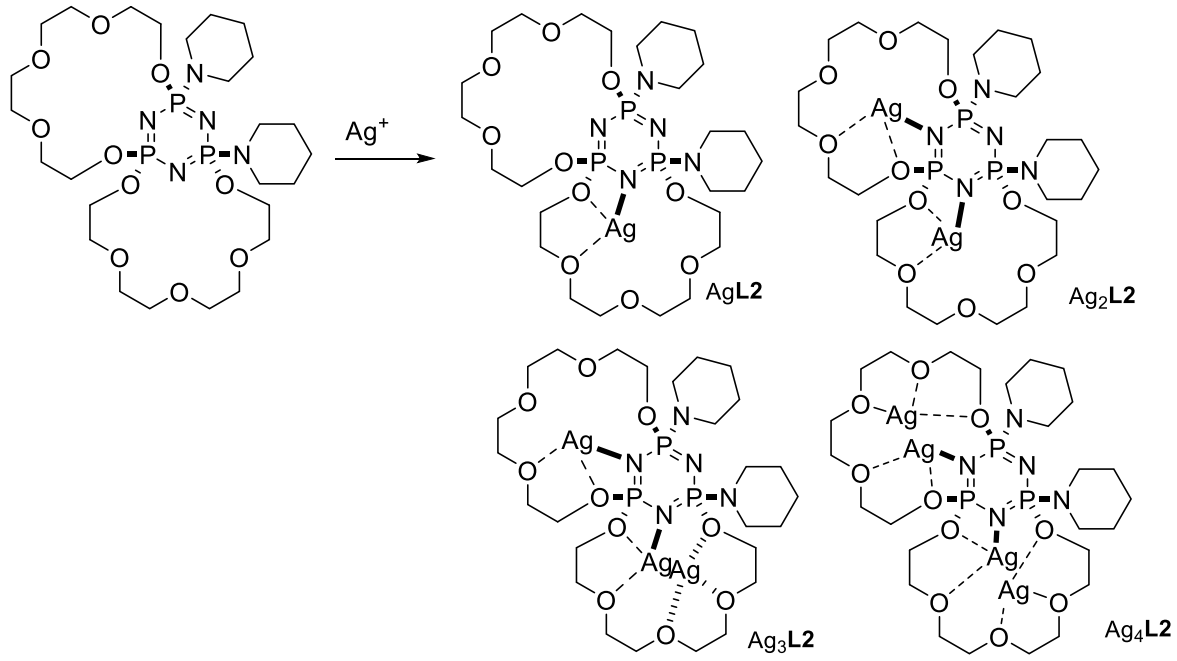

Figure 3-15. Ag^{+} binding with **L2**

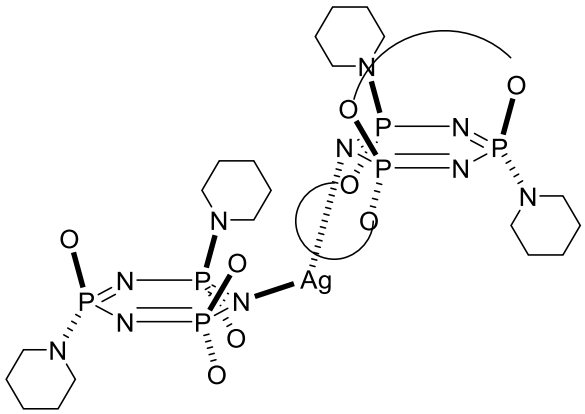

Figure 3-16. Ag^+ bound by two molecules of **L2**, Ag**L2**$_2$

The most stable complex was Ag**L1** in both solvents. On the other hand, **L2** generated more types of complexes, Ag**L2**$_2$, Ag**L2**, Ag_2**L2**, Ag_3**L2** and Ag_4**L2**. With **L2**, the most stable complex was Ag**L2**. In the case of MeOH/**L2**, the first Ag^+ is probably more trapped in the pocket of the crown moiety (higher stability constants in the case of the Ag**L2** and Ag_2**L2**). Introduction of one more Ag^+ into the crown did not allow such a close approach to the oxygen atoms. The piperidinyl substituents would promote to form Ag**L** complex. For both **L1** and **L2**, Ag^+ was trapped by the endocyclic phosphazene nitrogen atom and oxygen atoms of the crown ether moiety (Figures 3-15, 16).

3-1-9. Self-assemble polymer

Kato reported synthesis of cyclotriphosphazene-substituted diazoacetate homopolymer (polyPNDA') (PNDA' = hexaphenoxysubstituted phosphazene-containing methylene) and block copolymer, polyPNDA'-block-poly(hexyloxycarbonylmethylene) (polyPNDA'-b-polyHDA'), and self-assembly behavior of these polymers.[31] PolyPNDA'′ was synthesized by $[(\eta^3\text{-}C_3H_5)PdCl]_2/NaBPh_4$ catalyzed polymerization of diazoacetate of PNDA to afford a polymer (66% yield, Mn = 13.7 kg mol^{-1}, Mw/Mn = 1.09). Similarly, poly(hexyloxycarbonylmethylene) (polyHDA') was prepared from diazoacetate of hexyloxycarbonylmethylene (48% yield, Mn = 8.3 kg·mol^{-1}, Mw/Mn = 1.28). Block copolymer of PNDA and HDA was also prepared by sequential addition of PNDA and HDA (67% yield, Mn = 19.3 kg·mol^{-1}, Mw/Mn = 1.22).

Wide-angle X-ray diffraction analyses revealed that a hierarchically ordered, aggregated structure was formed within the polyPNDA' domain which then develops a hexagonally packed arrangement with an intercenter distance of 29 Å. Small-angle X-ray scattering and scanning transmission electron microscopy analyses revealed that a higher-ordered lamellar structure was formed by the self-assembly of the microphase-separated polyPNDA'-b-polyHDA' block copolymer (Figures 3-17, 3-18).

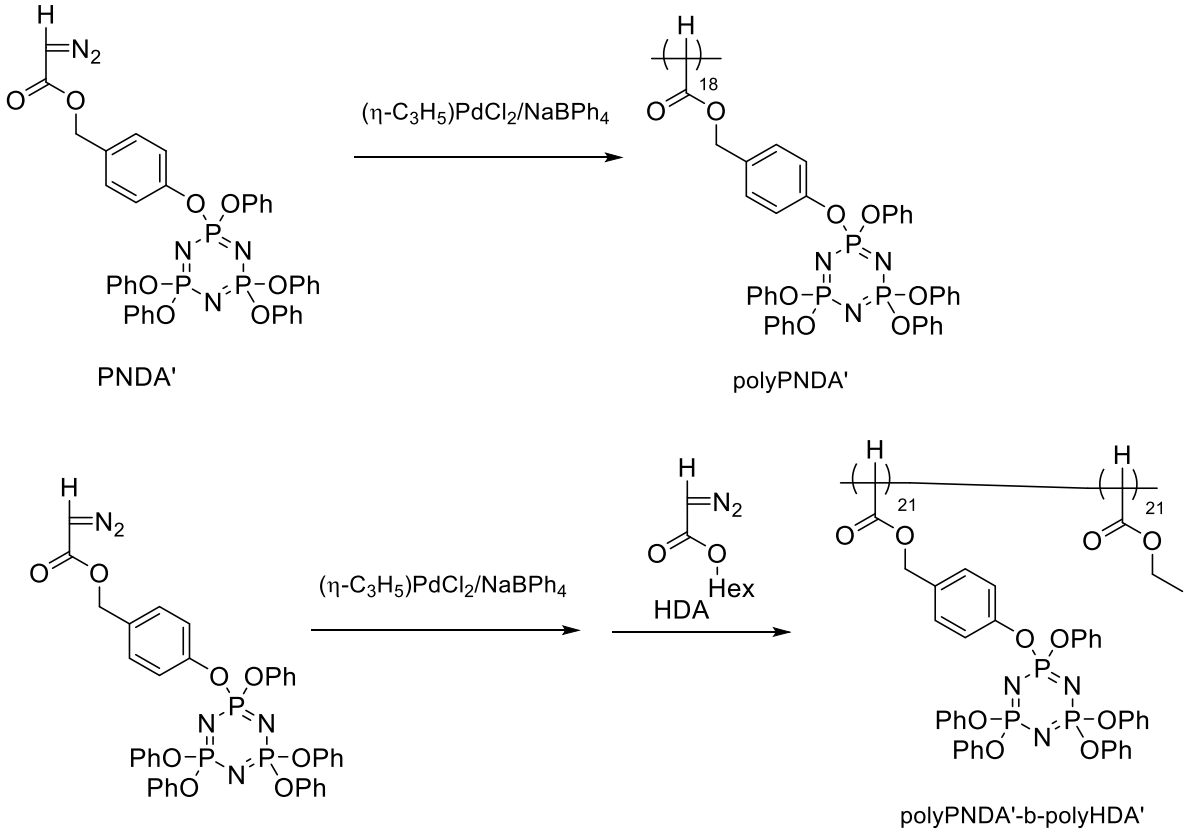

Scheme 3-9. Synthesis of polyPNDA’ and polyPNDA’-b-polyHDA’

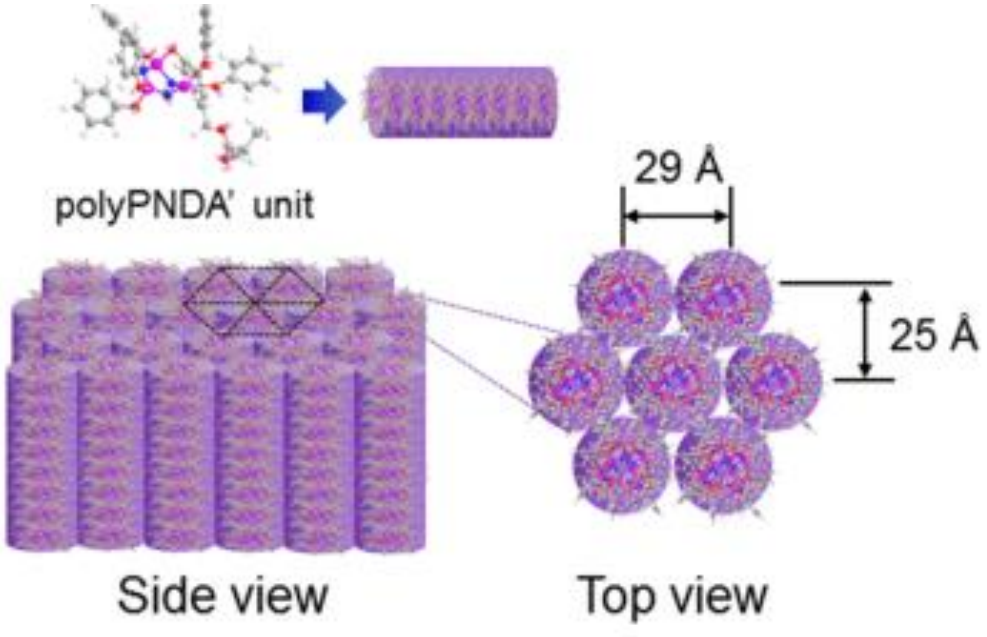

Figure 3-17. Schematic illustration of the ordered and aggregated nano-assemblies of polyPNDA’ within the homopolymer and the block copolymer polyPNDA’-b-polyHDA’. These figures were originally printed in lit. 31.

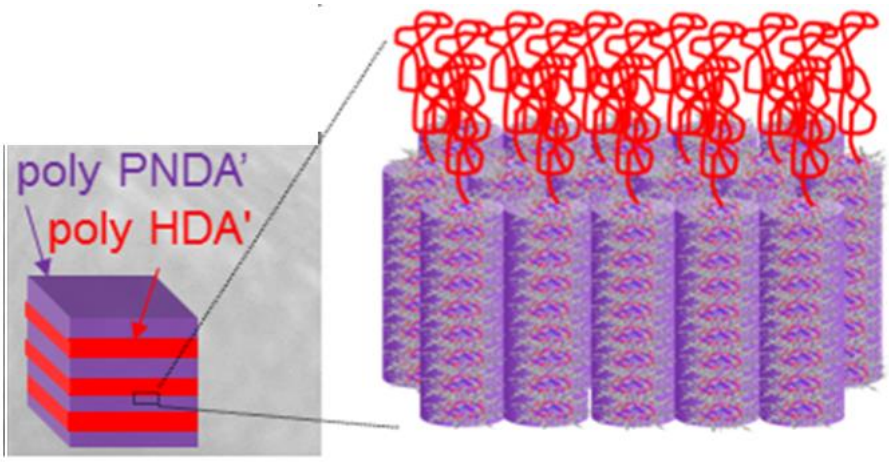

Figure 3-18. Schematic illustration of polyPNDA'-b-polyHDA' self-assembled nanostructures. These figures were originally drawn in lit. 31.

3-1-10. Photoresist

Glass photoresist compounds containing ^{t}BOC protecting group having well-defined molecular structure and definite molecular weight were designed and prepared.[32] The compounds exhibited excellent solubility in common organic solvents, fully amorphous character, and good film-forming property. Upon irradiation to 365 nm light, the photo-acid generator readily underwent photolysis to form H^{+}. The H^{+} generated in the photolysis can further catalyze the deprotection of ^{t}BOC protecting group.

Hexakis(4-formylphenoxy)cyclotriphosphazene (HAPCP), synthesized from HCCP with *p*-hydroxybenzaldehyde, was reduced by $NaBH_4$ to afford hexakis[4-(hydroxymethyl)phenoxyl]cyclotriphosphazene (HHPCP). The hydroxy group of HHPCP was protected by the reaction with di-*tert*-butyl dicarbonate in the presence of 4-dimethylaminopyridine (DMAP) as catalyst to give *tert*-butoxycarbonyl (^{t}BOC) protected HHPCP.

The patterning property of the ^{t}BOC-HHPCP derivative was measured by scanning electron microscopy obtained from a film prepared as follows. A photoresist was prepared from the ^{t}BOC-HHPCP, photo-acid generator (PAG), and DMF as the solvent, and it was coated onto silicon wafer. The substrate was exposed by 365 nm exposure source, followed by post-bake at 100 °C for 120 s. The acid-catalyzed deprotection converted the *tert*-butyl ester group of ^{t}BOC to carboxyl group, which provided fast dissolution rate in developing solution to form the Line/Space pattern. As seen in Figure 3-19, the SEM images showed that these molecular glass photoresists demonstrated clear and straight line.

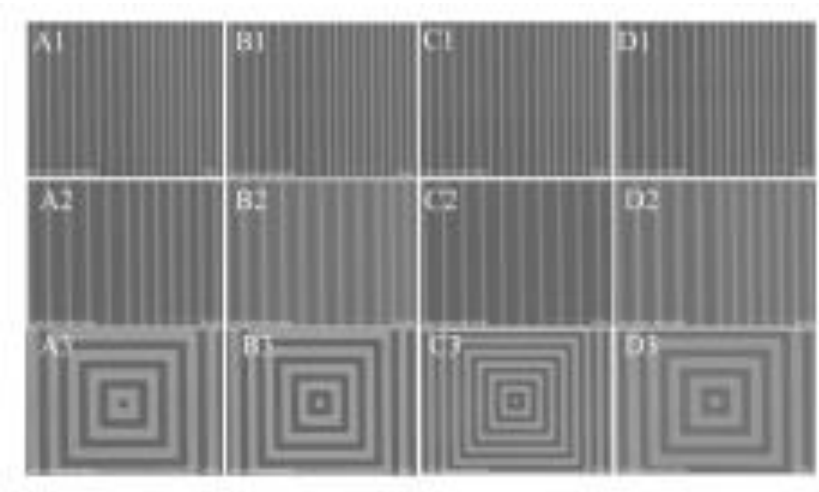

Figure 3-19. SEM images of patterns from the photoresist containing different ^{t}BOC protecting ratio. (A:60%, B:70%, C:80%, D:100%, respectively). This photo is originally reported in lit. 32.

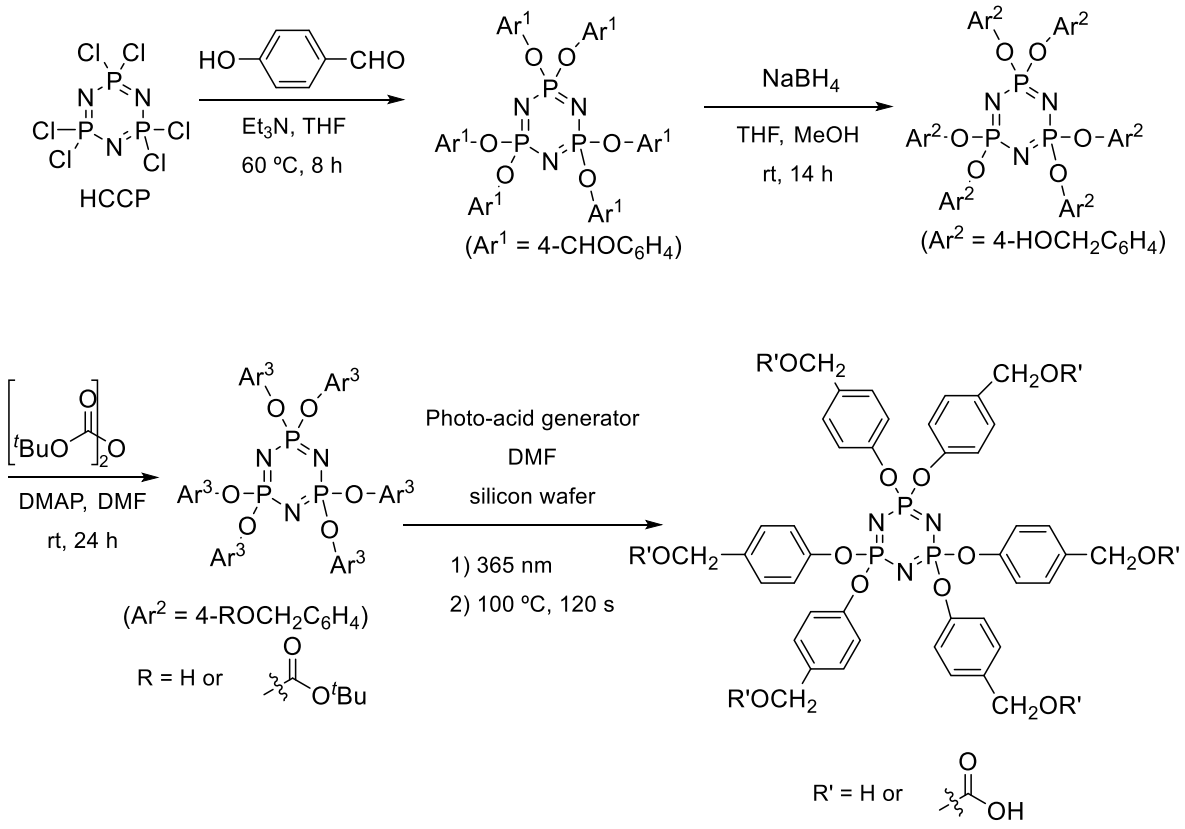

Scheme 3-10. Synthesis of photoresist compound

3-1-11. Fluorescence

Aslan reported cyclotriphosphazene-based fluorescence-emitting materials (Scheme 3-11).[33] Hexakis(4-formylphenoxy)cyclotriphosphazene (**33-2**) and hexakis(4-formyl-2-methoxyphenoxy)cyclotriphosphazene (**33-3**) were treated with 12 equiv. of anilines having different

substituted groups, such as hydroxy, cyano, mercapto, heterocyclic, carboxyl, and chloro, for synthesis of organocyclotriphosphazene derivatives incorporating six non-conjugated Schiff base groups **33-6N** and partially condensed imide products **33-5N** – **2N**.

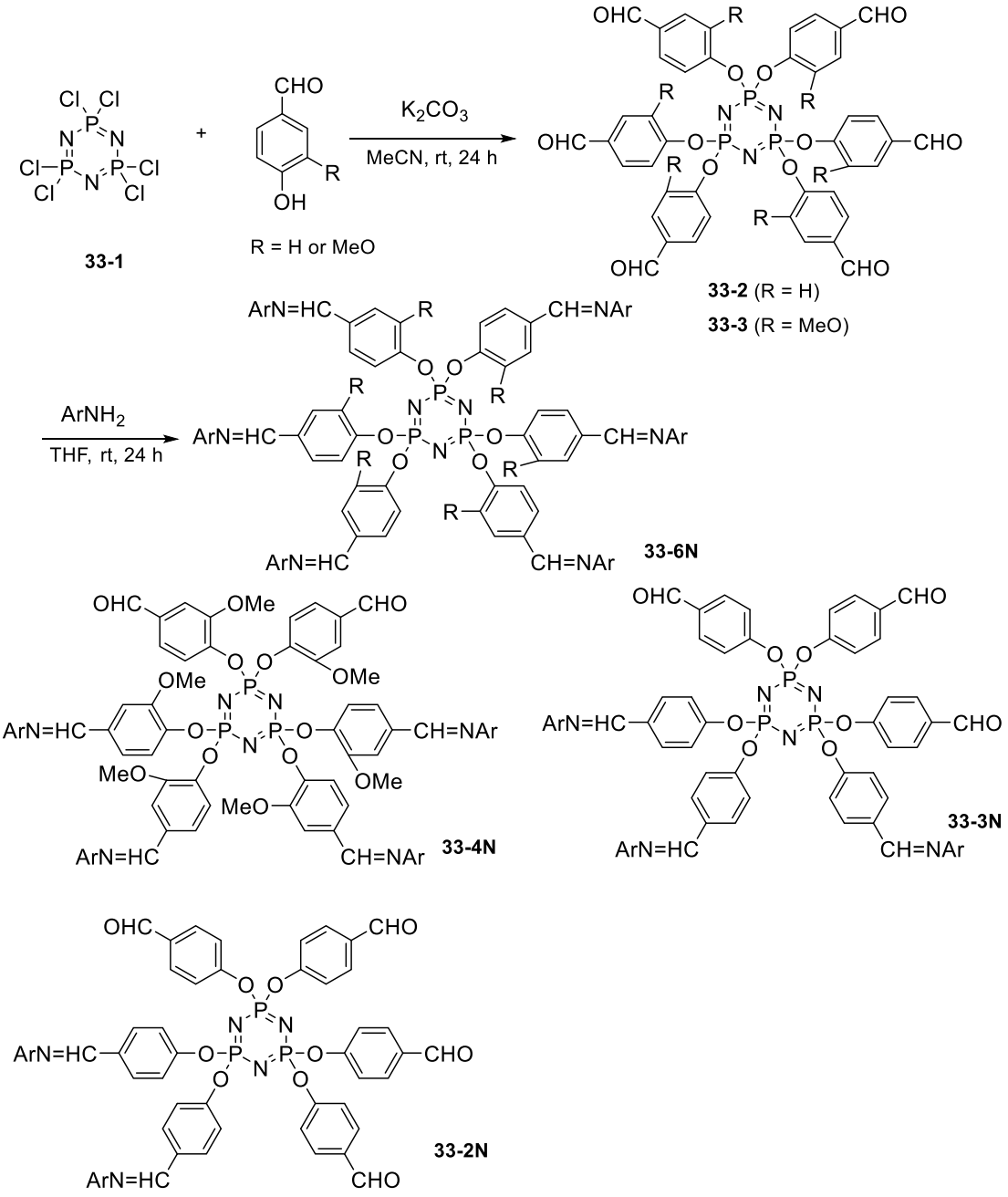

Scheme 3-11. Synthesis of organocyclotriphosphazene derivatives incorporating non-conjugated Schiff base groups

Synthesized compounds were photophysically investigated by UV absorption and fluorescence emission spectroscopy in solution state to indicate that HCCP (**33-1**) and all of the obtained compounds have

luminescence properties and large Stokes shifts. Some compounds showed blue-red emission peak having rather large Stokes shifts in the range of 390-800 nm.

Çiftçi synthesized the partially or fully substituted *spiro*-, *ansa*-, and *open-chain* forms of 2,2'-methylenediphenoxy, 1,1'-methylenedi-2-naphthoxy cyclotriphosphazene derivatives, and investigated their spectral properties.[34] HCCP (**34-1**) was treated with 2,2'-methylenediphenol (**34-2**) and 1,1'-methylenedi-2-naphthol (**34-3**) in THF to give new cyclotriphosphazene compounds, **34-4** – **11** (Scheme 3-12).

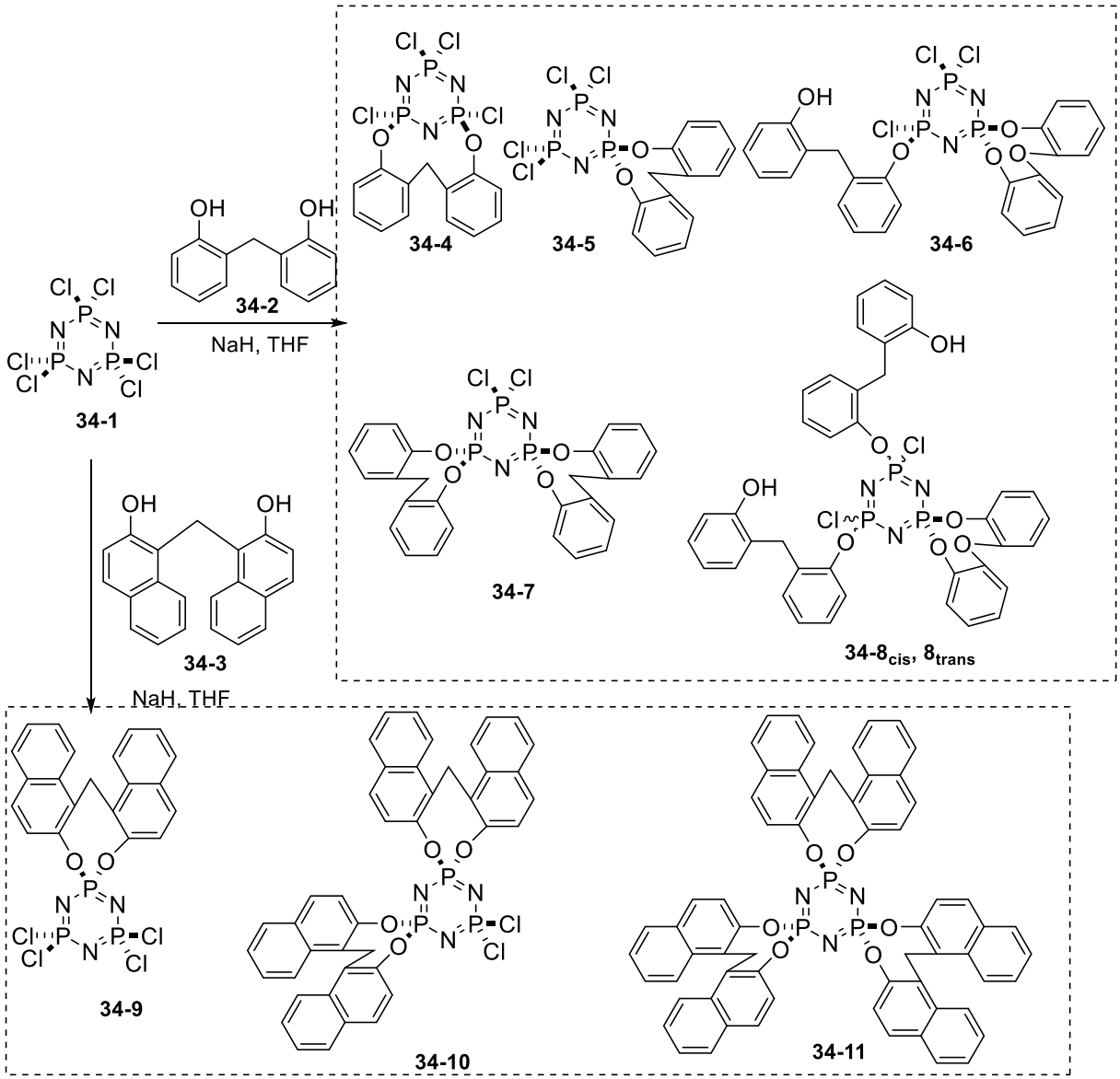

Scheme 3-12. Synthesis of 2,2'-methylenediphenoxy- and 1,1'-methylenedi-2-naphthoxy-cyclotriphosphazene derivatives

The electronic absorption and fluorescence behavior of **34-4**, **34-5**, **34-7**, **34-9** – **11** were determined in THF. Absorption bands were observed at approximately 260 and 270 nm for phenol-substituted cyclotriphosphazene compounds **34-4**, **34-5** and **34-7**, whereas 260, 275, 285 and 290 nm for naphthol-substituted cyclotriphosphazene compounds **34-9**, **34-10** and **34-11** (Figure 3-20). On the other hand, fluorescence emission peaks of **34-4**, **34-5** and **34-7** were observed at 285 nm. The trend in the emission maxima amongst the cyclic compounds was as follows: *dispiro*- (**34-7**) > *mono-spiro*- (**34-5**) > *ansa*-cyclotriphosphazene derivative (**34-4**). Among **34-9**, **34-10**, and **34-11**, **34-9** showed the highest fluorescence emission behavior. The fluorescence behavior increased with the number of the aromatic group increased because of the non-covalent π-π interactions between aromatic double bonds of naphthol groups.

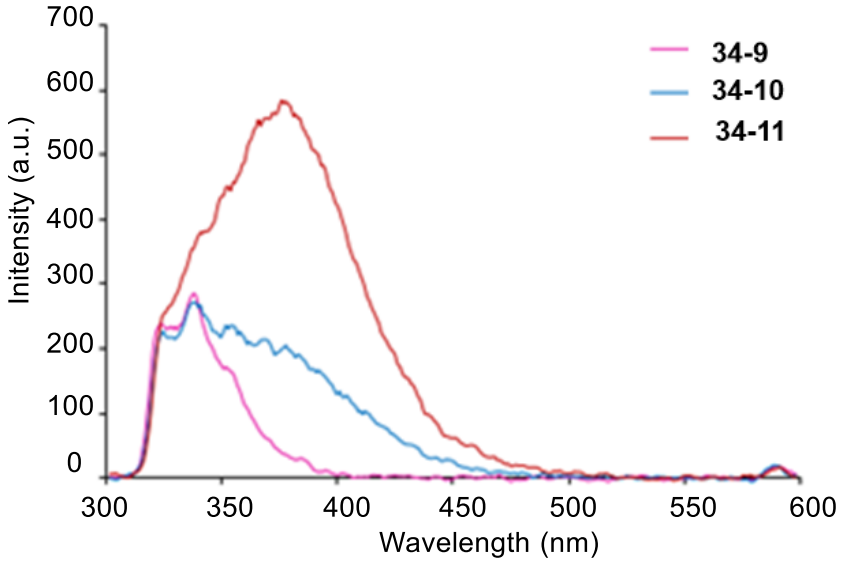

Figure 3-20. The fluorescence emission spectra of **34-9**, **34-10**, and **34-11** in THF. Concentration: 1 x 10^{-5} mol·dm^{-3}; excitation wavelength: 295 nm. The Figure was originally drawn in lit. 34.

3-1-12. Chemosensor for metal ions

Şenkuytu reported synthesis of aniline (**35-8** and **35-9**) and 2-naphthylamine (**35-10** and **35-11**) substituted 4,4'-(9-fluorenylidene)diphenol (FDP)-bridged cyclotriphosphazenes and aniline (**35-12**) and 2-naphthylamine (**35-13**) substituted 4,4'-(9-fluorenylidene)dianiline (FDA)-bridged cyclotriphosphazene derivatives (Scheme 3-13).[35]

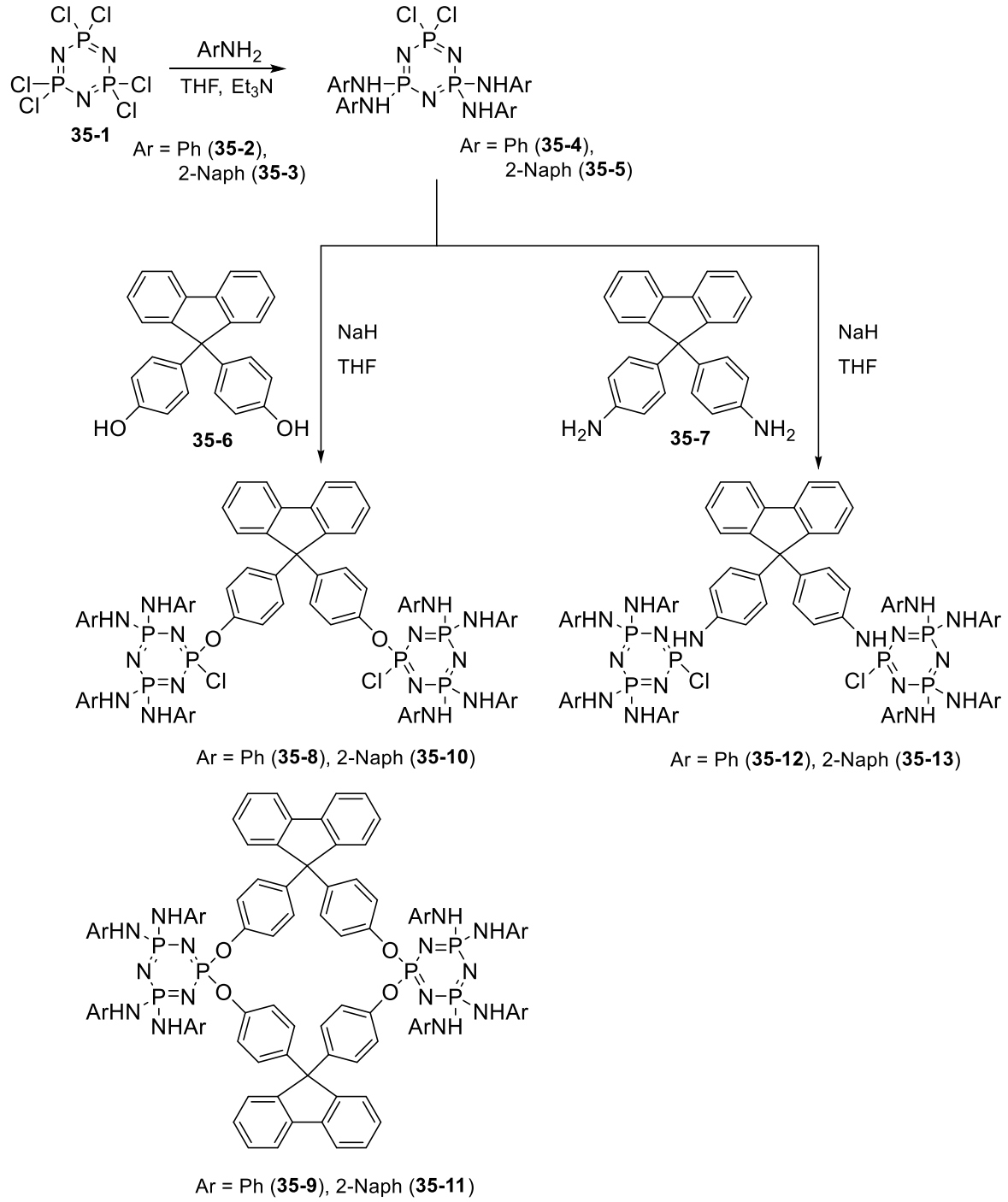

Scheme 3-13. Synthesis of ion sensors

When 2,2,4,4-tetraanilino-6,6-dichlorocyclotriphosphazene (**35-4**) and 2,2,4,4-tetrakis(2-naphthylamino)-6,6-dichlorocyclotriphosphazene (**35-5**) were treated with FDP (**35-6**) and FDA (**35-7**) in THF, **35-8** – **11** and **35-12** – **13** were obtained, respectively. The florescence properties of **35-8** – **13** were studied. The chemosensory behavior of the compounds against to metal ions was also investigated. The obtained fluorenylidene bridged 2-naphthylamine substituted cyclotriphosphazenes (**35-10**, **35-11**, and **35-13**) showed fluorescence chemosensor behavior with high selectivity for Fe^{3+} and Cu^{2+} ions in the solution.

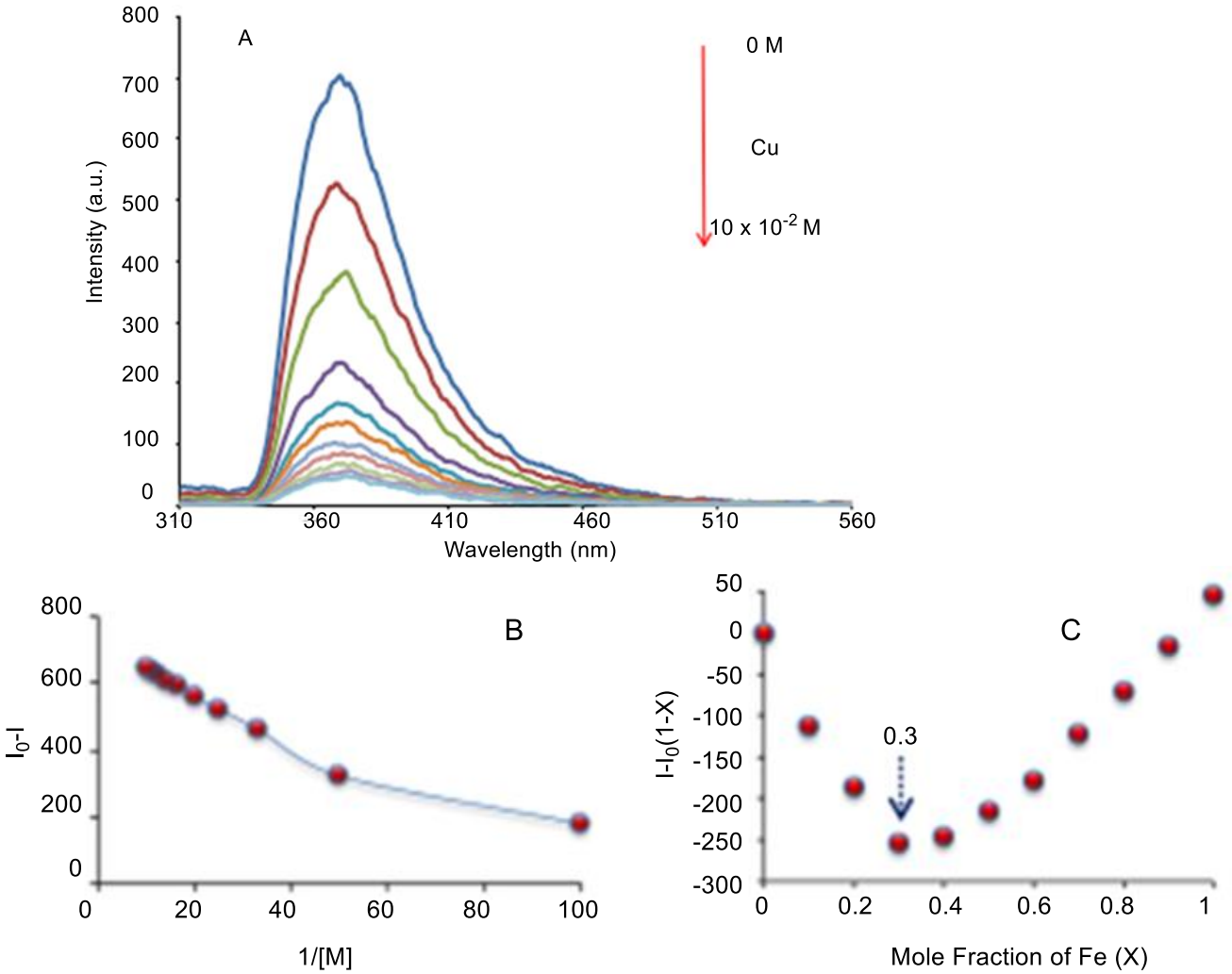

Figure 3-21. (A) Fluorescence response of chemosensor **35-10** to various equivalents of Cu^{2+}. (B) The Benesi–Hildebrand graph and (C) Job's plot of **35-10**-Cu^{2+} complexes in THF solutions. The total concentration of **35-10** and Cu^{2+} was 1 x 10^{-2} M. The excitation wavelength was 295 nm. The monitored wavelength was 370 nm (compound **35-10**, C: 5 x 10^{-6} M). These figures were originally illustrated in lit. 35.

Çiftçi reported synthesis of 3-[2-(diethylamino)ethyl]-7-oxy-4-methylcoumarin substituted cyclotriphosphazene (**36-4**) by reaction of HCCP with 3-[2-(diethylamino)ethyl]-7-hydroxy-4-methylcoumarin (**36-3**) (Scheme 3-14).[36] The quaternized cationic (**36-6**) and zwitterionic (**36-8**) derivatives were obtained by the reaction of **36-4** with dimethyl sulfate and 1,3-propanesultone, respectively. All these coumarin-substituted cyclophosphazene compounds, **36-4**, **36-6**, and **36-8**, were soluble in most of organic solvents and quaternized ionic and zwitterionic compounds, **36-6** and **36-8**, also showed excellent solubility in water.

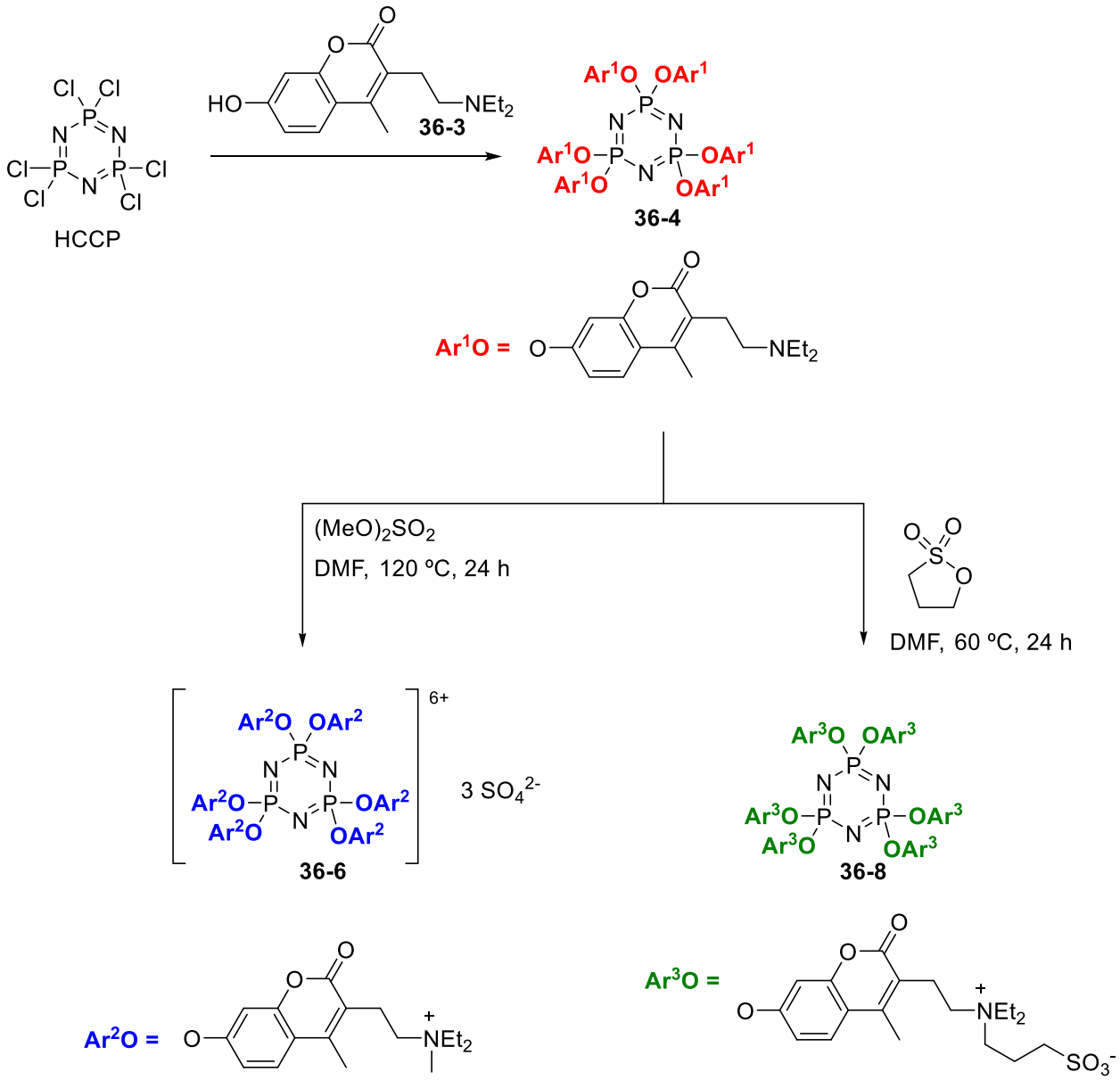

Scheme 3-14. Synthesis of chemosensors

The fluorescence behaviors of novel cyclophosphazene compounds were investigated in MeOH and aqueous solutions. The chemosensor properties of **36-6** and **36-8** were investigated in aqueous media. These cyclophosphazene derivatives showed fluorescence chemosensor behavior with high selectivity for Fe^{3+} ions in aqueous solution.

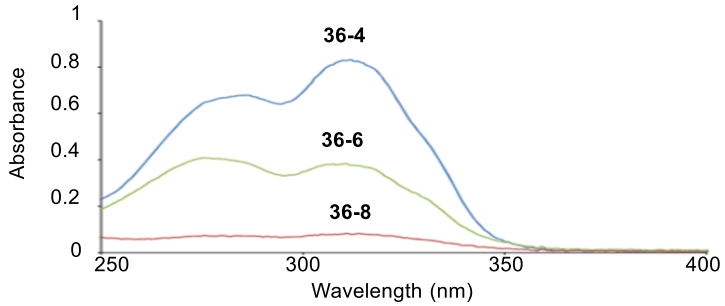

Figure 3-22. Electronic absorption spectra of compounds **36-4**, **36-6** and **36-8** in MeOH ($c = 2.5\times10^{-6}$ M). This figure was originally reported in lit. 36.

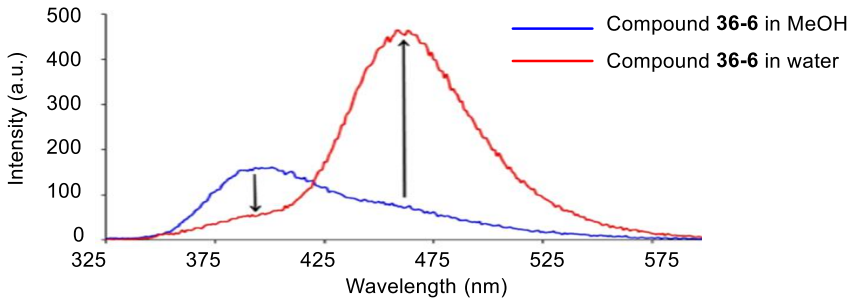

Figure 3-23. Fluorescence emission spectra of **36-6** in MeOH and aqueous solutions ($c = 1.00\times10^{-5}$ M, $\lambda_{ex} = 315$ nm). This figure was originally drawn in lit. 36.

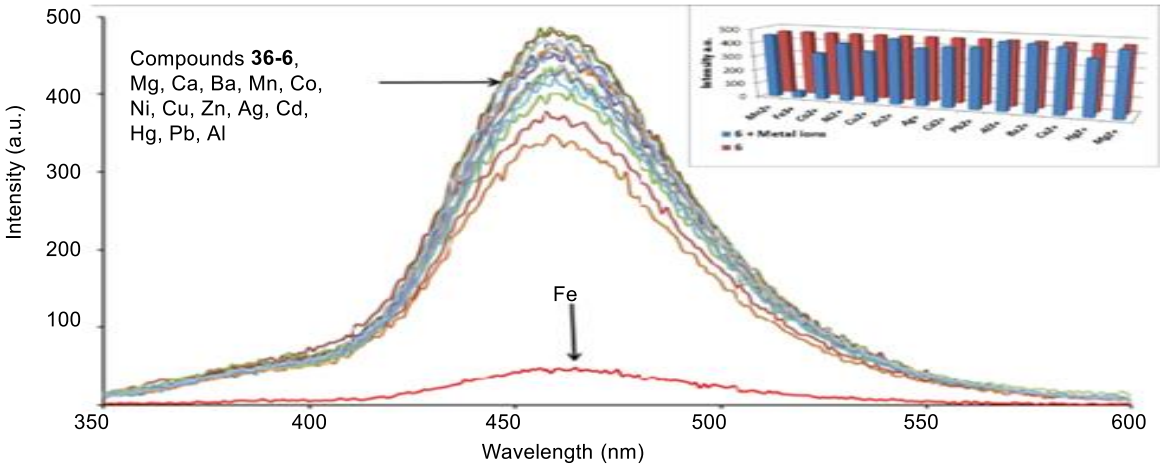

Figure 3-24. The fluorescence intensity of **36-6** with and without metal ions in aqueous solution. Addition of Fe^{3+} ions to the solution prevent fluorescent emission hence provide a selective detection. This figure was originally reported in lit. 36.

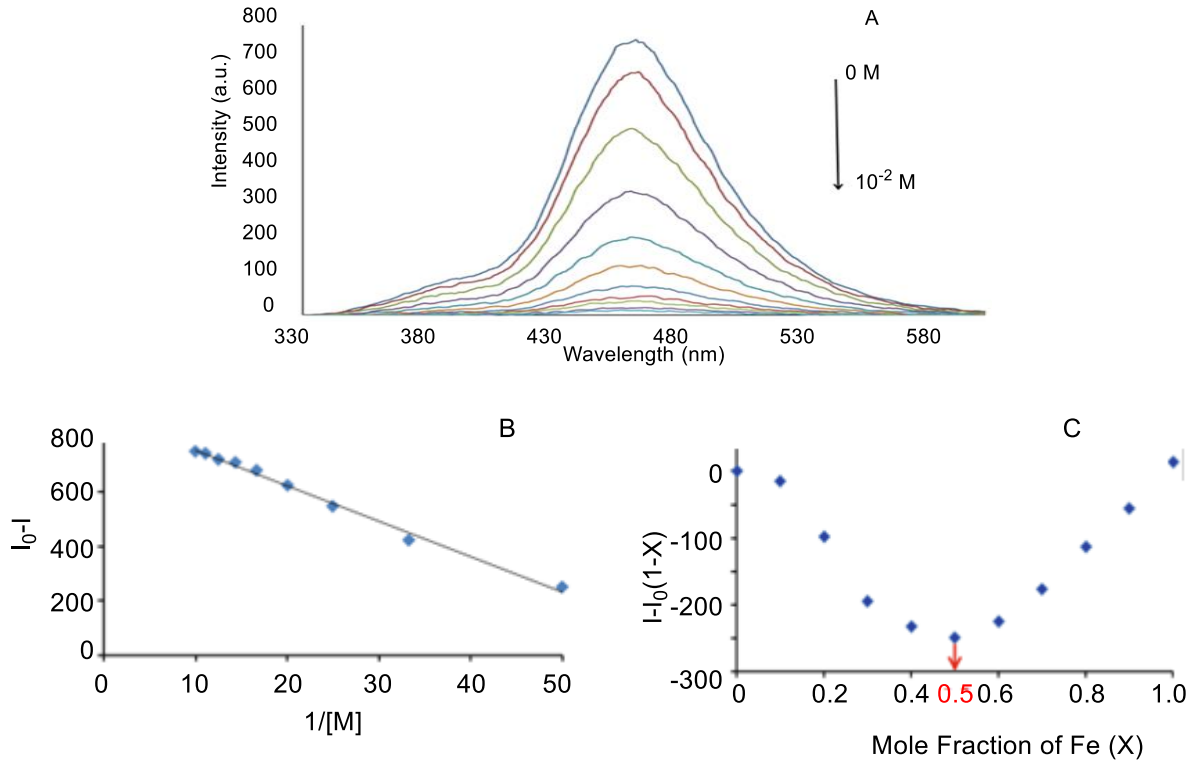

Figure 3-25. (A) Fluorescence response of chemosensor **36-6** to various equivalents of Fe^{3+}. (B) The Benesi-Hildebrand graph and (C) Job's plot of **36-6**-Fe^{3+} complexes in aqueous solutions. The total concentration of **36-6** and Fe^{3+} was 1×10^{-2} M. The excitation wavelength was 320 nm. The monitored wavelength was 460 nm. These figures were originally printed in lit. 36.

The cyclotriphosphazene compound (**37-2**) bearing 2-methoxy-4-formylphenyl group was obtained from reaction of 2,2-dichloro-4,4,6,6-bis[spiro(2',2"-dioxy-1',1"-biphenylyl)]cyclotriphosphazene (**37-1**) with 4-hydroxy-3-methoxybenzaldehyde in the presence of K_2CO_3 in THF (Scheme 3-15).[37] Oxime-cyclotriphosphazene compound (**37-3**) was obtained from **37-2** treated with hydroxylamine hydrochloride in pyridine. Compound **37-3** was allowed to react with alkyl and acyl halides to form C=N-OR (**37-4** – **6**) and C=N-OC(=O)R (**37-7** – **10**) derivatives, respectively. Dielectric constant, dielectric loss factors, and conductivity properties of cyclotriphosphazene compounds were measured over the frequency range from 100 Hz to 2 kHz at 25 ºC. It is found that ester-substituted cyclotriphosphazenes have higher dielectric constant. Among them, oxime-ester phosphazene containing 2-thienyl group **37-10** displayed higher conductivity than other cyclotriphosphazene. compounds.

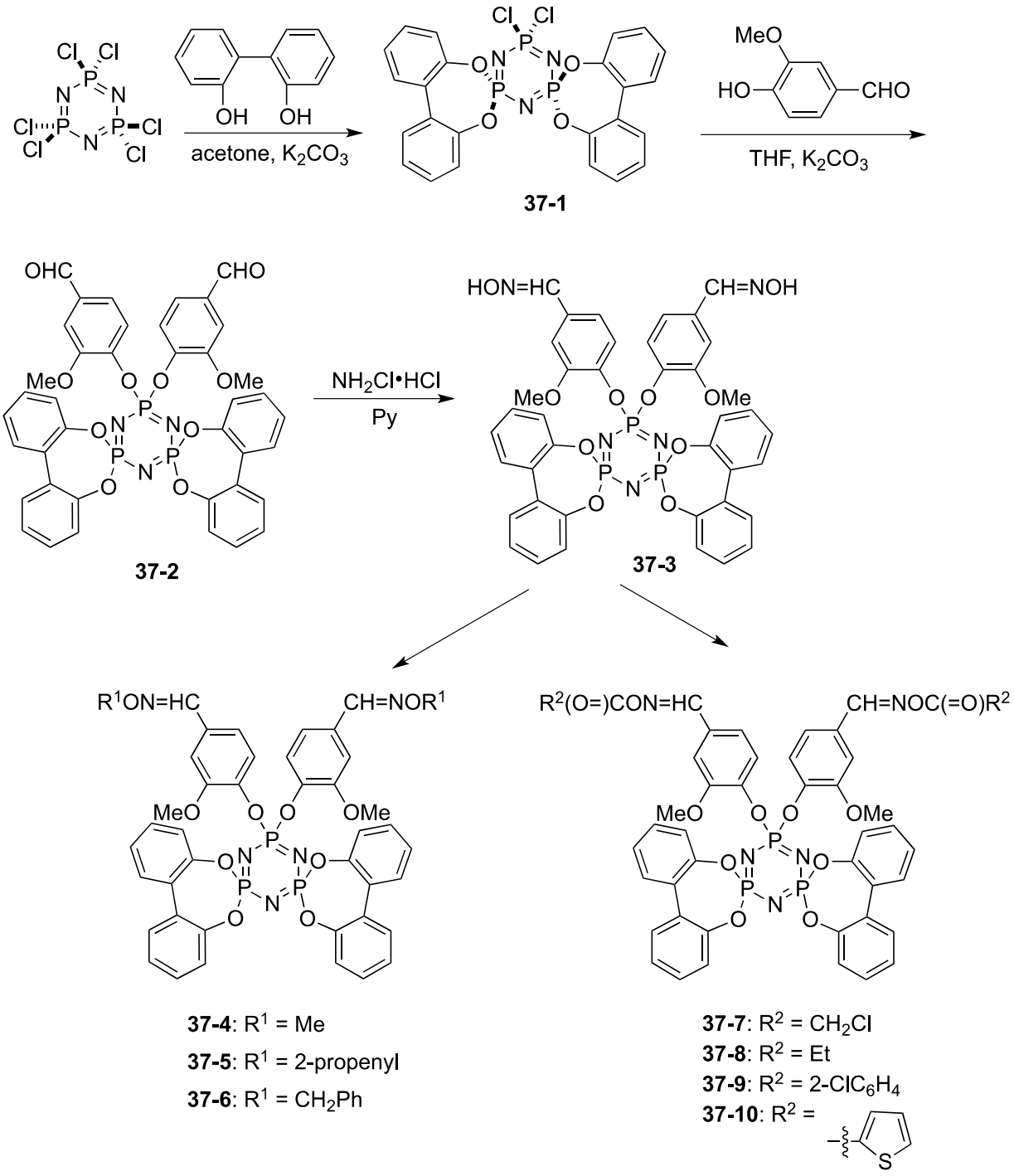

Scheme 3-15. Synthesis of oxime-ether and oxime-ester cyclotriphosphazene compound

Table 3-3. The dielectric constant (ε') and AC conductivity (σ) values of cyclotriphosphazene compounds (**37-2** – **10**) in the frequency of 1 kHz at 25 ºC

Compounds	ε'	σ x 10^{-6} (Siemens/cm)
37-2	2.95	0.95
37-3	3.80	1.79
37-4	3.37	1.99
37-5	3.02	2.17
37-6	3.80	2.24
37-7	6.44	2.88
37-8	5.96	2.57
37-9	6.95	3.19
37-10	7.87	3.41

3-1-13. Polyradicals-TEMPO

Badetti synthesized a cyclotriphosphazene functionalized with nitroxyl radicals (TEMPO) in its six branches (Scheme 3-16).[38] The radical compound **38-2** was prepared by imination of hexakis(4-formylphenoxy)cyclotriphosphazene (**38-1**) with 4-amino-2,2,6,6-tetramethylpiperidine *N*-oxyl (4-NH_2TEMPO). The radical was used as a probe to determine the orientation of the six branches in solution experimentally by Electron Paramagnetic Resonance (EPR) spectroscopy compared with the structure in the solid state obtained by X-ray diffraction. The orientation of the branches in solution was the same as in the solid state.

The EPR spectrum of a solution of **38-2** in a mixture of dichloromethane/toluene (1 : 1) at 350 K shows seven lines centered at g = 2.0066 and separated by ca. 5.0 G (Figure 3-26). This fitted with a spectrum generated by the interaction of three TEMPO radicals. However, the first, fourth, and seventh lines are more intense than those for the expected pattern. This result suggested that the observed spectrum was the sum of at least two different spectra. It is important to take into account the magnitude of the magnetic exchange interactions, *J* between the six radical units in **38-2**, and the fact that these interactions may be not constant in solution because the radical units move under such conditions. Consequently, the EPR spectra should depend on the conformation and mobility of the branches and, the shape of the spectra also depended on the temperature, viscosity, and nature of the solvent.

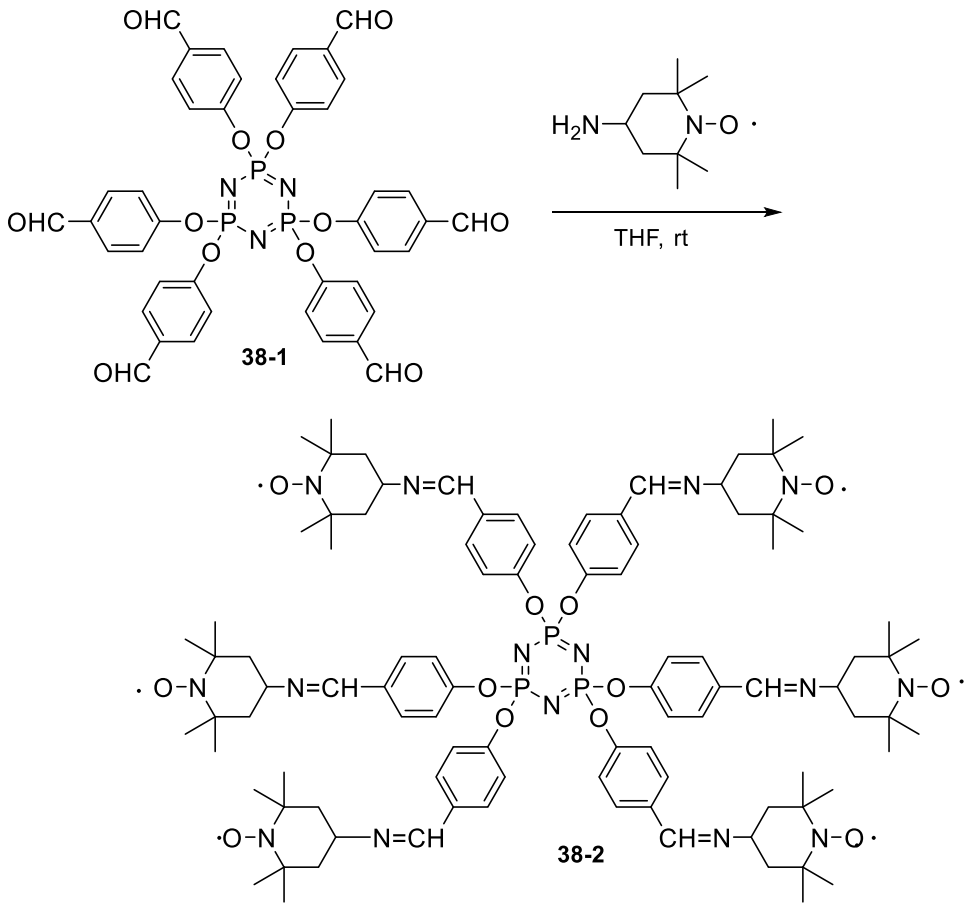

Scheme 3-16. Synthesis of polyradical **38-2**

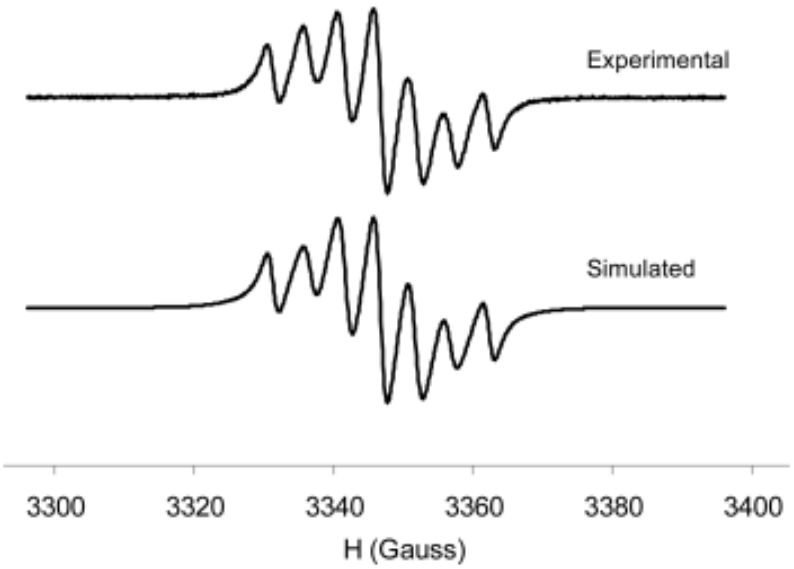

Figure 3-26. Experimental and simulated EPR spectra of a 10^{-4} M solution of **38-2** in dichloromethane/toluene (1 : 1) at 350 K. These figures were originally shown in lit. 38.

3-1-14. Spin crossover material

Spin crossover (SCO) materials have been suggested to have potential for use in quantum computers and massive data storage. However, since SCO materials are often crystalline, they are difficult and expensive to deposit and process.

Synthesis of cyclotriphosphazene ligand substituted with a pendant 2,6-bis(benzimidazol-2-yl)pyridine, namely (pentaphenoxy)[4-{2,6-bis(benzimidazol-2-yl)pyridin-4-yl}phenoxy]cyclotriphosphazene (**39-1**) was reported (Scheme 3-17).[39] Compound **39-1** is allowed to react with FeX_2 (X = ClO_4^- or BF_4^-) salts to form [Fe(**39-1**)$_2$]X_2 complexes **39-2** (X = ClO_4^-) and **39-3** (X = BF_4^-)**,** respectively (Figure 3-27).

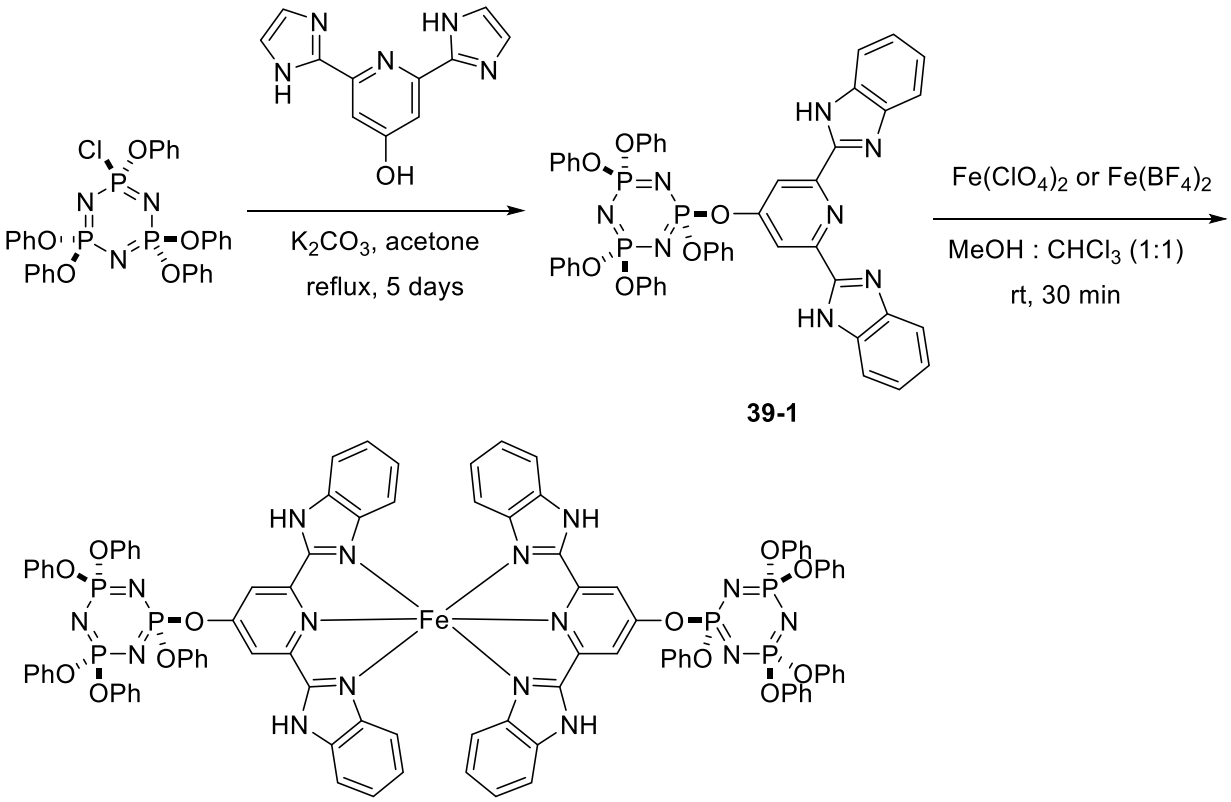

Scheme 3-17. Synthesis of Fe-complex **39-2** and **39-3** having cyclotriphosphazene units

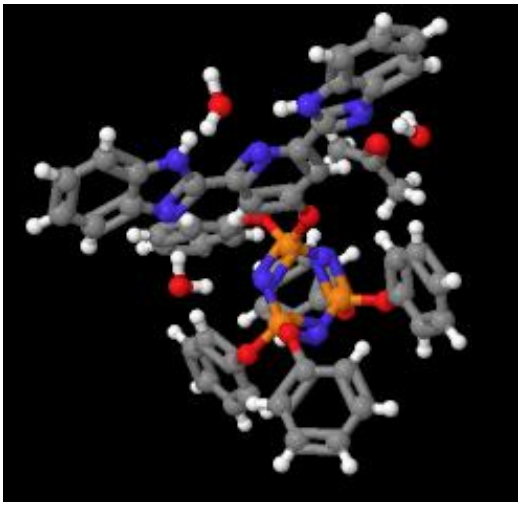

CCDC 904683: Experimental Crystal Structure Determination

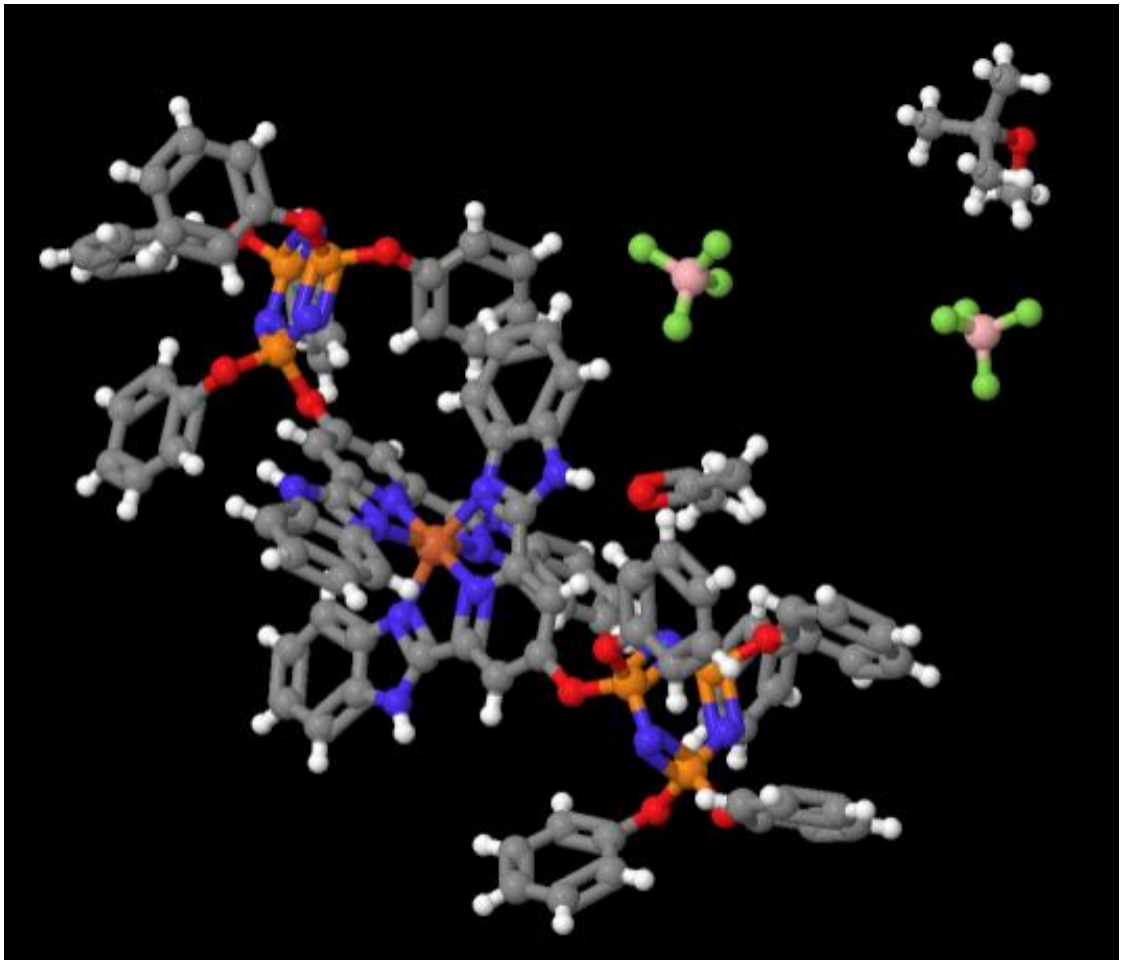

CCDC 904684: Experimental Crystal Structure Determination

Figure 3-27. Crystal structure of **39-1** (upper) and **39-2** (lower)

The complexes were in low spin state below 300 K, but displayed spin crossover (SCO) behavior above this temperature, hence showing that the addition of a phosphazene to a SCO moiety does not prevent

SCO. The temperature dependent electronic spectra for **39-2** are shown in Figure 3-28. Both **39-2** and **39-3** displayed identical MLCT (Metal to Ligand Charge Transfer) bands, with λ_{max} at 560 and 561 nm, respectively, typical of t_{2g} forms of $[Fe(bbp)_2]^{2+}$ complexes. There were red shifts of 8 and 9 nm, respectively, relative to the unsubstituted complex $[Fe(bbp)_2](ClO_4)_2$ (λ_{max} 552 nm in MeCN), which can be explained by electron-withdrawing effects of the phosphazene unit.

This investigation proves that the addition of a phosphazene to a SCO moiety does not prevent SCO and provides a new route for the creation of workable SCO materials based on the polyphosphazene scaffold.

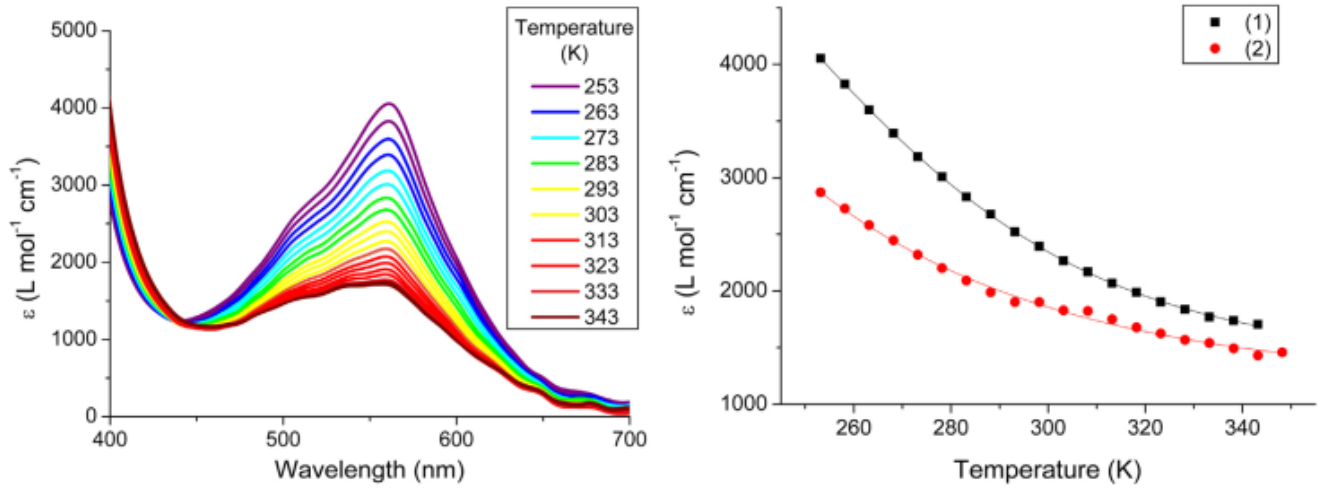

Figure 3-28. Left: the visible spectrum of **39-2** from 253 – 343 K. Right: εMCLT (Metal to Ligand Charge Transfer) vs. temperature for **39-2** (black squares) and **39-3** (red circles). This figure was originally shown in lit. 39.

3-2. Practical applications of cyclotriphosphazene Materials as Biomaterials

3-2-1. ^{19}F MRI contrast agent

A cyclotriphosphazene (**40-3**) substituted with six 3,5-bis(trifluoromethyl)benzyloxy units was designed as a ^{19}F MRI contrast agent (Scheme 3-18).[40] Compound **40-3** has 36 magnetically equivalent fluorine atoms and exhibited suitable MRI properties with high imaging sensitivity.

To test the ^{19}F MRI properties of **40-3**, ^{19}F MRI measurements of solutions in $CHCl_3$ were conducted at a field strength of 9.4 T. As illustrated in Figure 3-29a, samples with ^{19}F concentrations 3 - 100 mM could be detected successfully by ^{19}F MRI. The ^{19}F MRI signal/noise ratio (SNR) was calculated for illustrating the quantitative nature of the ^{19}F MRI experiments. As shown in Figure 3-29b, a good linear relationship of ^{19}F MRI SNR to the concentration of sample **40-3** was observed (R^2 = 0.982). These observations indicated that **40-3** is a promising quantitative ^{19}F MRI contrast agent with high imaging sensitivity due to the numerous chemically equivalent fluorine atoms in one molecule.

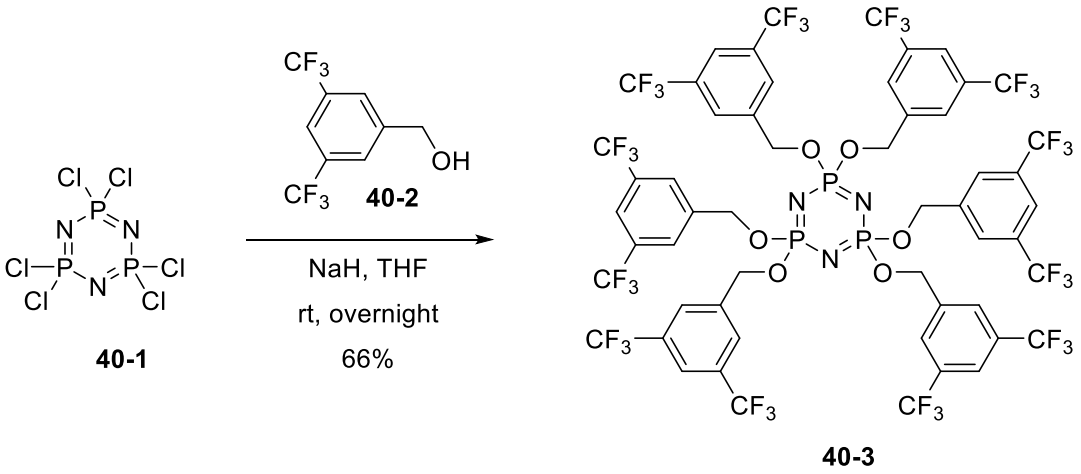

Scheme 3-18. Synthesis of ^{19}F MRI contrast agent **40-3**

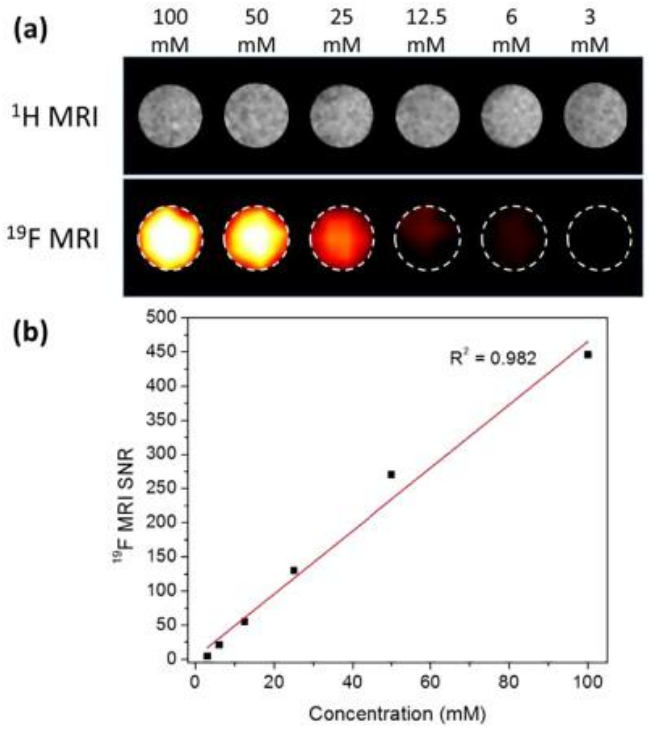

Figure 3-29. (a) ^{19}F MRI images of solutions of **40-3** ($CHCl_3$) at various concentrations. (b) Signal/noise ratio of **40-3**. Field strength: 9.4 T. These figures were originally reported in lit. 40.

3-2-2. Cytotoxic activity

Koran reported the relationship between the cytotoxic activity and dielectric properties of 2,2,4,4-tetrakis(4′-oxy-substituted-chalcone)-6,6-diphenylcyclotriphosphazene derivatives (**41-4** – **11**) (Scheme 3-19).[41] 2,2,4,4-Tetrachloro-6,6-diphenyl cyclotriphosphazene (**41-2**) was obtained through Friedel-Crafts reaction in the presence of HCCP, benzene, Et_3N, and anhydrous $AlCl_3$. Compounds **41-4** – **11** were synthesized from the reaction of **41-2** with the hydroxychalcone derivatives (**41-3a** – **h**) in

the presence of K_2CO_3 in acetone. The dielectric constant, dielectric loss factor, and AC conductivity of **41-4** – **11** were examined by an impedance analyzer.

The *in vitro* cytotoxic activities of compounds **41-4** – **11** in five different concentrations (1, 5, 25, 50, and 100 μM) were analyzed by colorimetric MTT (3-(4,5-dimethylthiazol-2-yl)-2,5-diphenyltetrazolium bromide) assay [measurement of cytotoxicity (loss of viable cells) or cytostatic activity (shift from proliferation to quiescence) of potential medicinal agents and toxic materials] which is based on reduction of MTT salt by mitochondria of alive cells over the human ovarian cancer (A2780) and human prostate cancer (PC-3 and LNCaP) cell lines. The obtained results suggest that the compounds have a powerful cytotoxic activity (especially for A2780, $p < 0.05$).

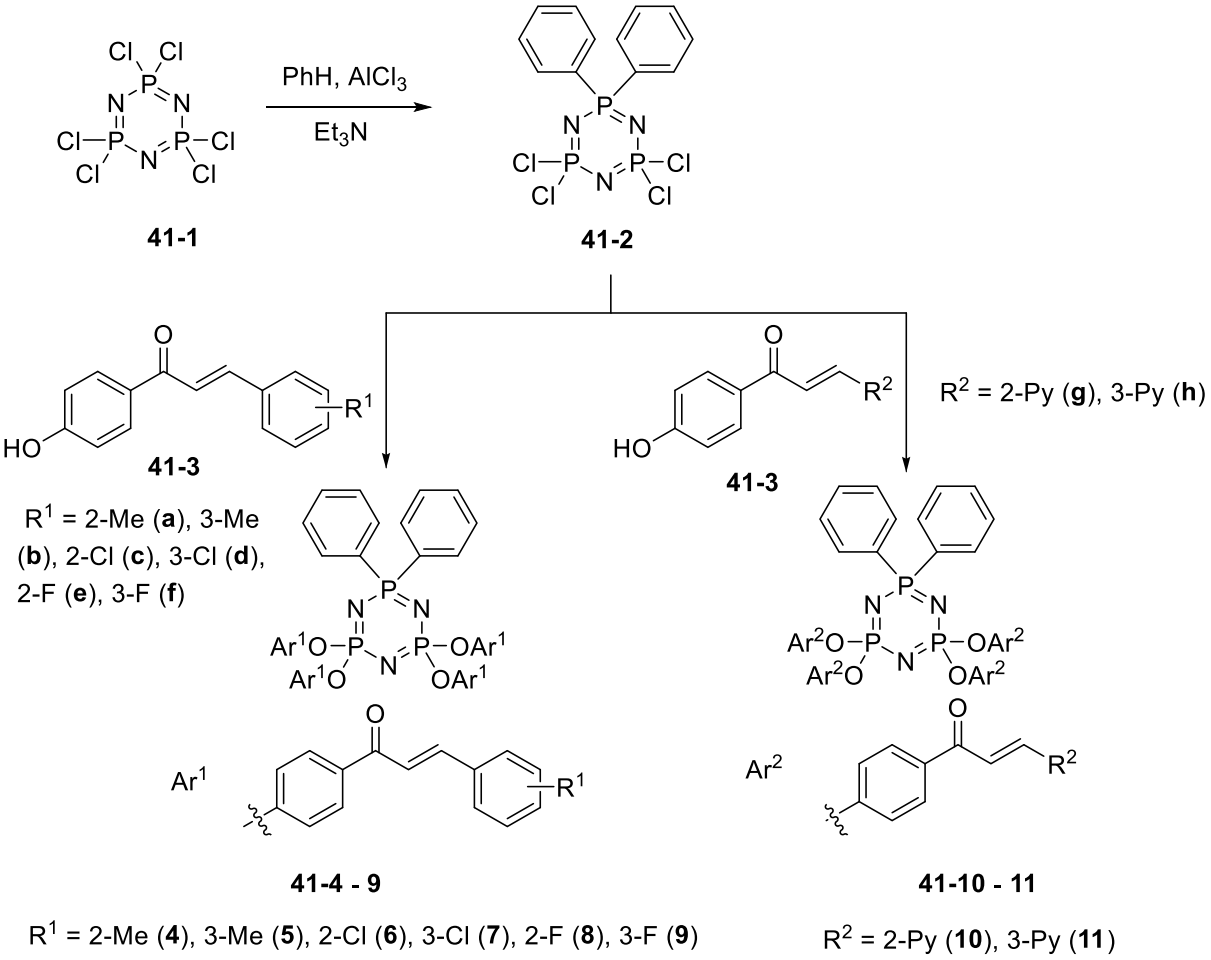

Scheme 3-19. Synthesis of 2,2,4,4-tetrakis(4′-oxy-substituted-chalcone)-6,6-diphenylcyclotriphosphazene derivatives **41-4** – **11**

3-2-3. Antiproliferative activity to cancer cell

A series of hexa-armed star-shaped thiosemicarbazones with different substitutions at *para* positions **42-3a** – **g** emanating from cyclotriphosphazene core were prepared (Scheme 3-20).[42]

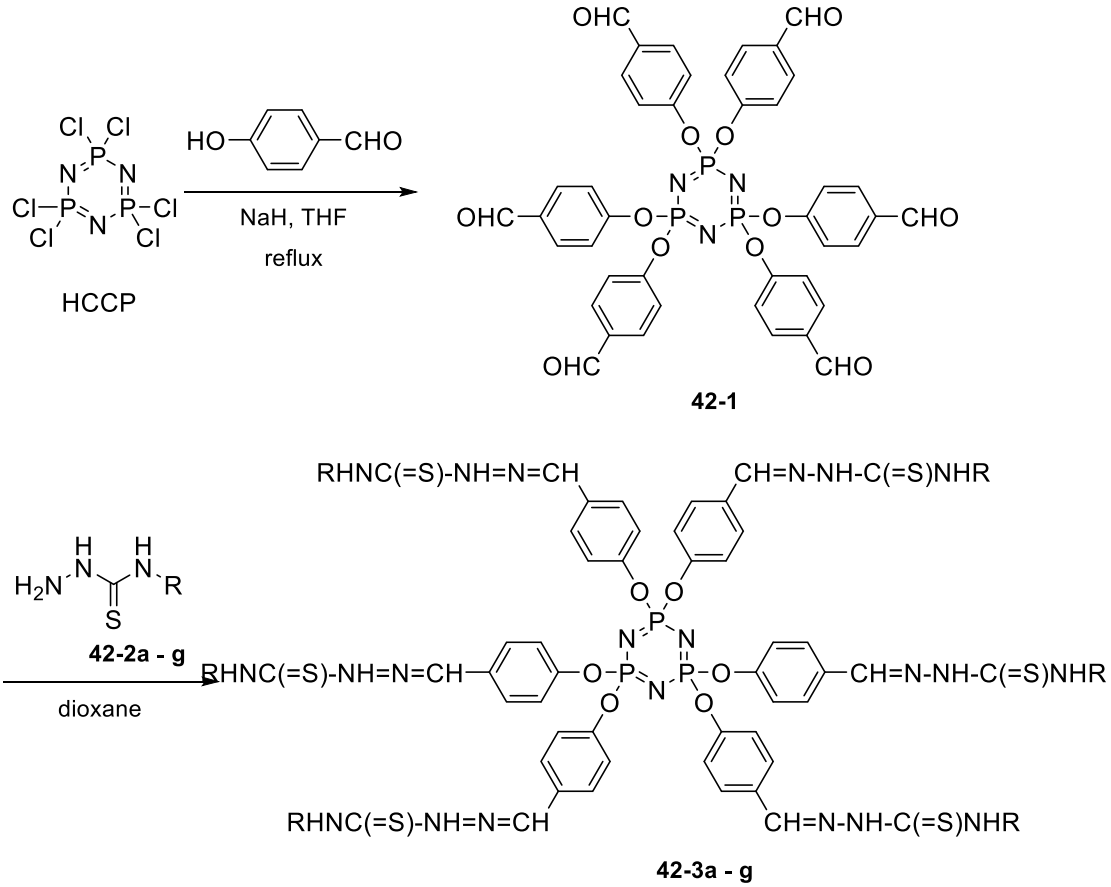

	a	b	c	d	e	f	g
R	Ph-	4-BrC_6H_4-	4-ClC_6H_4-	4-FC_6H_4-	4-HOC_6H_4-	4-$MeOC_6H_4$-	4-$CH_3C_6H_4$-

Scheme 3-20. Synthesis of hexa-armed star-shaped thiosemicarbazones **42-3a** - **3g**

These compounds were evaluated for *in vitro* antiproliferative activity against breast cancer (MCF7) and ovarian cancer (PA-1) cell lines using MTT assay to exhibit moderate to good activity against the tested cell lines. The compounds **42-3c**, **42-3f** and **42-3d** exhibit good activity against MCF-7, and **42-3c**, **42-3g**, and **42-3d** exhibit good activity against PA-1.

Table 3-4. Anticancer activity of **42-3a** - **3g** test compounds by MTT assay (% inhibition)

	MCF-7		PA-1	
	50 μmol	100 μmol	50 μmol	100 μmol
3a	58.28	63.11	54.4	61.88
3b	90.1	96.94	83.64	86.38
3c	78.08	87.74	71.91	73.02
3d	67.00	84.6	63.8	60.18
3e	67.18	70.86	59.64	66.48
3f	73.25	78.96	57.81	57.88
3g	53.40	63.03	67.9	68.31

The reactions of $[N_3P_3Cl_4(NCHMe_2)]_2$ with bidentate ligands, *N*-(4-fluorobenzyl)-*N'*-methylethane-1,2-diamine and *N*-(4-fluorobenzyl)-*N'*-methylpropane-1,3-diamine, at different molar ratios produced monospiro (**43-4a**, **43-4b**, **43-5a**, **43-5b**) and dispiro (**43-6a**, **43-6b**, **43-7a**, **43-7b**) biscyclotriphosphazenes with 4-fluorobenzyl pendant arms (Scheme 3-21).[43] The gel electrophoresis with plasmid DNA exhibited that **43-5a** and **43-7a** caused conformational changes and **43-7a** caused DNA cleavage. The conformational changes were due to the DNA binding of the compounds. *In vitro* studies showed that **43-5a** had high anticancer and apoptotic activities. Since DNA is one of the main targets for the anticancer agents, these two compounds, **43-5a** and **43-7a**, may have the promising results. Compounds **43-5a** and **43-7a** were also found to become significant growth inhibitors on Gram-negative (*E. coli*) and Gram-positive (*B. cereus*) bacteria.

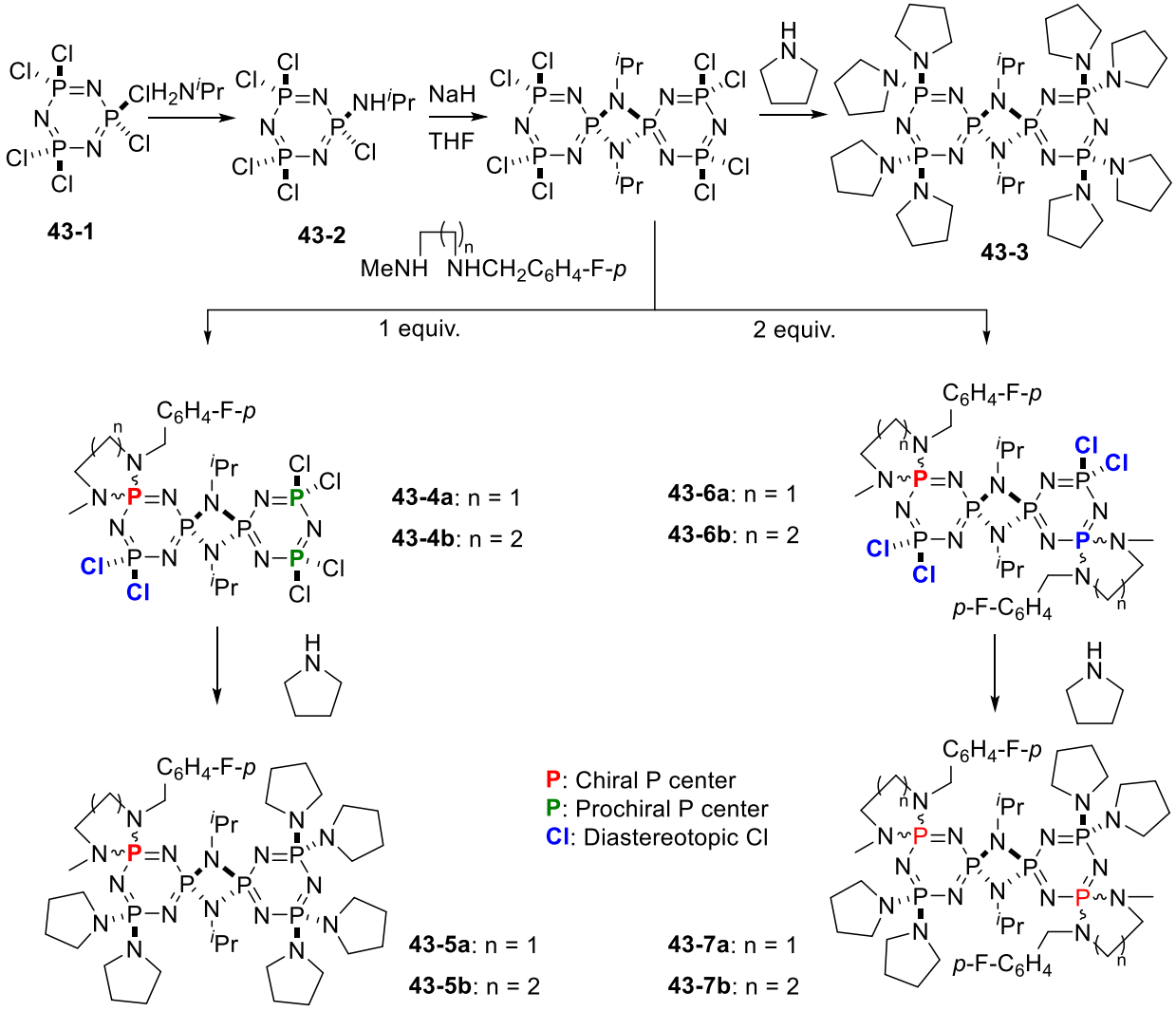

Scheme 3-21. Synthesis of compounds having DNA binding ability

3-2-4. Antimicrobial/Cytotoxicity

A cyclotriphosphazene ligand containing the *spiro*-2,2'-dioxybiphenyl group and 2-methyl-3-pyridyloxy moieties (**44-2**) was synthesized (Scheme 3-22). A Ru(II) complex **44-3** was prepared from the reaction of $[RuCl_2(p\text{-cymene})]_2$ with **44-2**.[44]

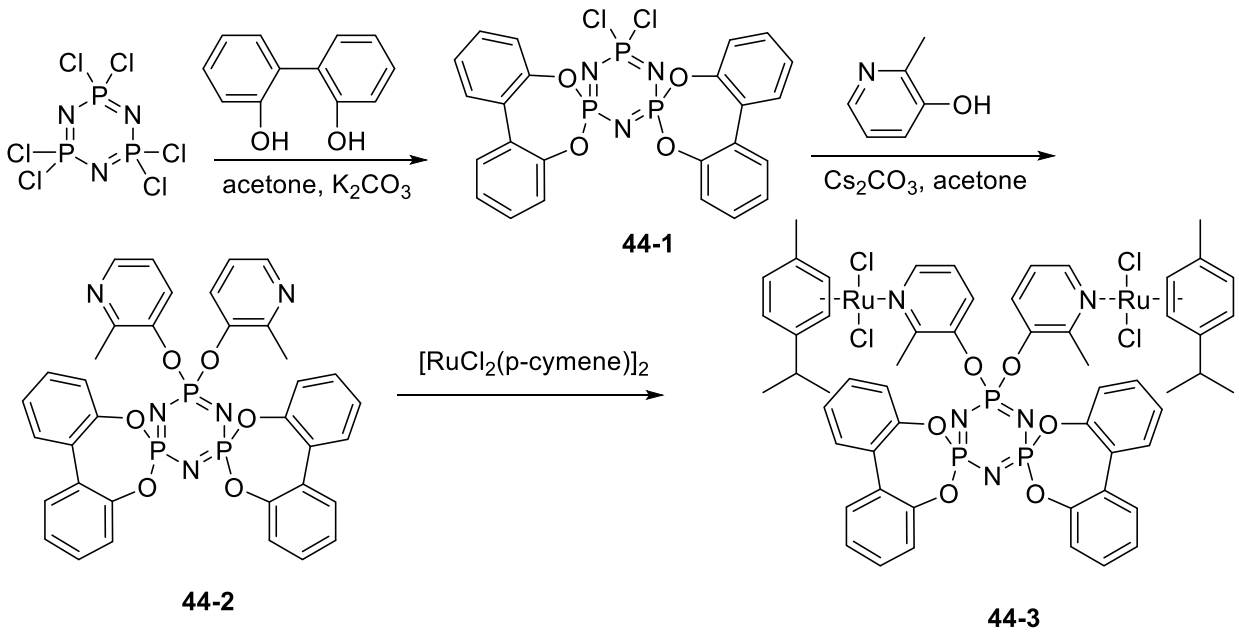

Scheme 3-22. Synthesis of Ru(II) complex **44-3**

Ru(II) complex **44-3** was used as a catalyst for the Catalytic Transfer Hydrogenation (CTH) of *p*-substituted acetophenone derivatives in the presence of KOH to afford the corresponding benzyl alcohol derivatives. The antimicrobial activities of the ligand **44-2** and the complex **44-3** was also studied.

The antimicrobial activities was screened *in vitro* against Gram-positive (*Staphylococcus aureus* ATCC 6538, *Bacillus cereus* ATCC 7064, *Listeria monocytogenes* ATCC 15313, *Micrococcus luteus* La 2971) and Gram-negative (*Escherichia coli* ATCC 11230, *Klebsiella pneumoniae* UC57, *Pseudomonas aeruginosa* ATCC 27853, *Proteus vulgaris* ATCC 8427, *Enterobacter aerogenes* ATCC 13048) bacteria and yeast cultures (*Candida albicans* ATCC 10231, *Kluyveromyces fragilis* NRRL 2415, *Rhodotorula rubra* DSM 70403) using two methods, disk diffusion and dilution methods (Tables 3-5, 3-6).

Table 3-5. Disk diffusion method: *In vitro* antimicrobial activity (mm zone) of **44-2**, **44-3**, and standard antibiotics

Microorganism	**44-2**	**44-3**	AM	CT	TE	NY	KE	CL
Gram (-)								
Proteus vulgaris	9	9	18	20	24	-	-	-
Escherichia coli	15	17	14	12	25	-	-	-
Klebsiella pneumoiae	14	17	15	16	30	-	-	-
Gram (+)								
Staphylococcus aureus	23	16	15	14	26	-	-	-
Bacillius cereus	12	10	14	14	22	-	-	-
Micricoccus luteus	-	10	30	34	20	-	-	-
Listeria monocytogenes	10	13	14	14	28	-	-	-
Fungi								
Candida albicans	-	9	-	-	-	20	22	16
Rhodotorula rubra	-	9	-	-	-	23	22	24
Kluyveromyces fragilis	13	14	-	-	-	16	15	18

-: inactive. AM: ampicillin 10 μg, CT: cefotaxime 30 μg, TE: tetracycline 30 μg, NY: nystatin 100 μg, KE: ketoconazole 20 μg, CL: clotrimazole 10 μg.

Table 3-6. Dilution method: *In vitro* antimicrobial activity of **44-2**, **44-3**, and standard antibiotics (MICs in mg/mL)

Microorganism	**44-2**	**44-3**	GEN	NY
Gram (-)				
Proteus vulgaris	25	25	6.25	-
Escherichia coli	12.5	6.25	6.25	-
Klebsiella pneumoiae	12.5	6.25	6.25	-
Gram (+)				
Staphylococcus aureus	12.5	12.5	25	-
Bacillius cereus	6.25	12.5	6.25	-
Micricoccus luteus	25	50	50	-
Listeria monocytogenes	25	25	12.5	-
Fungi				
Candida albicans	6.25	3.125	-	3.125
Rhodotorula rubra	3.125	3.125	-	3.125
Kluyveromyces fragilis	25	12.5	-	6.25

-: inactive. AM: GEN: gentamycin, NY: nystatin.

The results suggest that both ligand **44-2** and Ru(II) complex **44-3** exhibit good anti-microbial activities and can be further developed for application as effective antimicrobial agents. The antimicrobial data showed that the Ru(II) complex is more active than the free ligand against bacteria.

Çıralı also prepared cyclotriphosphazene ligands (**45-2** and **45-3**) bearing 3-oxypyridine groups and their corresponding Ru(II) complexes (**45-4** and **45-5**) (Scheme 3-23), and evaluated the cytotoxic activities of **45-2** –**5** against PC3 (human prostate cancer), DLD-1 (human colorectal cancer), HeLa (human cervical cancer), and PNT1A (normal human prostate) cell lines.[45] They also investigated the antimicrobial activities of **45-2** – **5** against a panel of Gram-positive and Gram-negative bacteria and yeast cultures. The compounds **45-2** – **5** were found to have moderate to high cytotoxic and antimicrobial activities, and complex formation with Ru(II) enhanced both cytotoxic and antimicrobial activities in comparison with the parent ligands, which is because lipophilicity of the Ru(II) complexes increased which would enhance the penetration of the complexes into cells and block the metal binding sites of receptors.

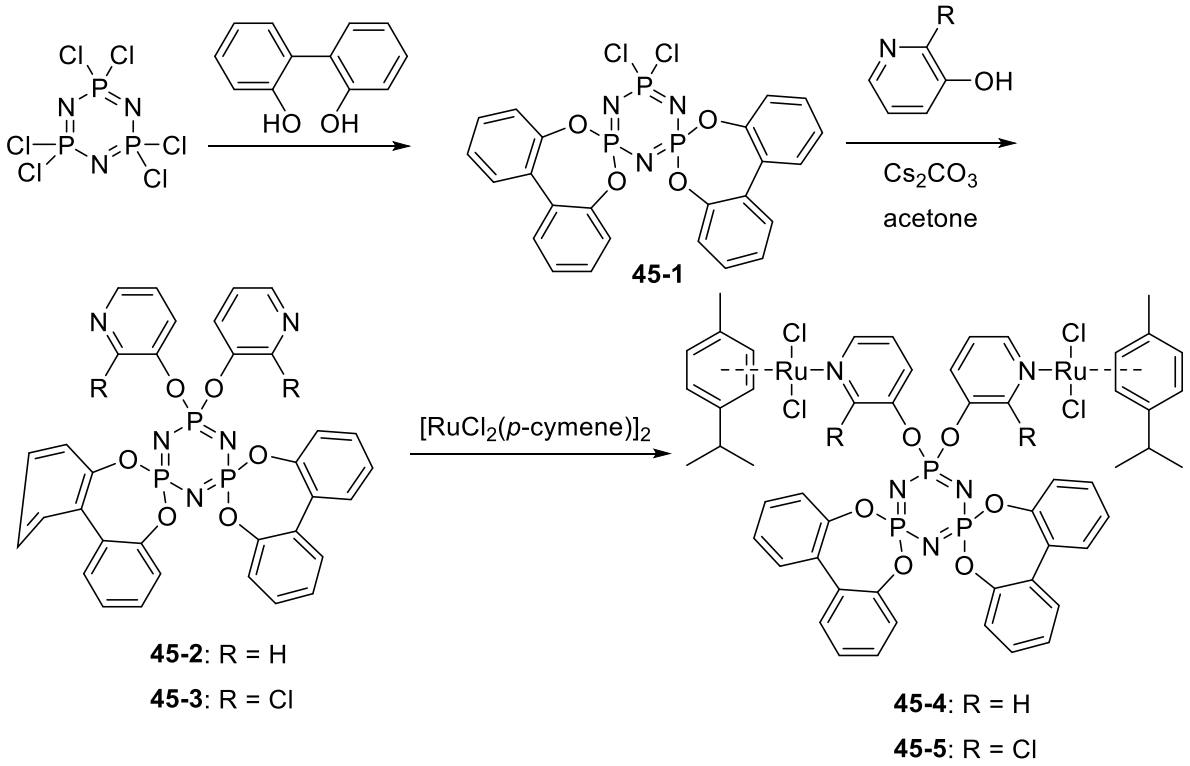

Scheme 3-23. Synthesis of ligands **45-2** – **3** and Ru(II) complex **45-4** – **5**

Against PC3 and DLD-1, **45-4** and **45-5** shows the highest antiproliferative effect, respectively (decrease of cell viability: 47% and 42% at 200 μM). Other compounds show around 30% reduction of cell viability for both PC3 and DLD-1 cells at 200 μM. Against HeLa cells, **45-2** and **45-3** reduced 16 and 35% cell viability, respectively. Ru(II) complexes **45-4** and **45-5** were more effective (the number of viable cells is observed (against HeLa cells, 46 and 48% reduction, respectively)) than **45-2** and **45-3.**

The data indicate that **45-4** and **45-5** show the highest cytotoxic activity against the tested cancer cells. However, **45-5** also shows severe toxic effects on normal PNT1A cells- 59% reduction. Since **45-4** is less toxic (25% decrease in cell viability), **45-4** may render it a candidate for potential drugs.

The results for *in vitro* antimicrobial activities of **45-2** – **5** together with inhibition zones of standard drugs are summarized in Table 3-7. The ligands **45-2** – **3** and complexes **45-4** – **5** show higher antibacterial activity against *M. luteus* and *S. aureus* than the commercial antibiotic gentamycin. Compounds exhibit about the same antibacterial activity against *K. pneumoniae* and moderate activity against the other bacteria in comparison with the standard drug. The results also show that Ru(II) complexes have generally better antimicrobial activities than metal-free ligands.

Table 3-7. *In vitro* antimicrobial activity of **45-2** – **5**, and standard antibiotics (MICs in mg/mL)

	Minimum Inhibitory Concentrations (MIC, μg/mL)					
Microorganism	**45-2**	**45-3**	**45-4**	**45-5**	GEN	NY
Bacteria						
M. luteus	12.5	12.5	12.5	12.5	50	-
S. aureus	6.25	12.5	6.25	12.5	25	
K. pneumoniae	12.5	6.25	6.25	12.5	6.25	
P. vulgaris	12.5	12.5	12.5	12.5	6.25	-
L. monocytogenes	25	25	25	25	12.5	
E. coli	50	12.5	25	6.25	6.25	-
B. cereus	25	25	6.25	25	6.25	-
Fungi						
R. rubra	6.25	3.125	3.125	3.125	-	3.125
C. albicans	6.25	6.25	3.125	3.125	-	3.125
K. fragiles	12.5	6.25	3.125	3.125	-	6.25

GEN: gentamycin, NY: nystatin. Red: Low activity, blue: Moderate acatibvity, Green: High activity

Çiftçi reported synthesis of *spiro* (**46-1a**), di*spiro* (**46-1b**, **46-2**, **46-3**), per-substituted spermine-bridged (**46-6** – **9**) and di*spiro-ansa* spermine (**46-10**) derivatives of cyclotriphosphazene (Scheme 3-24).[46]

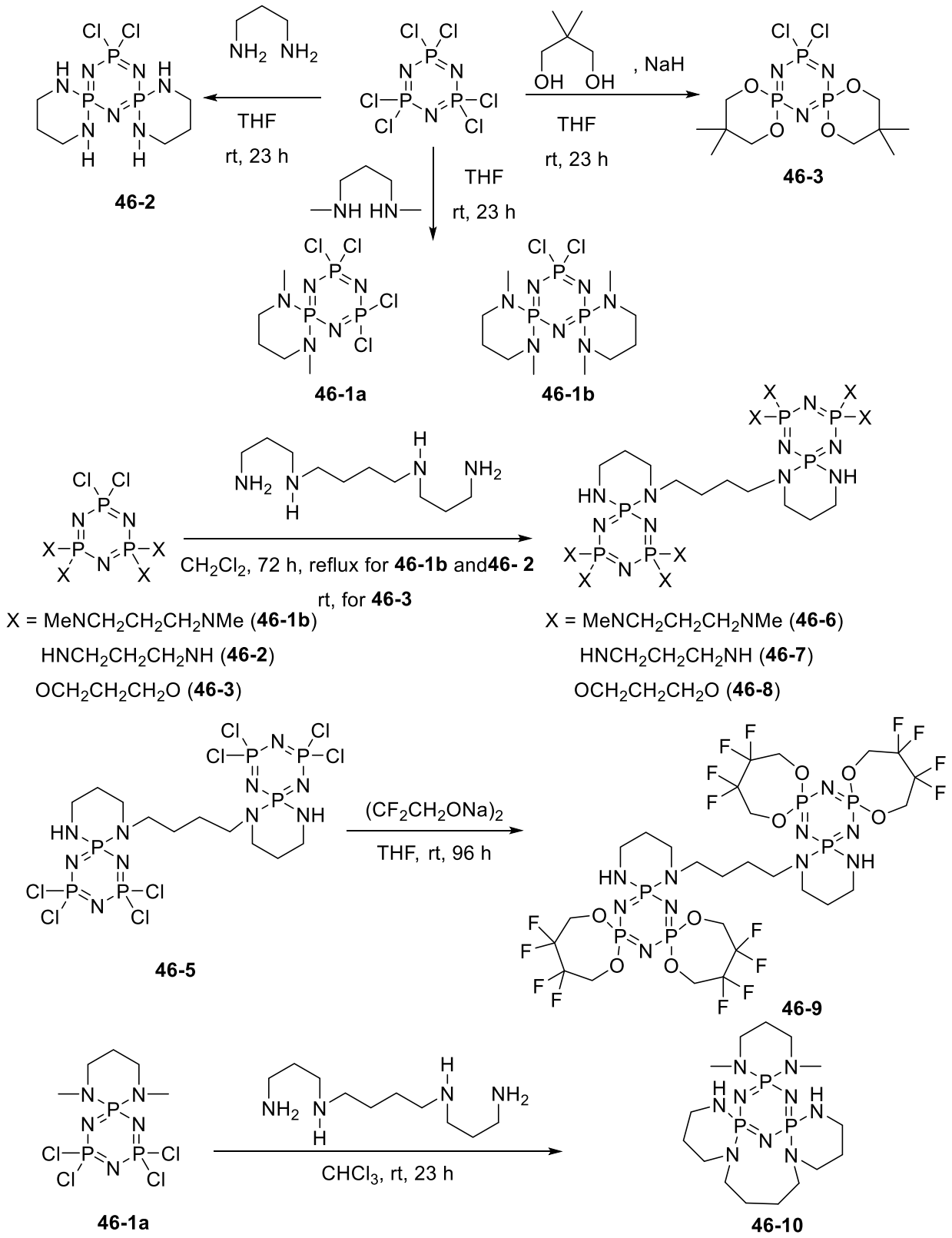

Scheme 3-24. Synthesis of **46-1** – **10**

In order to investigate the anti-tumor properties of the synthesized cyclotriphosphazene derivatives, *in vitro* cytotoxic activity test (MTT assay) has been performed using HT-29 (human colon

adenocarcinoma) and Hep2 (human epidermoid larynx carcinoma) cell lines. The result of the MTT assay showed that while **46-1a** has cytotoxic effect on both Hep2 and HT-29 cell lines, **46-3** has only cytotoxic effect towards the Hep2 cells. Compound **46-3** showed cytotoxic effect on Hep2 cells. On the other hand, **46-2**, **46-8**, **46-10**, **46-1b**, and **46-9** did not exhibit any cytotoxic effect on both cell lines.

3-2-5. DNA interaction

Tümer reported substitution of 2,2,4,4-tetrachlorocyclotriphosphazenes containing pendant NN or NO monoferrocenyl groups (**47-1a** – **1e**) with vanillin (Scheme 3-26).[47] The aim of this work is investigating antimicrobial and cytotoxic activities, and the DNA interactions of the mono- (**47-2a** – **2e**), di-substituted *gem* (**47-3a** – **3e**) and non-*gem/cis* (**47-4a** – **4e**), /*trans* (**47-5a** – **5e**), tri- (**47-6a** – **6e**) and tetra-substituted (**47-7a** – **7e**) monoferrocenylphosphazenes, since the vanillinatophosphazenes have reversible voltammograms with one-electron anodic and cathodic peaks which are attributed to ferrocenyl redox probe. Synthesis of **47-1a** – **1e** were reported in lit. 48 (Scheme 3-25).

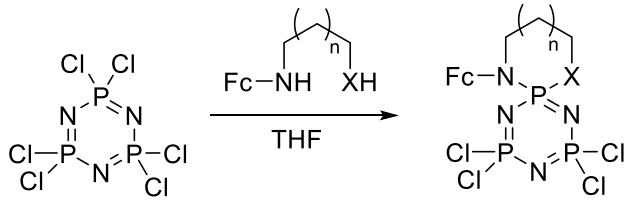

Compound	X	n
47-1a	NHMe	0
47-1b	NHEt	0
47-1c	NHMe	1
47-1d	OH	0
47-1e	OH	1

Scheme 3-25. Synthesis of 2,2,4,4-tetrachlorocyclotriphosphazenes containing pendant NN or NO monoferrocenyl groups (**47-1a** – **1e**)

In this study, HeLa cancer cell lines were used to determine the cytotoxic effects of **47-7b**, **47-4e**, and **47-4b** on mammalian cells by MTT assay (Figure 3-30). The MTT assay provided that anticancer activity of **47-7b** is negligible, while compounds **47-4e** and **47-4b** were little effective compared to cisplatin and paclitaxel.

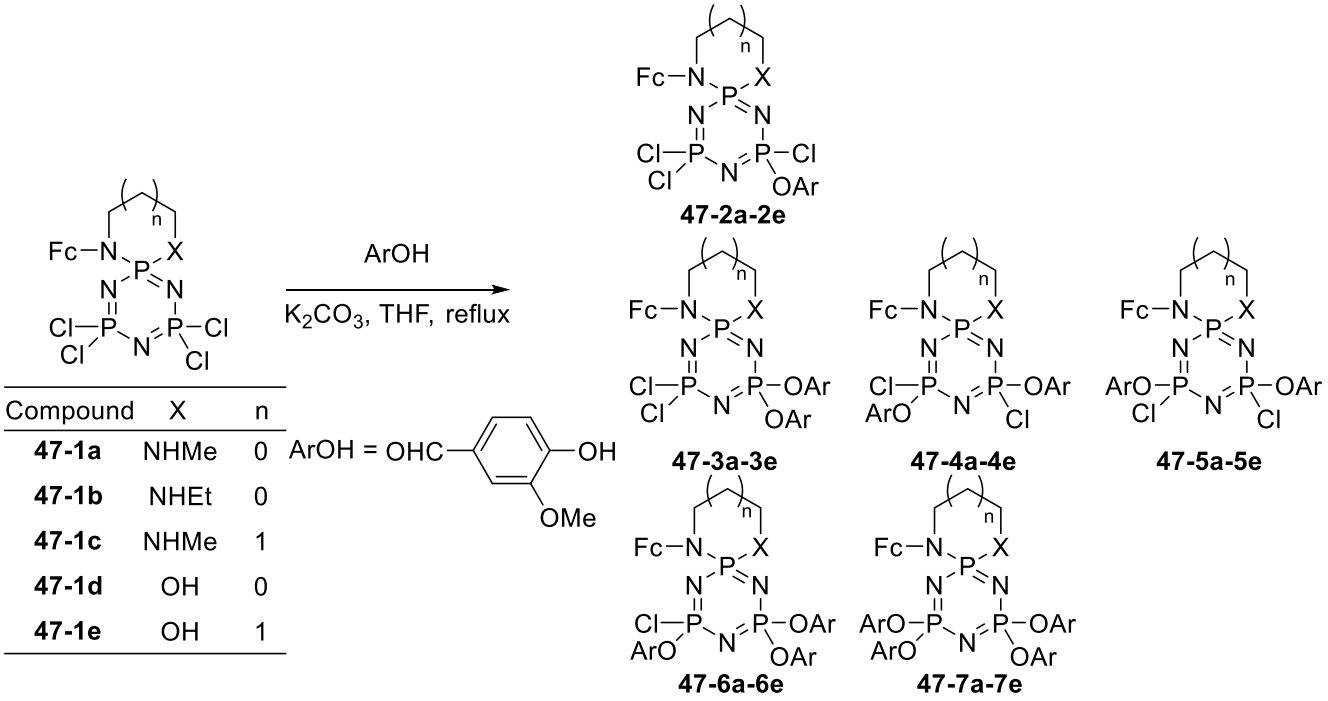

Compound	X	n
47-1a	NHMe	0
47-1b	NHEt	0
47-1c	NHMe	1
47-1d	OH	0
47-1e	OH	1

Scheme 3-26. Reaction of **47-1** with potassium vanillinate

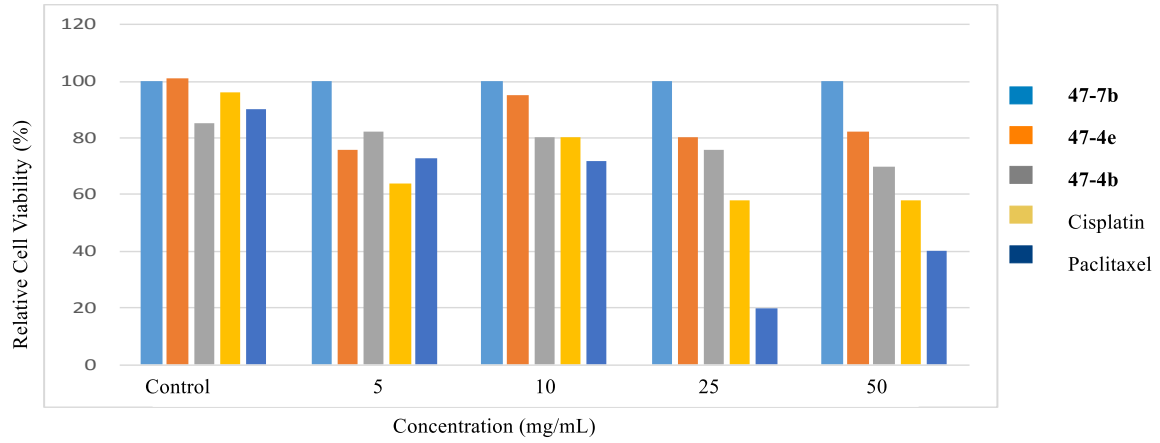

Figure 3-30. Relative cell viability (%) of HeLa cells following exposure of various concentrations of compounds **47-7e**, **47-4e**, **47-4b**, cisplatin and paclitaxel between 5 and 50 µg/mL and untreated control cell for 24 h

3-2-6. Cleavage of DNA

DNA cleavage activity of cyclotriphosphazene derivatives, **49-3**, and **49-4a** – **g**, was studied on double-stranded pBR322 DNA by gel electrophoresis experiments.[49] It was found that **49-4e** and **49-4f** caused the highest level of DNA damage. The interactions of **49-3** and **49-4e** with calf thymus DNA were also investigated using absorption spectrometry. The interaction of the compounds (**49-3** and **49-4b**) with the DNA (PDB ID:3V9D for A-DNA and PDB ID:1BNA for B-DNA) was investigated (Figure 3-32).

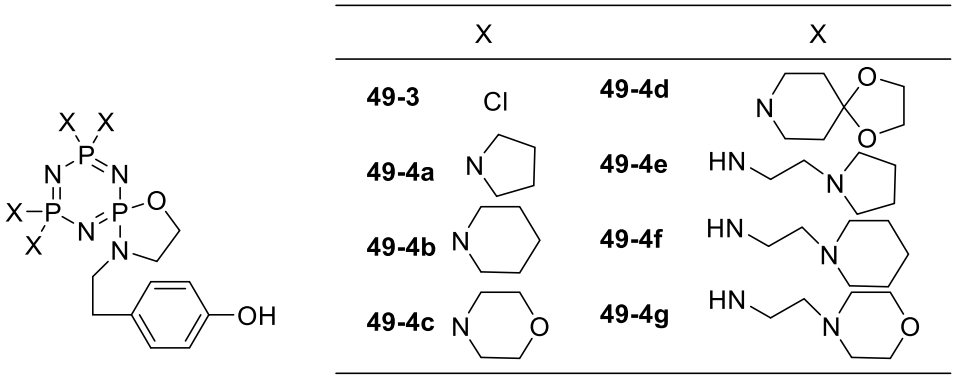

Figure 3-31. Structures of **49-3** and **49-4a** – **g**

DNA is a target molecule for anticancer drug development, and interaction of the synthetic products with DNA is essential in order to discover new drug candidates. Şenkuytu reported an electrochemical biosensor can be used to perform quantitative analysis of DNA/compound interactions (Scheme 3-27).[50] In this study, full paraben substituted fluorenylidene double bridged cyclotriphosphazene compounds (**50-5a** – **5e**) were synthesized and their interaction with DNA was investigated using an automated biosensor device MiSens. The reaction of fluorenylidene double bridged cyclotriphosphazene compound (**50-3**) with methyl 4-hydroxybenzoate (**50-4a**), ethyl 4-hydroxybenzoate (**50-4b**), propyl 4-hydroxybenzoate (**50-4c**), butyl 4-hydroxybenzoate (**50-4d**), and benzyl paraben (**50-4e**) were performed to give **50-5a** – **5e**.

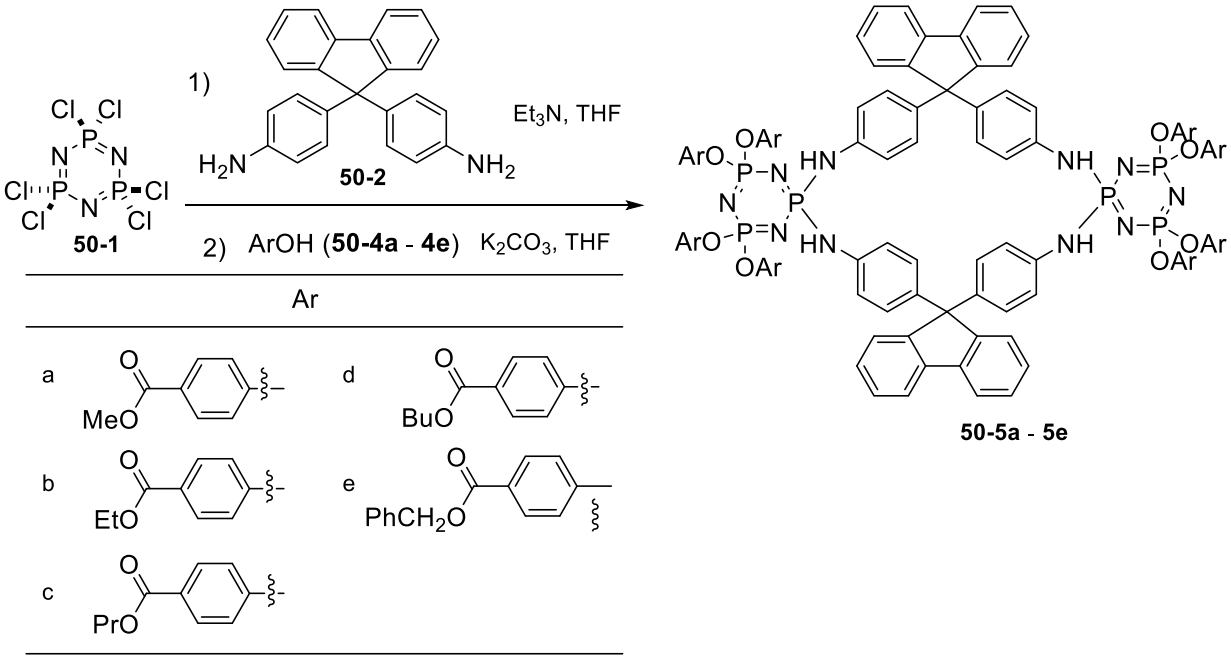

Scheme 3-27. Synthesis of paraben substituted fluorenylidene double bridged cyclotriphosphazene compounds (**50-5a** – **5e**)

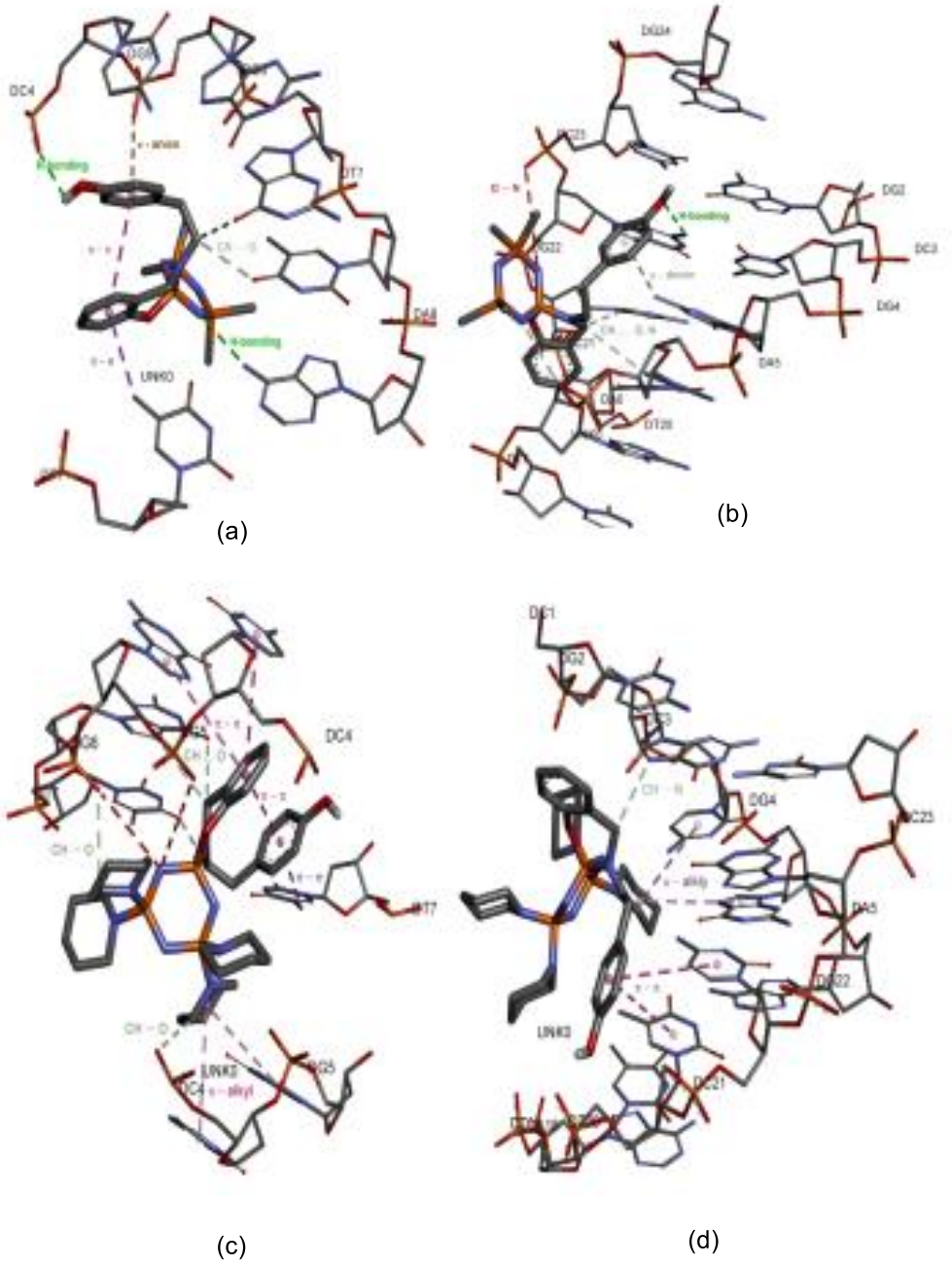

Figure 3-32. Binding interactions of the compounds (a) **49-3** with A-DNA, (b) B-DNA, (c) **49-4b** with A-DNA and (d) with B-DNA. These figures were originally drawn in lit. 49.

Biosensor based screening tests were used to investigate DNA interaction properties of **50-5a** – **5e** by measuring efficiency of DNA hybridization on biochip surface. The effects of **50-5a** – **5e** on the plasmid DNA structure were also analyzed by agarose gel electrophoresis. In addition, antimicrobial activities of **50-5a** – **5e** were investigated. The biosensor assay and the agarose gel electrophoresis investigation indicated that **50-5d** and **50-5e** gave severe damage on DNA and might be potent candidates

as anticancer agents. On the other hand, no compound among **50-5a** – **50-5e** show any antibacterial activity against *P. aeruginosa* ATCC 27853, *E. coli* ATCC 35218, and *S. aureus* ATCC 25923.

3-2-7. Proliferation

Two different families of bifunctional water-soluble dendrimers containing cyclotriphosphazene core having 5 units of proliferation of human osteoblasts and one unit of immobilizing unit on Au metal are synthesized (Figure. 3-33).[51] Dendrimers are grown from the 5 remaining functions, up to generation 2. Water-solubility is attained in the last step of the synthesis by grafting either ammonium terminal groups or carboxylate terminal groups, on generations 1 and 2 of these bifunctional dendrimers. The function linked to the core is thioctic acid, suitable for grafting onto Au metal, thus both types of water-soluble dendrimers can be used to coat Au surfaces. The Au surfaces were modified by either positively or negatively charged dendrimers and studied their interaction with cells. Containing cyclotriphosphazene as an exposed to human osteoblast cells, the influence of the surface coatings on the cell responses is investigated. Polycationic dendrimers provoke cell apoptosis, whereas negatively charged dendrimers support cell adhesion and proliferation.

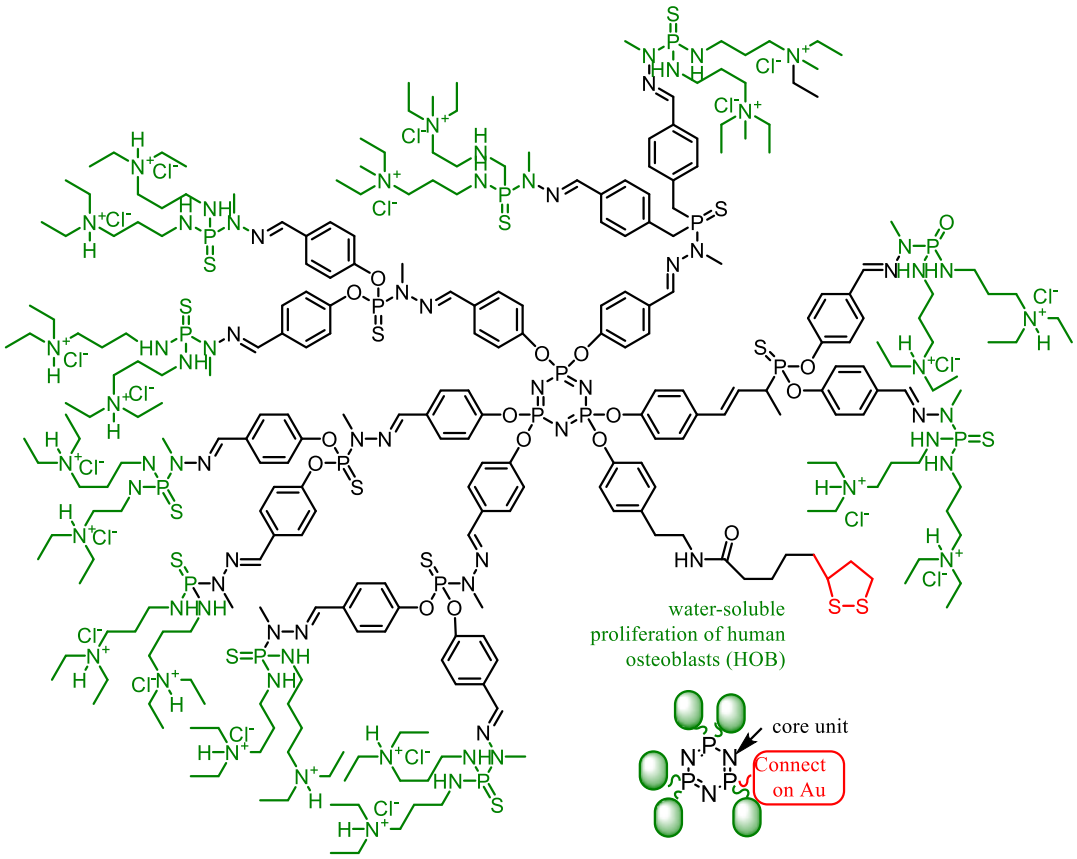

Figure 3-33. Bifunctional water-soluble dendrimers containing cyclotriphosphazene core having 5 units of proliferation of human osteoblasts and one unit of immobilizing unit un Au metal

4. SUMMARY and PERSEPECTIVE

Cyclotriphosphazene ($N_3P_3R_6$) has a 6-membered N-P ring and six substituents from three phosphorus atoms. The ring is almost flat, and six substituents are located upper side (three substituents) and lower side (three substituents) of the ring. Therefore, the substituents can interact each other. Similar compounds would be hexa-substituted benzene derivatives and hexa-substituted cyclohexane derivatives. However, in hexa-substituted benzene derivatives, all substituents are located in the same plane of benzene ring, and in all-*trans* hexa-substituted cyclohexane derivatives, all substituents are likely located at equatorial position because of steric hindrance. Therefore, interaction between the substrates should become small. Moreover, hexa-substituted cyclotriphosphazene can be prepared much easier than hexa-substituted benzene derivatives and hexa-substituted cyclohexane derivatives because of the high reactivity of P-Cl bond of their staring material hexachlorocyclotriphosphazene (HCCP). Therefore, though HCCP does not show a special property, it can be used as a pinholder of flowers (‘Kenzan’ in Japanese, a tool for flower arrangement). HCCP itself is an inorganic compound, but it becomes a base of inorganic/organic hybrid materials.

Though six P-Cl bonds in HCCP are equivalent, once a substituent is introduced, not all the remaining reaction sites, P-Cl bonds, are equivalent. Therefore, numbers of substituents, regio-, and stereochemistry vary depending on the reaction conditions and the nature of the firstly introduced substituent. Cyclotriphosphazenes have ^{31}P nuclei, and if the other ^{31}P nuclei is not included in the reaction conditions (such as in solvents), the reaction can be monitored easily by ^{31}P NMR technics because the sensitivity of ^{31}P is relatively high.[52] One disadvantage can be pointed out that examples of the ^{31}P NMR data are insufficient compared with those of ^{1}H and ^{13}C NMR data. Therefore, the researchers should face difficulty to determine the structure of the compounds they obtained. But in some days, cyclotriphosphazene chemistry would be developed more and more, database would be prepared.

Historically, phosphazene derivatives were used as a frame retardant, but now a day, cyclotriphosphazene derivatives are used as highly functionalized materials and biomaterials. Though number of the literatures about “cyclotriphosphazene” is still small, it is now increasing and new materials are reported.

LITERATURES AND NOTES

1. J. Liebig and J. Wöhler, *Liebigs Ann. Chem.*, 1834, **11**, 139.
2. H. N. Stoke, *J. Am. Chem. Soc.*, 1895, **17**, 275.
3. L. O. Brockway and W. M. Bright, *J. Am. Chem. Soc.*, 1943, **65**,1552.
4. (a) A. Wilson and D. F. Carroll, *J. Chem. Soc.*, 1960, 2548; (b) G. J. Bullen, *J. Chem. Soc. (A)*, 1971, 1450.

5. M. Kuroboshi, M. Morita, Y. Masumoto, M. Mikasa, R. Toza, and H. Tanaka, *Heterocycles*, 2019, **98**, 931.
6. M. Kuroboshi, M. Mikasa, and H. Tanaka, *Heterocycles*, 2019, **98**, 940.
7. (a) J. Reuben, *Magn. Reson. Chem.*, 1987, **25**, 1049; (b) Y. W. Chen-Yang, S. J. Cheng, and B. D. Tsai, *Ind. Eng. Chem. Res.*, 1991, **30**, 1314.
8. S. Beşli, C. M. Balcı, C. Köseoğlu, D. Palabıyık, and C. W. Allen, *Inorg. Chim. Acta*, 2019, **492**, 23.
9. (a) M. Kajiwara, "Fosufazen Kagaku no Kiso", CMC Press, Tokyo, 1986; (b) M. Kajiwara, *CREATIVE*, 2011, **10**, 3.
10. S. BeŞli, C. Mutlu, F. Yuksel, and A. Kılıç, *Polyhedron*, 2014, **81**, 777.
11. S. Beşli, C. Mutlu, and F. Yukse, *Dalton Trans.*, 2013, **42**, 16709.
12. S. Beşli, C. M. Balcı, C. Köseoğlu, D. Palabıyık, and C. W. Allen, *Inorg. Chim. Acta*, 2019, **492**, 23.
13 S. Beşli, C. M. Balcı, S. Doğan, and C. W. Allen, *Inorg. Chem.*, 2018, **57**, 12066.
14. D. Palabıyık, C. M. Balcı, and S. Beşli, *Inorg. Chim. Acta*, 2019, **487**, 15.
15. S. Beşli, S. Doğan, C. M. Balcı, and F. Yukse, *Polyhedron*, 2017, **122**, 61.
16. P. I. Dron, K. Zhao, J. Kaleta, Y. Shen, J. Wen, R. K. Shoemaker, C. T. Rogers, and J. Michl, *Adv. Funct. Mater.*, 2016, **26**, 5718.
17. J. Kaleta, G. Bastien, J. Wen, M. Dracinsky, E. Tortorici, I. Cisarova, P. D. Beale, C. T. Rogers, and J. Michl, *J. Org. Chem.*, 2019, **84**, 8449.
18. M. Cipolloni, J. Kaleta, M. Mašát, P. I. Dron, Y. Shen, K. Zhao, C. T. Rogers, R. K. Shoemaker, and J. Michl, *J. Phys. Chem.* C, 2015, **119**, 8805.
19. J. Tian, P. Thallapally, J. Liu, G. J. Exarhos, and J. L. Atwood, *Chem. Commun.*, 2011, **47**, 701.
20. H. R. Allcock, M. L. Levin, and R. R. Whittle, *Inorg. Chem.*, 1986, **25**, 41.
21. Sozzani, S. Bracco, A. Comotti, L. Ferretti, and R. Simonutti, *Angew. Chem. Int. Ed.*, 2005, **44**, 1816.
22. G. Gahungu, B. Zhang, and J. Zhang, *J. Phys. Chem. B*, 2007, **111**, 5031.
23. H. Eserci, E. Şenkuytu, and E. Okutan, *J. Mol. Struct.*, 2019, **1182**, 1.
24. A. Uslu and Ş. Guvenaltın, *Dalton Trans.*, 2010, **39**, 10685.
25. E. Okutan, H. Eserci, and E. Şenkuytu, *Spectrochim. Acta Part A: Mol. Biomol. Spectr.*, 2019, **222**, 117232.
26. H. A. Alidagi, S. O. Tümay, A. Şenocak, Ö. F. Çiftbudak, B. Çoşut, and S. Yeşilot, *New J. Chem.*, 2019, **43**, 16738.
27. D. Davarcı, *CBU J. Sci.*, 2016, **12**, 535.
28. Z. Jamain, M. Khairuddean, and S. A. Saidin, *J. Mol. Struct.*, 2019, **1186**, 293.

29. H. AkbaŞ, A. Karadağ, A. Destegül, Ç. Çakırlar, Y. Yerli, K. C. Tekin, U. Malayoğlu, and Z. Kılıç, *New J. Chem.*, 2019, **43**, 2098.
30. N. Gutowska, P. Seliger, G. Andrijewski, M. Siwy, M. Małecka, and J. Kusz, *RSC Adv.*, 2015, **5**, 38435.
31. F. Kato, A. Chandra, M. Tokita, H. Asano, H. Shimomoto, E. Ihara, and T. Hayakawa, *ACS Macro Lett.*, 2018, **7**, 37.
32. H. Li, Z. Zhou, J. Liu, X. Zheng, W. Xu, C. Ji, W. Shi, R. Liu, and X. Liu, *J. Polym. Res.*, 2017, **24**, 62.
33. F. Aslan, A. Oztürk, and B. Söylemez, *J. Mol. Struct.*, 2017, **1137**, 387.
34. G. Y. Çiftçi, Y. Eker, E. Şenkuytu, and F. Yuksel, *J. Mol. Struct.*, 2016, **1117**, 164.
35. E. Şenkuytu, E. T. Eçik, M. Durmuş, and G. Y. Çiftçi, *Polyhedron*, 2015, **101**, 223.
36. G. Y. Çiftçi, E. Şenkuytu, M. Bulut, and M. Durmuş, *J. Fluoresc.*, 2015, **25**, 1819.
37. K. Koran, F. Özen, F. Biryan, and A. O. Görgülü, *J. Mol. Struct.*, 2016, **1105**, 135.
38. E. Badetti, V. Lloveras, K. Wurst, R. M. Sebastian, A.-M. Caminade, J.-P. Majoral, J. Veciana, and J. Vidal-Gancedo, *Org. Lett.*, 2013, **15**, 3490.
39. R. J. Davidson, E. W. Ainscough, A. M. Brodi, G. B. Jameson, M. R. Waterland, B. Moubaraki, K. S. Murray, K. C. Gordon, R. Horvath, and G. N. L. Jameson, *Polyhedron*, 2013, **55**, 37.
40. E. Önal, C. Zhang, D. Davarcı, Ü. Işci, G. Pilet, A. K. Whittaker, and F. Dumoulin, *Tetrahedron Lett.*, 2018, **59**, 521.
41. K. Koran, Ç. Tekin, F. Biryan, S. Tekin, S. Sandal, and A. O. Görgülü, *Med. Chem. Res.*, 2017, **26**, 962.
42. S. S. Machakanur, B. R. Patil, G. N. Naik, R. P. Bakale, S. W. A. Bligh, and K. B. Gudasi, *Inorg. Chim. Acta*, 2014, **421**, 459.
43. E. Öztürk, A. Okumuş, Z. Kılıç, A. Kılıç, H. Kayalak, L. Açık, N. A. Çerçi, M. Türk, and T. Hökelek, *Inorg. Chim. Acta*, 2019, **486**, 172.
44. D. E. Çıralı, O. Dayan, N. Özdemir, and N. Hacıoglu, *Polyhedron*, 2015, **88**, 170.
45. D. E. Çıralı, Z. Uyarb, İ. Koyuncu, and N. Hacıoğlu, *Appl. Organomet. Chem.*, 2015, **29**, 536.
46. G. Y. Çiftçi, E. T. Eçik, T. Yildirim, K. Bilgin, E. Şenkuytu, F. Yuksel, Y. Uludag, and A, Kiliç, *Tetrahedron*, 2013, **69**, 1454.
47. Y. Tümer, L. Y. Koç, N. Asmafiliz, Z. Kılıç, T. Hökelek, H. Soltanzade, L, Açık, M. L. Yola, and A. O. Solak, *J. Biol. Inorg. Chem.*, 2015, **20**, 165.
48. E. E. Ilter, N. Asmafiliz, Z. Kılıç, L. Açık, M. Yavuz, E. B. Bali, A. O. Solak, F. Büyükkaya, H. Dal, and T. Hökelek, *Polyhedron*, 2010, **29**, 2933.

49. S. PektaŞ, S. B. Koçak, N. S. BaŞterzi, Z. Kılıç, C. T. Zeyrek, B. Coban, U. Yildiz, and Ö. Çelik, *Inorg. Chim. Acta*, 2018, **474**, 51.
50. E. Şenkuytu, T. Yıldırım, Z. Ölçer, Y. Uludağ, and G. Y. Çiftçi, *Inorg. Chim. Acta*, 2018, **477**, 219.
51. E. R. de Jong, N. Deloch, W. Knoll, C.-O. Turrin, J.-P. Majoral, A.-M. Caminade, and I. Köper, *New J. Chem.*, 2015, **39**, 7194.

52. Monitoring of reaction by ^{31}P NMR: D_2O is sealed in a capillary (i.d. ca. 2 mm, length ca. 70 mm). In a 5 mm i.d.-NMR sample tube were put the capillary and an aliquot of the reaction mixture (ca. 0.5 mL). Lock of the NMR is set on D_2O. If the concentration of the substrate is 1 mmol/5 mL-solvent, 32-64 acquisition times would be enough for detecting of main products.

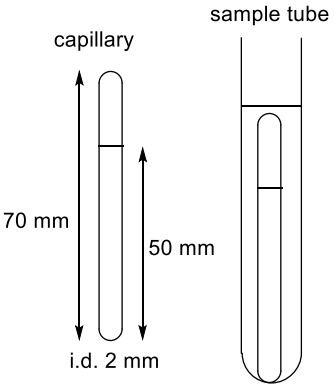

Manabu Kuroboshi completed his PhD at Kyoto University in 1989. From 1989 to 1992, he worked in Sagami Chemical Research Center, and from 1992 to 1995, he worked in Tokyo Institute of Technology with Prof. Tamejiro Hiyama. He moved to Okayama University in 1995 as a lecturer, worked with Prof. Sigeru Torii and Hideo Tanaka, and now he is an associate professor in Okayama University.